Forward Dynamic Simulation of a Golf Drive: Optimization of Golfer Biomechanics and Equipment

by

William McNally

A thesis
presented to the University of Waterloo
in fulfillment of the
thesis requirement for the degree of
Master of Applied Science
in
Systems Design Engineering

Waterloo, Ontario, Canada, 2018

I hereby declare that I am the sole author of this thesis. This is a true copy of the thesis, including any required final revisions, as accepted by my examiners.

I understand that my thesis may be made electronically available to the public.

Abstract

Advances in golf club performance are typically based on the notion that golfer biomechanics do not change when modifications to the golf club are made. A full-swing forward dynamic golf drive model, including impact and ball flight, has been developed to provide a deeper understanding of the interaction between golfer biomechanics and the physical properties of golf clubs. A three-dimensional, six degree-of-freedom biomechanical model of a golfer, a Rayleigh beam model of a flexible club, an impact model based on volumetric contact, and a spin-rate dependent ball flight model have been integrated to dynamically simulate a golf drive.

Data from a golf swing motion capture experiment with ten elite golfers was used to validate various components of the golf drive model. Using the flexible club model in full-swing simulations driven by experimental grip kinematics, the simulated shaft deflections matched the motion capture experiment with a high level of accuracy. In the same simulations, the grip forces were obtained via inverse dynamics. The simulated grip forces showed that the majority of the grip force at impact is centripetal, and very little torque is applied about the shaft axis throughout the golf swing.

The impact model was added to the multibody framework so that impact effects from the shaft and golfer could be investigated. Parameter identification was performed using full-club impact simulations initialized at the moment of impact and driven by extrapolated grip forces. Using a training dataset, the differences between the simulated and experimental ball velocity and angular velocity were minimized, and the impact model was validated against a test dataset. In a simulation experiment, the shaft was removed from the impact model to examine the validity of a long-held assumption in golf science – that the impact is accurately modelled as a free-body collision between the clubhead and ball. Comparing free-body and full-club impact simulations, the shaft was shown to create a stiffening effect that resists the twisting of the clubhead during contact, corresponding to a significant increase in ball speed and a suppression of the gear-effect.

To validate the biomechanical model, a custom optimization routine combining genetic and search-based algorithms was implemented to maximize carry distance. Comparing the simulated grip kinematics to the motion capture experiment, the biomechanical model effectively reproduced the motion of an elite golf swing. The golf drive model was used to investigate the complex interaction between clubhead mass, the golfer's ability to generate clubhead speed, and impact efficiency. By varying clubhead mass, it was shown that a golfer can potentially generate greater ball speed with a lighter clubhead. This simulation experiment, among others conducted in this work, demonstrate the model's ability to provide valuable insights relating to golfer biomechanics and equipment performance.

Acknowledgements

I would like to thank my supervisor, Prof. John McPhee, for the opportunity to conduct this research and the invaluable advice and support throughout this project.

I would like to thank PING Inc., and in particular Dr. Erik Henrikson, for his supervision during my internship and the experimental support of this research.

I would like to acknowledge my committee members, Prof. David Clausi and Prof. Glenn Heppler, for providing suggestions to improve this work.

I would like to acknowledge the Natural Sciences and Engineering Research Council of Canada, the Canada Research Chairs program, and the Government of Ontario for financial supporting this research.

Finally, I would like to thank all the members of the Motion Research Group at the University of Waterloo for their suggestions and modelling support over the past two years.

Table of Contents

List of Tables

List of Figures

Chapter 1

Introduction

It is estimated that golf is played by 80 million people worldwide [1]. The sport is most popular in North America, where 54% of the world's golf facilities reside [2]. In Canada, golf has had the highest participation rate of any sport since 1998 [3]. In recent years, the sport has been considered by many to be in decline [4, 5]. However, statistics indicate that golf is in position for future growth. In 2016, the total number of new golfers (those playing on a golf course for the first time) in the U.S. rose to a new high of 2.5 million, surpassing the previous record set in 2000, when Tiger Woods was at the peak of his career and drawing newcomers to the game at unprecedented rates [6]. The growth of golf is supported more than ever by off-course participation from driving ranges and indoor golf simulators. Driven primarily by the success of Topgolf, a form of golf entertainment, there was an estimated 20 million off-course participants in the U.S. in 2016 [6]. Furthermore, golf returned to the Summer Olympics in 2016, following a 112-year hiatus.

To capitalize on golf's $70 billion market [7], golf equipment companies are perpetually innovating, releasing new lines of clubs and balls year after year with promises of improved performance. The amount of innovation that flows into the design of golf equipment is astounding. In 2016, 831 patents containing the word "golf" in their title were issued by the United States Patent and Trademark Office, five times more than North America's five major sports combined (baseball, football, basketball, hockey, and soccer). The driver is the most expensive golf club and as such it is the most highly marketed. Each year, golf companies claim to find innovative ways to improve driver performance while abiding by design restrictions imposed by the sport's governing bodies. Despite these supposed advancements, the average driving distance on the PGA Tour has increased by only 3 yards in the past decade [8], causing consumers to contemplate the credibility of driver marketing information.

1.1 Motivation and Goals

Modern driver design involves advanced modelling and simulation of clubhead-ball impacts. Current design methods are exceedingly computationally intensive and as a result, prototype driver designs are evaluated based on stand-alone free-body impact simulations that do not consider the interaction between the club and golfer, let alone the interaction between the clubhead and shaft. The goal of this thesis is to develop and validate a predictive dynamic simulation of a golf drive including the golfer, club, impact, and ball flight. Existing models of this nature have lacked the experimental validation required to support results from virtual experiments (i.e., simulations). For this reason, experimental validation is one of the primary focuses of this work. Furthermore, no models to date have contained an impact model compatible with the shaft and golfer, so the development of such an impact model is another focus of this work. The overall model seeks to build our scientific understanding of the biomechanical interaction between the golfer and club, and golf impact mechanics.

1.2 Document Structure

This document is divided into six chapters:

- Chapter 1 provides a brief introduction that outlines the motivation for the work and summarizes the main contributions of this research.
- Chapter 2 provides some background information and a literature review on existing golf swing and impact models.
- Chapter 3 describes each component of the overall golf drive model, which contains four sub-models. Each sub-model is described within its own section. The fifth and final section of this chapter describes how the model is implemented using optimal control.
- Chapter 4 contains experimental validations for the biomechanical, flexible club and impact sub-models. These validations exploit data collected from a golf swing motion capture study with ten elite golfers.
- Chapter 5 applies the golf drive model or some of its sub-models to investigate different aspects of golf swing mechanics, impact dynamics, and equipment performance in four simulation experiments.

- Chapter 6 concludes the project with a summary of the work that was completed, makes recommendations based on the results of the simulation experiments, and outlines areas for future research.

1.3 Contributions

- A full-swing forward dynamic model of a golf drive including a three-dimensional six degree-of-freedom biomechanical model.
- A continuous concentric-eccentric torque-velocity scaling function for biomechanical joint torque production using parameters found in existing golf swing models.
- The accurate simulation of shaft dynamics in full-swings using experimental grip kinematics as inputs and empirically determined clubhead properties.
- Characterization of the grip forces applied to the golf club in the swings of elite golfers.
- A volumetric clubhead-ball impact model, compatible with the shaft and golfer in a multibody framework and validated for impact locations close to the center of the clubface.
- A quantitative comparison of full-club and free-body clubhead-ball impact dynamics and launch conditions.
- The golfer's dynamic contribution to impact and corresponding influence on launch conditions.

Chapter 2

Background & Literature Review

The golf drive is a unique golf shot taken from the tee with a special club known as a driver. In terms of modelling, the golf drive is regarded as a physical system spanning many fields of engineering, namely biomechanics, multibody dynamics, optimal control, solid mechanics, and aerodynamics. To simplify this multifaceted modelling problem, the golf drive is broken down into three components: the golf swing, the impact, and the ball flight. The golf swing is a full body movement and therefore has many degrees of freedom. It begins with the activation of the golfer's muscles, generating joint torques that guide a flexible club in a controlled arcing motion. The shaft, flexed from the swing, unloads its stored energy just before impact and the clubhead strikes the golf ball with tremendous force. The peak force during impact often surpasses a metric ton and causes significant elastic deformation to both the clubface and the ball during a brief contact period lasting approximately half a millisecond [9]. The goal of a drive is to transfer as much kinetic energy as possible to the ball while maintaining a high level of consistency and control. Performance is measured by the distance the golf ball travels through the air and depends on the initial launch conditions of the golf ball and its aerodynamics in flight. The longer and straighter the drive, the easier the subsequent shot into the green and the better chance of making a good score on the hole.

The predictive simulation of a golf drive requires the integration of multiple models to capture various physical phenomena. Each component is modelled individually and ultimately pieced together to simulate a complete golf drive. It should be noted that in this work, the golf swing itself is broken down further into two sub-models: the biomechanics of the golfer, and the behaviour of the golf club. However, the two sub-models may be collectively referred to as a golf swing model, and are often referred to as such in the literature. Although the simulation of a golf drive requires the integration of all four sub-

models, the main contributions in this work lie within golf swing and impact modelling. This chapter provides an overview of existing golf swing and impact models, and highlights opportunities for improvement.

2.1 Golf Swing Models

From a high-level perspective, a golf swing model consists of two components: a biomechanical model, and some representation of the golf club. A biomechanical model is a mathematical representation of the human body and its motion, and biomechanical analysis is performed by running simulations (i.e., virtual experiments) with the model. The complexity of a biomechanical golfer model can range from a single rigid body representing the leading arm connected to a fixed torso by a one-dimensional (1D) rotational joint [9], to a three-dimensional (3D) 15 segment full-body model [10]. Biomechanical models are classified based on whether they employ inverse or forward dynamics [11]. It is necessary to discuss the differences between these two approaches as they have both been used extensively to model the golf swing [12], and each have their strengths and weaknesses.

2.1.1 Inverse Dynamics versus Forward Dynamics

Inverse dynamics is the more commonly used approach to biomechanical modelling in general, and is frequently used for biomechanical analysis of the golf swing [12]. With inverse dynamics, a motion capture system collects position data on a subject performing a specific movement, which is then used to drive a biomechanical model at the joint level. A model such as this is said to be *kinematically driven*. Joint velocities and accelerations are obtained by numerically differentiating the position data or by direct measurement using inertial measurement units. Complex biomechanical models are developed within multibody dynamics software packages that generate the equations of motion automatically. The forces and torques required to produce the imposed motion are calculated by substituting the joint accelerations into the equations of motion. Joint torques are useful for the comparison of energy metrics such as power and work across subjects, and such an energy analysis was applied to the golf swings of four amateur golfers using a 15 segment full-body model in the work of Nesbit and Serrano [13].

Due to discretization error associated with numerical differentiation, force histories are noisy and often require smoothing algorithms to interpret. The accuracy of numerical differentiation inherently depends on data resolution, which relates to the frequency of the

motion capture system. The more markers used in the experiment, the lower the motion capture frequency. Because the golf swing is a full-body movement, many markers are required to capture the motion of all the segments, thus limiting the accuracy of the estimated forces. Furthermore, because inverse dynamic models are driven using measured kinematic data, they are ill-equipped to make predictions and consequently cannot be used for optimization. However, inverse dynamics facilitates the modelling of a large number of degrees of freedom, which is important for an accurate representation of golfer biomechanics. Furthermore, solving the underlying linear algebraic equations of inverse dynamic models is straightforward.

Conversely, forward dynamics uses internal forces to create motion. A forward dynamic model is said to be *dynamically driven*. The creation of motion implies that a forward dynamic model has predictive capabilities, and is well-suited for optimization. For that reason, forward dynamics is a more insightful modelling approach than inverse dynamics. However, forward dynamics requires knowledge of how the internal forces are generated and also needs solvers for ordinary differential equations or differential algebraic equations. Forward dynamics is therefore is not as widely used as inverse dynamics. In forward dynamic biomechanical models, internal forces are typically generated using parameterized joint torque functions based on the underlying theory of muscles, and parameters are identified using subject-specific experimental data. Advanced joint torque functions incorporate the mechanical characteristics of muscles such as the force-velocity and force-length relationship, but are only accurate under the conditions for which their parameters were experimentally identified, such as maximum voluntary contraction [14]. As a result, forward dynamics is not fit to control coordinated full-body movements with a large number of degrees of freedom.

Despite forward dynamics' general incompatibility with full-body movements, the golf drive is a defensible case for the use of a forward dynamic model as players try to generate as much power as possible using their upper body and core in order to maximize clubhead speed. Researchers have recognized this and therefore forward dynamic golf swing models, or simply put, dynamic golf swing models, are an active area of research. To control a golf swing dynamically, biomechanical simplifications must be made, and there exists a trade-off between biofidelity (i.e., the number of degrees of freedom) and difficulty in controlling the swing. Accordingly, dynamic golf swing models to date have focused on the motion of the upper body during the downswing with a particular focus on the leading arm, assuming the lower limbs and trailing arm play a more passive role. Starting out as planar double pendulums, dynamic golf swing models have progressed to 3D models with multiple biomechanical degrees of freedom featuring flexible clubs.

The dynamic golf swing model presented in Chapter 3 advances the state-of-the-art,

and was developed on a foundation of existing models. Sections 2.1.2 through 2.1.5 review these models in chronological order.

2.1.2 The Double Pendulum Model

The Search for the Perfect Swing, co-authored by Cochran and Stobbs and first published in 1968, presents a compilation of scientific studies examining all areas of golf [9]. Their pioneering work is the first comprehensive scientific analysis of the sport. To gain insights on optimal golf swing mechanics, Cochran and Stobbs idealized the golf swing using a double pendulum. The two-lever system, as they called it, consisted of an upper lever representing the golfer's arms and shoulders that rotated on an inclined plane about a fixed pivot point located in the middle of the golfer's upper chest. The lower lever represented the club and was attached to the upper lever via a hinge representing the wrists. The wrist hinge behaved passively but was restricted by a "stop" that prevented the wrist from "jack-knifing" beyond 90°. The two-lever system is illustrated in Fig. 2.1.

The model was initially positioned so that the two levers roughly corresponded to the top of a golfer's backswing, with the lower lever pressed against the stop. As the upper lever began rotating to commence the downswing, the lower lever remained pressed against the stop until centrifugal force started to throw the lower lever outwards. Due to conservation of angular momentum, the upper lever's angular velocity slows down while the lower lever speeds up. Cochran and Stobbs emphasized that this radial transfer of kinetic energy could generate a well-coordinated swing if the correct torque was applied at the fixed pivot, implicating a natural wrist release where the hands do not apply any forces. Albeit appreciative of this model's simplicity, Cochran and Stobbs were not blind to the fact that more kinetic energy could be generated at the clubhead if the wrist hinge were to activate during the downswing. They discussed the trade-off between increased clubhead speed and difficulty in timing the activation of both pivot points, and even suggested that a three-lever system would be more efficient if it could be timed correctly [9].

Cochran and Stobbs used the double pendulum model to explain some of the basic principles of golf swing mechanics, but did not apply the model in a forward dynamics sense. Having said that, the double-pendulum model has been applied in many forward dynamics studies using both rigid [15–19] and flexible [20] shafts. Perhaps most notable is the work of Jorgensen [15], who in 1970 used the Lagrangian method to formulate the differential equations of the double pendulum golf swing model. The equations of motion were simplified using a torque equivalent representation of gravity. The wrist joint was initially set to 90°, and a torque was applied at the wrist joint to prevent the uncocking of the wrist. The

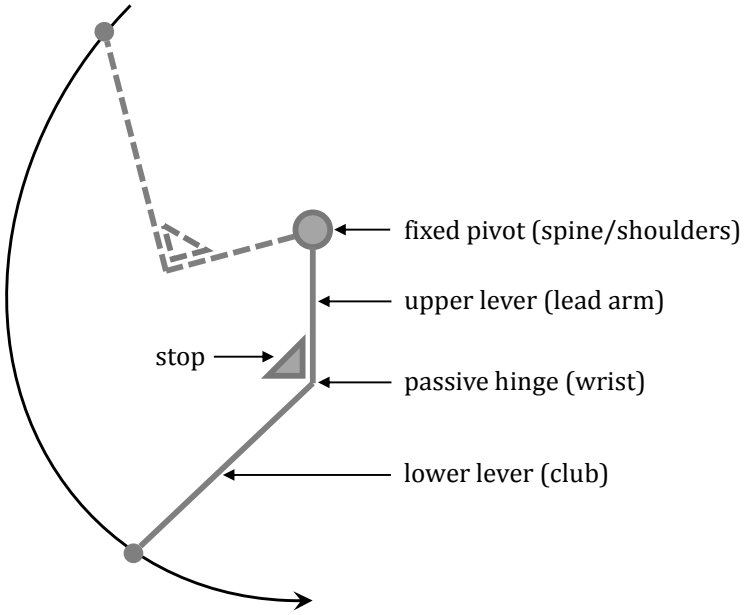

Figure 2.1: Author's rendition of the double pendulum golf swing model of Cochran and Stobbs [9].

wrist torque was initially positive (using the right-hand rule) and decreased as the swing progressed, eventually becoming negative before being deactivated in order to release the club before impact. Solving the equations of motion numerically, Jorgensen demonstrated using a constant torque input at the shoulder joint that clubhead speed increased with the "hindrance to the uncocking of the wrists." This effect was confirmed in the more recent forward dynamic studies by Lampsa [16] and Pickering and Vickers [17]. The delayed release of the wrist is known among today's golfers as *lag*, and is widely considered to be a major contributor to the generation of clubhead speed. A secondary conclusion from the work of Jorgensen suggested the backswing may be shortened substantially without a significant loss of clubhead speed [15].

Although Jorgensen studied the effects of a torque *hindering* the uncocking of the wrist, he did not report on the effects of a torque *facilitating* the uncocking of the wrist, so as to accelerate the club just before impact. With advancements in computer technology, Jorgensen revisited his simulations in the 1990s. After further investigation, Jorgensen concluded that using a wrist torque to accelerate the club was ill-advised, reporting a negligible increase in clubhead speed with an optimally timed wrist torque activation.

This supported the idea of the natural wrist release and the "free-wheeling" of the clubhead through impact as suggested by Cochran and Stobbs. The results of Jorgensen's simulation experiments were published in his book, *The Physics of Golf* [21].

2.1.3 A Planar Three-Segment Model

Fast-forward to the early 2000s, and golf swing research is burgeoning in Canada. After all, golf is the sport with the highest participation rate amongst Canadians [3]. Skeptical of Jorgensen's conclusions, Sprigings and MacKenzie [22] used a planar three-segment model, originally developed by Sprigings and Neal [23], to examine the delayed release of the club in the golf swing. The model contained an extra segment representing the torso that rotated on a plane inclined 60° from the ground about a fixed point representing the spine. The model is illustrated in Fig. 2.2, positioned at the top of the backswing.

Unlike the constant input torques of Jorgensen, this model's joint torque functions were based on the activation rate and force-velocity properties of human muscles. Hill's force-velocity relationship [24] was adapted for rotation, as previously done by Alexander [25]. The resulting torque profiles were predicted by Eq. 2.1,

$$T = T_{max}(1 - e^{-t/\tau})\frac{(\omega_{max} - \omega)}{(\omega_{max} + \Gamma\omega)} \tag{2.1}$$

where T was the instantaneous torque, T_{max} was the maximum isometric torque, ω_{max} was the maximum angular speed of the joint, ω was the instantaneous angular speed of the joint, Γ was a shape factor controlling the curvature of the torque-velocity relationship, t was the elapsed time from initial activation, and τ was the activation time constant. Body segment parameters (length, mass, center of mass, and moment of inertia) were taken from the work of de Leva [26], and the club properties were assigned values published by Cochran and Stobbs [9]. Γ was given a value of 3.0 [25], and τ a value of 40 ms [27]. The maxmimum isometric torques and angular velocities were estimated from an inverse dynamics study by Neal et al. [28]. Passive linear stiffnesses were applied to the joints when they were close to exceeding their anatomical joint limits.

Powell's method [29] was used to optimize the activation times and durations of the active torques in three different swing simulations. The first was a normal club release where no resistive torque was added to delay the release of the club, and an active wrist torque was used to accelerate the club. The second used both resistive and active torques at the wrist joint. The third was opposite the first in that it only used a resistive torque, and the club was accelerated only by centrifugal force. The results showed that the second

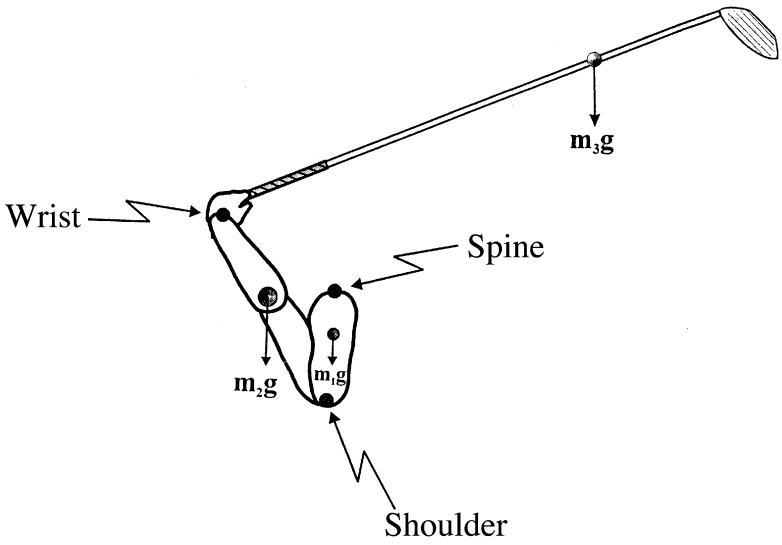

Figure 2.2: The three-segment golf swing model of Sprigings and Neal/MacKenzie [22,23]. Reproduced with kind permission from *Sports Engineering*.

swing produced the greatest clubhead speed, but was only marginally faster (0.7 m/s) than the third swing [22], confirming that the forward activation of wrist is not a significant contributor to clubhead speed.

2.1.4 A Three-Dimensional Forward Dynamic Model of the Golf Swing

In 2009, MacKenzie and Sprigings published the first 3D forward dynamic model of the golf swing [30], motivated by evidence that the golf swing is not planar [31,32]. The biomechanical model contained three body segments (torso, lead arm, and hand) and had four degrees of freedom: torso rotation, horizontal abduction of the shoulder, longitudinal rotation of the lead arm, and ulnar deviation of the wrist. The shoulder joint was constrained to rotate in a plane inclined 50° from the ground. This constraint resulted in planar arm motion, but the longitudinal rotation of the arm allowed the club to move out-of-plane. The active muscle torque generators used in the planar three-segment model [23] were modified to incorporate the deactivation time of the muscle when the torque generator

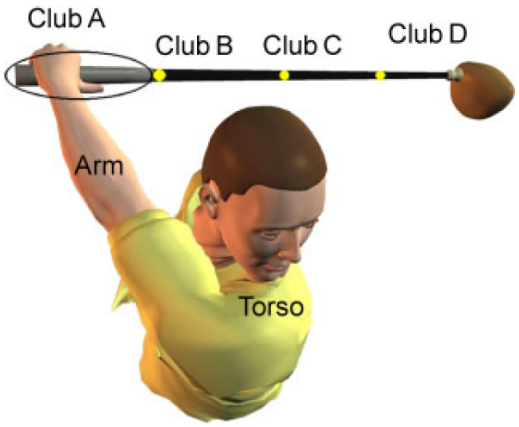

Figure 2.3: MacKenzie and Sprigings' 3D golfer model [34]. Reproduced with kind permission from Dr. MacKenzie.

disengaged, and took the form

$$T = \left[T_{max}(1 - e^{-t/\tau_{act}}) - T_{max}(1 - e^{-t'/\tau_{deact}})\right] \frac{(\omega_{max} - \omega)}{(\omega_{max} + \Gamma\omega)} \tag{2.2}$$

where τ_{act} and τ_{deact} were the activation and deactivation time constants, and t' was the time elapsed from disengagement of the torque generator. The biomechanical model was paired with a discretized flexible shaft comprised of four rigid sections interconnected by rotational spring-damper elements to simulate shaft deflection during the downswing. The inertia of the hand was grouped into the proximal shaft segment giving the model a total of six segments. The model is shown with the segmented shaft in Fig. 2.3. To validate the model, the simulated kinematics were regressed onto motion capture data of a "category-1" golfer using a custom genetic algorithm. Optimization of the golf swing was then performed by maximizing the horizontal clubhead speed at impact. The optimization results supported the idea that an optimal downswing follows a proximal to distal sequencing of movement [33].

In a separate work, MacKenzie and Sprigings applied the model to investigate the role of shaft stiffness in the golf swing [35]. After running biomechanical optimizations with four nominal stiffnesses (flexible, regular, stiff, and completely rigid), they showed that shaft stiffness only affected clubhead orientation (dynamic loft, face angle) and not clubhead speed. This idea was later confirmed by MacKenzie and Boucher using motion capture experiments [36]. They found that a more flexible shaft would increase the speed of the

clubhead relative to the grip, but reduce grip speed resulting in no significant difference in clubhead speed relative to the ball. This is a primary example of how a forward dynamic model was able to predict a golf swing peculiarity that was previously unknown.

2.1.5 A Three-Dimensional Forward Dynamic Model of the Golf Swing Optimized for Ball Carry Distance

Balzerson et al. [37] improved the model of MacKenzie and Sprigings by supplementing the biomechanical model with non-linear passive stiffnesses fit to experimental data from the literature and using an analytical flexible beam based on Rayleigh beam theory to model the golf shaft. The flexible beam allowed for continuous bending in the transverse directions, axial twisting, and variable stiffness as function of length. Developed using the multibody software MapleSim (Maplesoft, Waterloo, Canada), their golf swing model was combined with a momentum-based free-body impact model [38] (discussed in Section 2.2.3) and a spin-rate dependent aerodynamic ball flight model [39] (discussed in Section 3.4) to enable biomechanical optimization through maximization of carry distance as opposed to clubhead speed. Although providing a notable improvement to the model and optimization scheme of MacKenzie and Sprigings, the shaft deflection results of Balzerson et al. displayed spurious oscillations that were inconsistent with experimental measurements. The oscillations were thought to be caused by a lack of damping [37]. The model of Balzerson et al. is the predecessor of the model presented in Chapter 3.

2.1.6 Opportunities for Improvement

- In a study examining the role of upper torso and pelvic rotation in driving performance for golfers of various skill levels [40], it was found that the relative rotation of the upper torso with respect to the pelvis, referred to as the X-factor in the golf community, is correlated with ball velocity ($r = 0.54$, $p < 0.001$). Balzerson et al. [37] made an initial step toward modelling the X-factor by including a passive stiffness acting on the torso as a function of the torso's rotation angle. However, correctly modelling the X-factor using a relative angle of separation requires the addition of the pelvis. This is a noteworthy improvement area for the biomechanical model, due to the X-factor being linked to increased driving performance [40–45], as well as an increased risk of developing or exacerbating lower back pain [46].
- The flexible beam model in the latest version of MapleSim has been updated to include internal beam damping. The shaft oscillations observed in the simulations

of Balzerson et al. [37] may be eliminated using beam damping parameters, thereby improving the accuracy of the flexible club model.

- Existing dynamic golf swing models have only considered the downswing. Moreover, in models with flexible clubs, the shaft has been initialized with no deflection (unflexed). Although this was not explicitly stated by MacKenzie and Sprigings [30] or Balzerson et al. [37], it is evident from their plots of shaft deflection in Fig. 9 and Fig. 18 of their works, respectively. In reality, the shaft experiences significant toe-up deflection at the top of the backswing caused by the quick transition from backswing to downswing [20]. An unflexed shaft at the top of the backswing may alter the swing mechanics and for this reason the addition of the backswing is an opportunity to improve the existing models.

2.2 Golf Impact Models

The impact model is a crucial component of a predictive golf drive simulation. It estimates the initial launch conditions (velocity, angular velocity) of the golf ball given information regarding clubhead kinematics at the moment of impact, mass properties, and impact location on the clubface. The launch conditions are used to initialize an aerodynamic model that simulates the flight of the golf ball. In general, ball speed and spin grossly affect carry distance, the main performance indicator of a drive. Because maximizing carry distance is a method for optimization, accurate estimation of the launch conditions is critical.

2.2.1 The Free-Body Assumption

Regarding the collision between the clubhead and ball, Cochran and Stobbs [9] claim that the clubhead "free-wheels" through impact such that all the resistance to impact is borne by the inertia of the clubhead. In other words, the shaft nor player can influence the impact dynamics. Their accompanying experimental validation involved using a two-wood with a hinge at the hosel, the point of connection between the clubhead and shaft. The hinge was designed to give way upon impact, allowing the clubhead to behave like a free-body. Compared to 30 shots with a normal-shafted club, the shots hit with the hinged club averaged 215 yards (197 m), 5 yards (4.57 m) less than the normal club. The scientists dismissed the loss of yardage, attributing it to a decrease in clubhead speed caused by the "useless" weight of the hinge, or the "wobbly feel" of the club that may have

caused the golfers to swing easier. Since this study, a critical assumption in golf science and engineering is that the driver impact is accurately modelled as a free-body collision. Consequently, many of the impact models discussed in this section are based on free-body collisions.

2.2.2 Normal Force Models

Modelling the golf impact is a challenging undertaking due to the energy losses associated with the compression of the golf ball and the deformation of the clubface. A golf ball can compress to three-quarters its original size [47] due to a normal force reaching values as high as 15 kN [48]. Multiple researchers have implemented 1D mass-spring-damper systems to model the deformation of the golf ball and clubface during a normal impact [49,50]. These models adequately reproduced normal force histories for golf balls impacting a rigid barrier. In one study, Iwatsubo and Yamaguchi [51] employed mechanical impedance matching to optimize the flexibility of the driver clubface. The major asset of these models is their ability to effectively capture the decrease in coefficient of restitution (COR) with increasing impact velocity, an experimentally confirmed characteristic of golf ball impacts [52, 53]. However, 1D models cannot capture the 3D effects that clubhead moment of inertia (MOI), center of gravity (CG), and loft have on the golf ball's exit velocity. Furthermore, they do not contain a tangential force (i.e., friction) so they cannot predict spin.

It is advantageous to design a golf ball with high COR in order to maximize ball speed; however the golf ball's maximum COR is restricted by the sport's governing bodies – the United States Golf Association (USGA) and the Royal and Ancient (R&A) [54]. After noticing that thinner clubfaces were generating greater ball speeds due to their spring-like nature, the USGA restricted the COR between the driver clubhead and the golf ball to a value of 0.83 in 1998 [51]. The cumbersome experimental setup of the clubhead COR test lead to a new experimental test implemented in 2004 to measure the flexibility of a driver clubface. It involved striking the clubface with a small steel pendulum and measuring the contact time, which is called the "characteristic time," or CT. The CT of a clubhead cannot exceed 257 μs [55].

2.2.3 Impulse-Momentum Models

These models are free-body collisions between the clubhead and ball based on the principle of impulse-momentum (IM), where the clubhead and ball are assumed to be rigid. They typically impose a constant COR of 0.83 to account for the loss of translational kinetic

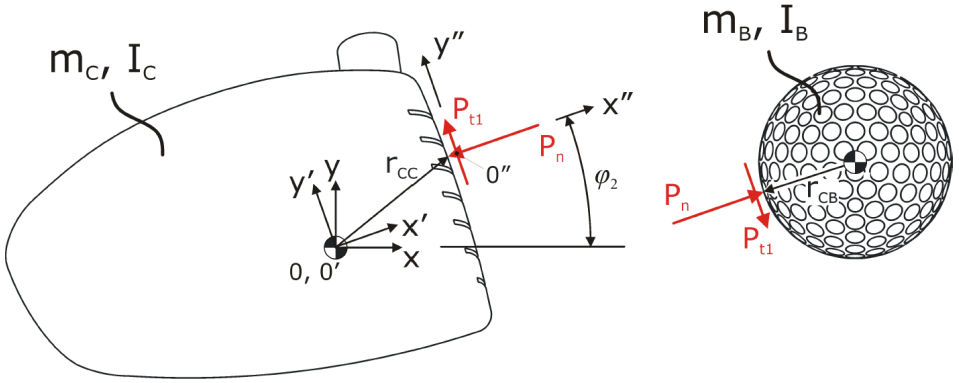

Figure 2.4: Side view of 3D impulse-momentum impact model of Petersen and McPhee [60]. Reproduced with kind permission from Dr. Petersen.

energy. The impact is assumed to be instantaneous, and as opposed to modelling friction, these models assume the golf ball is in a state of rolling when it leaves the clubface (i.e., the clubhead and ball have equal tangential velocities at the contact point the instant the golf ball leaves the clubface). Both Cochran and Stobbs [9] and Chou et al. [52] found that spin did not change significantly with changes to the clubface surface for standard driver loft angles, thus supporting the rolling hypothesis.

Winfield and Teong were the first to formulate the 3D momentum-based driver impact model and exploited it to find the loft angle [56] that maximized carry distance and the clubface curvature that minimized the dispersion of off-center hits [57]. Similar studies were conducted later by Penner [58, 59]. Petersen and McPhee [38] enhanced the model of Winfield and Teong using an ellipsoidal clubface representation, and compared the launch conditions generated by the model with those of finite-element (FE) simulations. The momentum and FE models showed reasonable agreement for ball velocity, but substantial differences in spin. The IM model of Petersen and McPhee was used in the predictive golf drive simulations of Balzerson et al. [37]. A side view of Petersen and McPhee's IM model is shown in Fig. 2.4, where P_n and P_{t1} are the normal and tangential impulses acting on the clubhead and ball at the contact point.

2.2.4 Finite-Element Models

Using FE models to simulate the golf impact is an active area of research. If done correctly, these models can provide a deeper understanding of clubhead-ball impact mechanics with

regards to the structural integrity of the clubhead, clubface deflection, spin generation, and overall clubhead and golf ball performance. For these reasons, golf equipment manufacturers use FE models to assess the design of clubhead prototypes. Modelling the impact using this method is a challenging task due to the golf ball's viscoelastic core and the complexity of its construction, not to mention the meshing of intricate clubhead geometries[1]. Constitutive models for viscoelastic materials have many parameters [61], and because a golf ball can have as many as five layers, creating an accurate golf ball model requires extensive experimental work to identify all the material parameters.

Tamaogi et al. [48] used a split Hopkinson bar test as a means for determining the dynamic characteristics of the materials in a two-piece (i.e., ionomer resin cover and single-material polybutadiene core) golf ball. The split Hopkinson bar was made of a polymeric material to account for the impedance mismatch between a soft test specimen and the standard metallic bar. Similar setups are used to evaluate material models for biological soft tissues [62]. Using experimentally determined material parameters in FE simulations, Tamaogi et al. demonstrated that the three-element standard linear solid model [61] is capable of describing the dynamic behaviour of the cover and core materials within a given frequency range. The standard linear model was also used by Tanaka et al. [63] to model a three-piece (i.e., two-layer core) golf ball obliquely impacting a rigid plate. Tanaka et al. performed a sensitivity analysis to observe the effects of varying the elastic moduli of the three layers independently. It was found that the stiffness of the innermost layer correlated negatively with ball speed and positively with spin, yet the stiffness of the middle layer correlated negatively with spin. The results support the use of softer mantle layers (i.e., between the innermost and outermost layers) to attenuate spin generation.

Optimizing driver clubheads using FE simulations is a tedious process because of the computational expense of each simulation. Furthermore, optimization results are met with a high level of skepticism because of the aforementioned challenges associated with creating an accurate golf ball model. Nonetheless, several researchers have performed optimizations in this manner, where effects of the shaft were assumed to be negligible (see free-body assumption in Section 2.2.1). Iwatsubo et al. [64] studied the effects of the clubhead's vertical MOI and CG depth on ball speed and spin, with the intent of developing a superior clubhead. They found that the greater the vertical MOI and the shallower the CG depth, the less side spin was produced for off-center hits. Conversely, the shallower the CG, the more back spin was generated. Additionally, the size of the uniform restitution area, also known as the "sweet-spot", increased in proportion to the increase in vertical MOI. The results of Iwatsubo et al. reflect the clubhead design goals of manufacturers – to

[1]Meshing is the practice of generating a polygonal mesh that approximates a geometry. It is used in FE methods for discretization.

maximize vertical MOI and CG depth in order to improve forgiveness and decrease back spin, respectively. Generally speaking, less backspin leads to greater carry distance [65]. The vertical MOI of a driver clubhead is now limited by the USGA to a maximum value of 5900 g-cm^2 [66].

The mass property insights observed by Iwatsubo et al. can also be found using IM models [67]; however the same cannot be said for other FE clubhead optimizations. For example, Hocknell [68] used experimentally validated clubhead modal characteristics and correlated them with performance and the concept of "feel", and Petersen and McPhee [69] devised a routine for determining optimal clubface shape.

Tanaka et al. [70] offers the only study on the effects of the shaft during impact, comparing experimentally validated FE impact simulations featuring highly simplified clubs to those with the clubhead alone. The simplified clubs were constructed using custom-made hollow cylindrical clubheads that were fitted to steel shafts at the top of the cylinder using a locking ring. The clubs were fixed at the butt end of the shaft and an air gun fired golf balls into the clubheads at various locations on the clubface. The experiment showed good agreement with the FE simulations. Subsequent simulation experiments using the full-clubs and clubheads alone showed an increase in ball speed at all impact locations and a suppression of the gear-effect [71] using the full-clubs, implicating that the inclusion of the shaft may have meaningful effects on clubhead-ball impact dynamics. More work needs to be done to determine whether or not the results of Tanaka et al. are upheld using realistic golf club models. Furthermore, the dynamic loading of the shaft at impact could alter the shaft's influence on impact dynamics, and was not taken into account by Tanaka et al.

2.2.5 Opportunities for Improvement

- Advances in multibody simulation present a new opportunity to investigate clubhead-ball impact dynamics. Analytical models for the contact forces may be applied to the clubhead and ball in 3D multibody impact simulations, permitting the observation of force histories, transient effects, and the influences of clubhead properties on golf ball launch conditions. In addition, the multibody framework can support a layered golf ball model, where the layers are interconnected by rotational springs and dampers. A rotationally compliant golf ball model could help predict spin generation accurately. In essence, such a model possesses all the favorable aspects of the models discussed in Section 2.2 and preserves the computational efficiency required for optimization. Moreover, the clubhead may be connected to an analytical beam model of the golf

shaft to compare full-club and free-body impact simulations. The computational efficiency of a symbolic multibody impact model could potentially enable clubhead and shaft optimization using full-club impact simulations.

- Volumetric contact is an analytical model of interest for the normal force. With volumetric contact, the normal force is proportional to the intersection volume between the colliding objects. Moreover, volumetric contact has already been implemented successfully in multibody simulations [72–74]. An analytical model of interest for the tangential force is the continuous velocity-based friction model recently published by Brown and McPhee [75]. This friction model has physically meaningful parameters and was designed primarily for optimal control and real-time dynamic applications such as the golf drive.

Chapter 3

Dynamic Model of the Golf Drive

The complete dynamic golf drive model is composed of four sub-models: the golfer biomechanics, the flexible club model, the impact model, and the ball flight model. This chapter describes each sub-model in detail and discusses how they are integrated and implemented using an optimal control strategy. It should be noted that the biomechanical, flexible club, and impact models were developed in MapleSim, version 2016.2 (Maplesoft, Waterloo, Canada).

3.1 Biomechanical Model

3.1.1 Degrees of Freedom

The golfer biomechanics are modelled using a series of rigid bodies interconnected by revolute (1D rotational) joints. Each rigid body represents a different body segment of the golfer. In total, four body segments are used. They are the pelvis, torso, leading arm (i.e., the left arm of a right-handed golfer), and the hand. The model does not include the lower limbs or the trailing arm. It is assumed the lower limbs and trailing arm play a passive role in the golf swing. Moreover, their addition would increase the number of degrees of freedom considerably and render optimal control impractical due to a large number of optimization variables. The body segments are interconnected using eight revolute joints, and the system is constrained by two algebraic equations, resulting in six biomechanical degrees of freedom.

The pelvis is fixed translationally at a height h_pH above the origin of the model, where h_p is the ratio of the model pelvis height to the overall height of the golfer standing upright,

H. The pelvis rotates about its longitudinal axis, which is positioned vertically. The torso is connected to the pelvis via a universal joint, allowing the torso to rotate about its independent longitudinal axis tilted forwards towards the golf ball. The universal joint is constrained algebraically such that the sternum of the golfer does not translate. The addition of the pelvis facilitates the analysis of thorax-pelvis separation, known in golf as the X-factor [76], and its effects on the golf swing.

The shoulder joint is positioned at a constant distance from the center of the torso and is horizontally aligned with the suprasternale. The default value used for this distance is 20 cm. Unlike the single-DOF shoulder joints in previous biomechanical models [30, 37], the shoulder joint in this model has two degrees of freedom. It is capable of horizontal adduction-abduction and vertical flexion-extension. This improvement means the arm plane is dynamic and is not constrained to rotate in a single plane, as was the case in previous models.

Another joint allows the rotation of the arm about its longitudinal axis. This joint is positioned at the elbow to prevent gimbal lock[1] from occurring at the shoulder joint. Its corresponding DOF is the pronation and supination of the forearm. Alternatively, this DOF could represent the internal-external rotation of the shoulder, however both rotations are not considered in this model. The final joint is positioned at the wrist to allow radial and ulnar deviation. The inertial reference frame and rotational degrees of freedom of the biomechanical model are displayed in Fig. 3.1, where the golfer is positioned at the top of the backswing. The axes of rotation are represented by the dashed lines. The inertial reference frame of the golfer model was given the subscript M to distinguish it from the inertial reference frame used in the motion capture experiment in Section 4.1.

The body segment lengths and mass properties (mass, center of mass, and moments of inertia) are based on experimental values from young adult Caucasian males, obtained by Zatsiorsky et al. [78] using a gamma-ray scanning technique. However, the properties reported by Zatsiorsky et al. were given in relation to bony landmarks. De Leva [26] later adjusted the properties to correspond to joint centers. De Leva's adjusted body segment properties are used in this model. The body segments are implemented in such a way that allows them to be scaled based on the golfer's height and mass. The golfer's default height and mass are 1.74 m and 73.0 kg. In relation to de Leva's body segments, the pelvis corresponds to the lower trunk, and the torso was formed by combining the middle and upper trunk segments. Similarly, the arm was formed by combining the upper arm and forearm segments.

[1]Three-DOF Euler rotations, formed by concatenating three single-axis rotations, suffer from gimbal lock when two of the three rotation axes align, causing a rotational DOF to be lost [77].

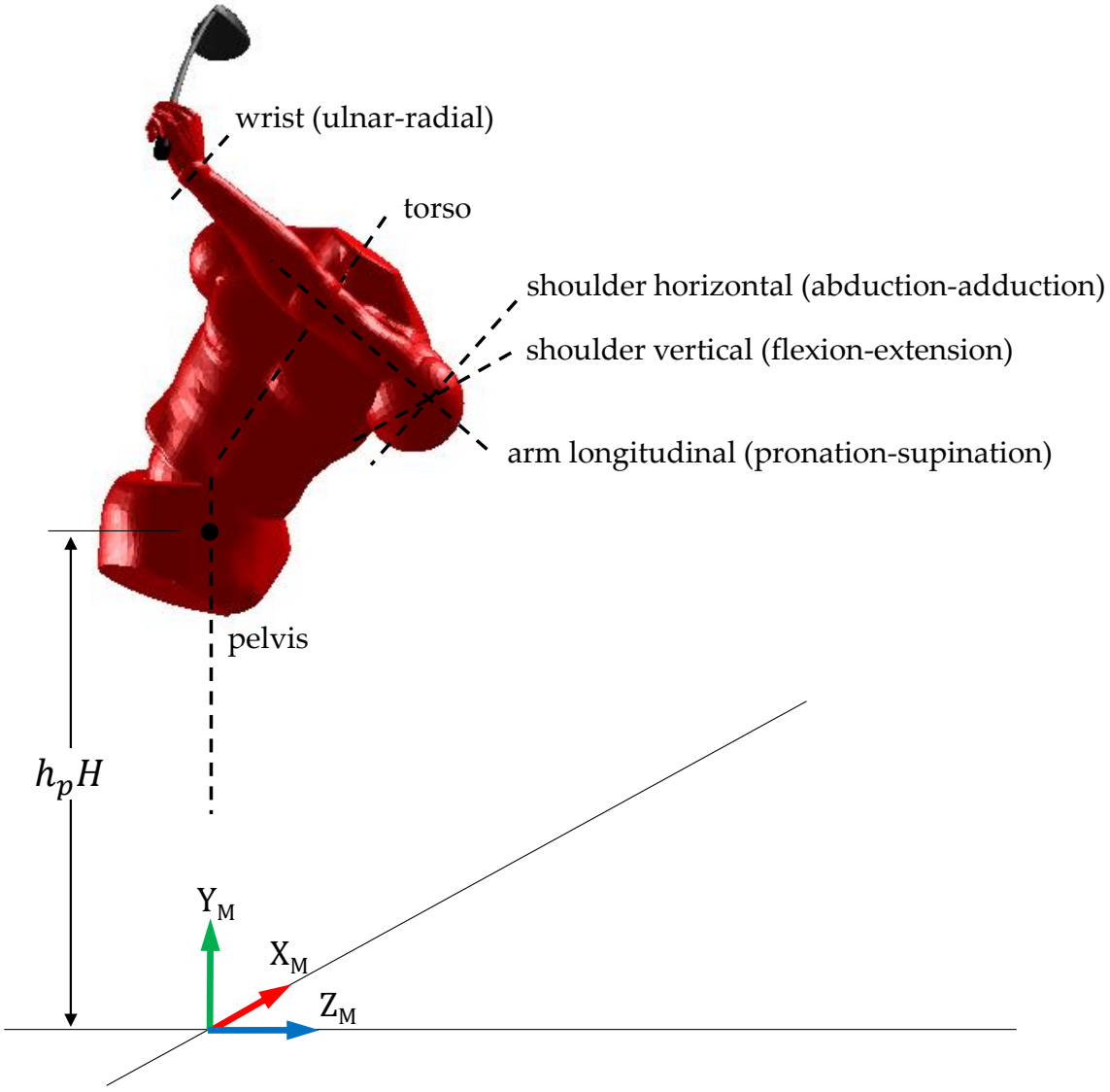

Figure 3.1: Golfer model inertial reference frame and biomechanical rotational degrees of freedom. Rotation axes represented by dashed lines.

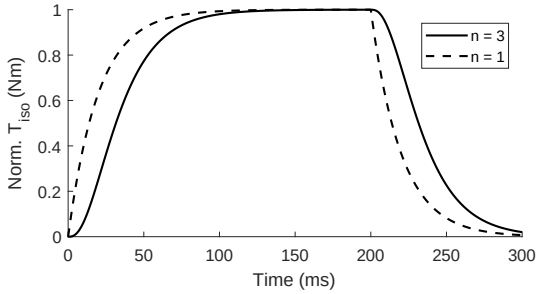

(a) Isometric torque generation function using τ_{act}, τ_{deact} = 20 ms.

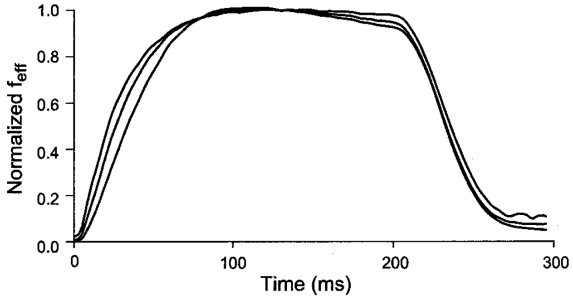

(b) Measured mammalian skeletal muscle force activation curves [80]. Reproduced with kind permission from the *Journal of Muscle Research and Cell Motility*.

Figure 3.2: Comparison of active joint torque profiles with experimental muscle force activation curves.

3.1.2 Active Joint Torques

The active joint torques are similar to those used by Sprigings and Neil [23] and MacKenzie and Sprigings [30]. A small modification was made to the isometric torque generation function used by MacKenzie and Sprigings (part of Eq. 2.2) to reduce its stiffness[2]. The exponential functions were raised to the power of n to create smooth transitions at the onset of activation and deactivation. The new isometric torque function is given by

$$T_{iso} = T_{max}(1 - e^{-t/\tau_{act}})^n - T_{max}(1 - e^{-t'/\tau_{deact}})^n \tag{3.1}$$

Apart from reducing the stiffness of the active joint torque equations, the resulting torque profiles from Eq. 3.1 resemble experimental measurements more precisely, as shown by Fig. 3.2. In total there are 12 active muscle torque generators, two for each DOF, where one controls the backswing and the other controls the downswing. As mentioned in Chapter 2, previous models incorporated the Hill force-velocity relationship [24] into their muscle

[2] A stiff equation is a differential equation for which a numerical method must take small steps to avoid numerical instabilities in the solution [79].

torque generators by scaling their instantaneous isometric torque using the equation

$$T = T_{iso}\frac{\omega_{max} - \omega}{\omega_{max} + \Gamma\omega} \tag{3.2}$$

where ω is the joint's current rate of shortening, ω_{max} is the joint's maximum rate of shortening, and Γ is a shape factor affecting curvature. With the incorporation of the backswing into this new model, some of the torque generators driving the downswing may be lengthening at the time of activation (i.e., $\omega < 0$), potentially creating a singularity as ω approaches $-\omega_{max}/\Gamma$. The pioneering experiments of Katz [81] suggest that the force-velocity relationship diverges from Hill's model when a force greater than isometric tension is applied. The divergence was illustrated by a discontinuity in velocity at the onset of lengthening and an exponential increase in the rate of lengthening with increasing applied force. Van Soest et al. [82] provide a generic equation for the eccentric force-velocity relationship observed in the experiments of Katz. The rotational equivalent of this equation was manipulated to use the same parameters as Eq. 3.2. The overall torque scaling function is now represented by the following piecewise function

$$T = \begin{cases} T_{iso}\left(\dfrac{\omega_{max} - \omega}{\omega_{max} + \Gamma\omega}\right) & \omega \geq 0 \\ \\ T_{iso}\left(\dfrac{(1 - T_r)\omega_{max} + S\omega T_r(\Gamma + 1)}{(1 - T_r)\omega_{max} + S\omega(\Gamma + 1)}\right) & \omega < 0 \end{cases} \tag{3.3}$$

where S is the slope-factor, defined by van Soest et al. [82] as the ratio between the eccentric and concentric derivatives of force with respect to velocity at isometric force, and T_r is the ratio between the maximum eccentric and isometric force. A slope-factor of 2 and a force ratio of 1.5 is used in this model, matching the values used by van Soest et al. For simplicity it is assumed the maximum rate of lengthening is equal to the maximum rate of shortening, hereafter referred to as the maximum angular velocity of the joint. Using Eq. 3.3, an example torque-velocity scaling profile is shown in Fig. 3.3 for a nominal isometric torque of 50 Nm, a maximum angular velocity of 10 rad/s, and a shape factor of 3. The muscle torque generators controlling the backswing use the same parameters as those controlling the downswing, except with negative maximum torques and scaled-down maximum angular velocities.

To control the 2-DOF shoulder joint, the horizontal and vertical muscle torque generators at the shoulder joint are assumed to activate and deactivate simultaneously. The total maximum isometric shoulder torque is decomposed into horizontal and vertical components

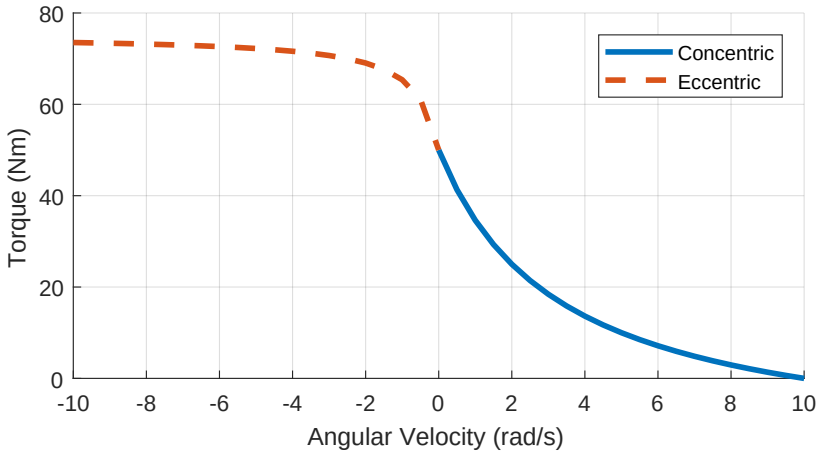

Figure 3.3: Torque-velocity scaling for concentric and eccentric contraction. Generated using Eq. 3.3 with $T = 50$ Nm, $\omega_{max} = 10$ rad/s, $\Gamma = 3$, $S = 2$, and $T_r = 1.5$.

using the following equations

$$T_{s,h} = \sqrt{\frac{T_s^2}{(1+r^2)}} \tag{3.4}$$

$$T_{s,v} = rT_{s,h} \tag{3.5}$$

where T_s is the maximum isometric shoulder torque, $T_{s,h}$ is the horizontal component, $T_{s,v}$ is the vertical component, and r is the shoulder torque ratio. The r value effectively controls the plane of the swing.

3.1.3 Passive Joint Torques

The total joint torque is the sum of passive and active torques. Passive torques are internal resistive torques that develop when muscle tissue, tendons, and ligaments surrounding the joint are stretched [14]. Passive joint torques have been shown to increase dramatically near the anatomical joint limits and therefore the torque-angle relationship is typically modelled using exponentials [14, 83, 84]. The equation chosen for this model was proposed by Yamaguchi [85] and includes joint damping. The passive torque is given by

$$T(\theta, \dot{\theta}) = k_1 e^{-k_2(\theta - \theta_1)} - k_3 e^{-k_4(\theta_2 - \theta)} - c\dot{\theta} \tag{3.6}$$

where θ is the joint angle, and the remaining parameters are determined by fitting the non-linear function to experimental data. Eq. 3.6 generates a large restoring torque when θ falls outside the range set by the breakpoints θ_1 and θ_2. A value of 0.1 $\frac{\text{Nms}}{\text{rad}}$ is used for c, as recommended by Yamaguchi.

Eq. 3.6 was fit to experimental resistive torque measurements of the torso [86], both directions of the shoulder [87, 88], the forearm [89], and the wrist [90] using MATLAB's (R2017a, MathWorks, Natick, MA, USA) `nlinfit` function. The fitted equations are plotted against joint angle in Fig. 3.4. For the wrist joint, Formica et al. [90] reported mean linear stiffnesses for the radial and ulnar directions. To generate the desired non-linear torque profile, four data points were generated using the linear stiffnesses. For Fig. 3.4b and 3.4c, a joint angle of zero corresponds to the mean neutral position of the shoulder joint for all the subjects in the experiment [87,88]. The shoulder angles used in the model were adjusted accordingly. No experimental data was found for the passive resistance of the pelvis with respect to the ground, so the torso's passive torque profile was also applied to the pelvis. The parameters of each passive joint torque are given in Table 3.1.

Table 3.1: Passive joint torque parameters

Joint	θ_1 (rad)	θ_2 (rad)	k_1	k_2	k_3	k_4
Torso	-0.09	0.09	5.56	1.97	5.57	2.02
Shoulder Vertical	-1.14	1.27	7.03	2.31	4.30	1.65
Shoulder Horizontal	-1.35	1.23	3.13	2.13	4.38	1.62
Forearm	-1.24	1.34	3.21	2.62	2.22	1.75
Wrist	-0.31	0.22	0.55	4.70	0.79	7.82

3.2 Flexible Club Model

MapleSim's standard flexible beam component is used to model the deformation of the golf shaft. The symbolic formulation is based on Rayleigh beam theory [91] and was implemented via the principle of orthogonality by Schmitke and McPhee [92]. A point on the beam is located using four deformation variables associated with the beam's centroidal

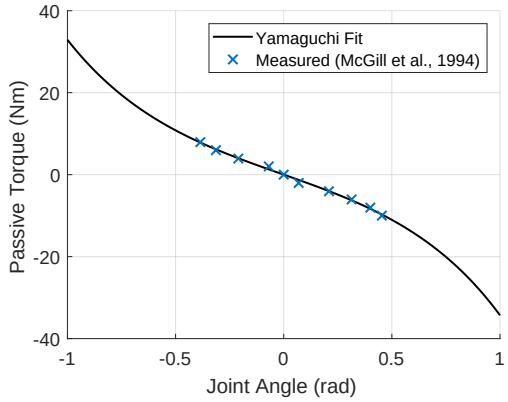

(a) Torso

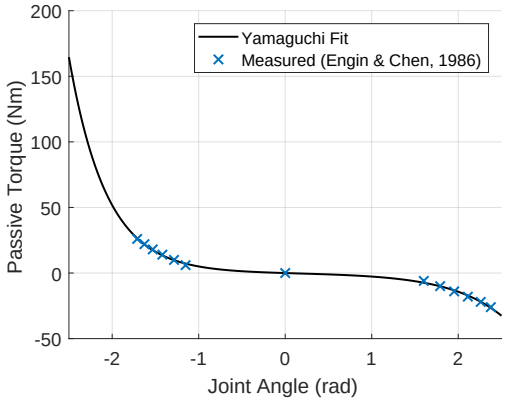

(b) Shoulder (vertical)

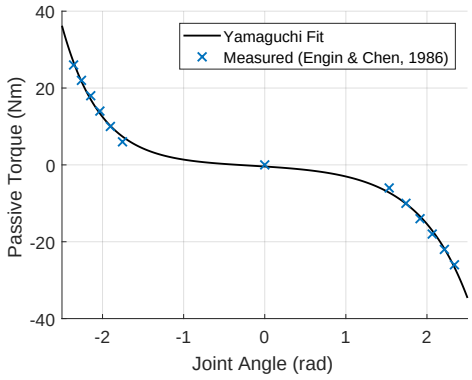

(c) Shoulder (horizontal)

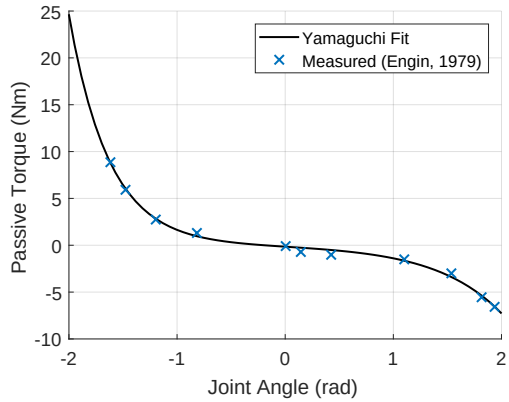

(d) Forearm

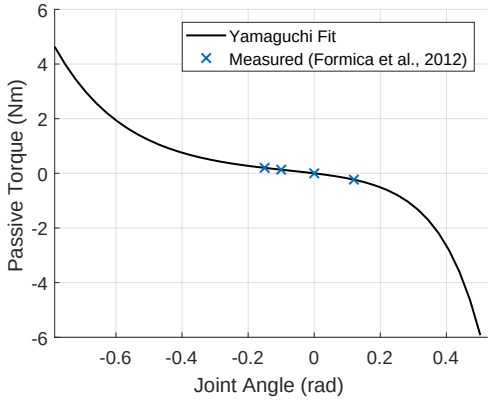

(e) Wrist

Figure 3.4: Passive joint torque profiles.

axis, x. The four variables are $u(x,t)$ for axial deformation, $v(x,t)$ and $w(x,t)$ for transverse deformations, and $\phi(x,t)$ for torsional deformation about the centroidal axis. The deformation in each of these directions is approximated using Taylor series polynomial shape functions and time-varying elastic coordinates [93]. In the transverse directions, using one elastic coordinate equates to a second-order polynomial approximation of bending. In the other directions, using one elastic coordinate equates to a linear approximation of deformation.

The elastic coordinates are represented using the following notation: $u0221$ corresponds to zero elastic coordinates for axial deformation, two for each transverse deformation, and one for torsional deformation. Increasing the number of elastic coordinates refines the approximation of deformation at the expense of computational efficiency, and is analogous to decreasing the element size in a FE simulation. The flexible beam component also incorporates varying stiffness and cross-sectional area as functions of the beam's length from its base. The internal damping parameters of the beam are defined in proportion to the stiffness moduli using units of s^{-1}. The clubhead is considered a rigid body and is fixed to the shaft at the hosel, where the shaft penetrates the hosel a distance of 25.4 mm, as illustrated in Fig. 3.5.

MapleSim's flexible beam component was previously applied to model golf shaft deformation in the works of Sandhu et al. [94] and Balzerson et al. [37]. Sandhu et al. compared simulation results of the analytical model to golf swing motion capture experiments. However, results were only provided for the ten milliseconds leading up to impact, and reasonable agreement was reported only for droop and dynamic loft. In this work, the flexible club model is validated using motion capture data for full swings from 10 golfers (Section 4.2). Balzerson et al. used the analytical model in forward dynamic simulations of the golf swing, but the flexible club demonstrated unrealistic oscillations, possibly caused by a lack of damping. MacKenzie and Sprigings [35] suggested the soft tissues in a golfer's hands contribute to damping during the swing. The foreseen challenges associated with empirically determining the amount damping caused by a golfer's grip led MacKenzie and Sprigings to choose a level of damping that provided the best agreement between their simulations and previously published golf swing data. A similar error minimization process is utilized in Section 4.2 to determining the damping coefficients for this model.

3.3 Impact Model

To simulate the contact dynamics between clubhead and ball, a seven-parameter impact model is proposed. It includes a normal force based on volumetric contact, continuous

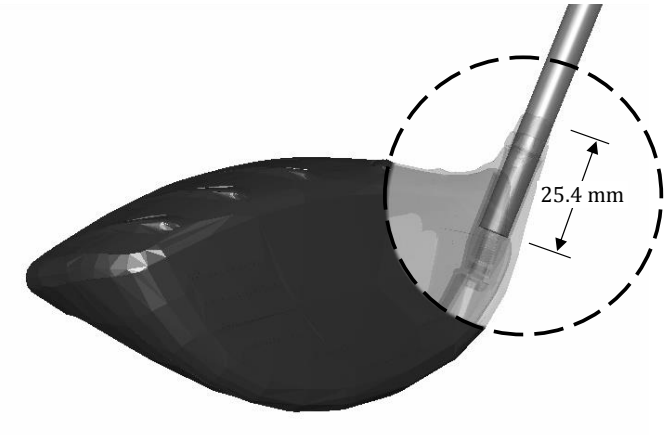

Figure 3.5: Clubhead attached to the shaft at the hosel.

velocity-based tangential friction, and a tangentially compliant golf ball. The proposed model includes favorable aspects of the prevalent impact models used in golf research, namely FE and IM models. The proposed impact model effectively captures four important phenomena that are observed in FE simulations but absent in IM models: the transient dynamics that occur through the duration of contact, the hysteretic behaviour caused by the viscoelasticity of the golf ball [95, 96], the tangential compliance of the golf ball, and friction. Moreover, in a multibody framework, the effects of the shaft can be studied using full-club impact simulations while maintaining a level of computational efficiency suitable for parameter identification and optimization, akin to IM models.

3.3.1 Normal Force

The normal force, first formulated by Gonthier et al. [72] and experimentally validated by Boos and McPhee [73], is directly related to the volume of interference between the two colliding bodies through a volumetric stiffness parameter k_v, having units of force per unit volume. For the case of a clubhead impacting a golf ball, the interference volume is the intersection volume between two spheres, where the clubface shape is considered to be spherical with a radius chosen to best approximate the clubface's radii of curvature, known as bulge and roll. The normal force is given by

$$F_n = k_v V(1 + a v_n) \tag{3.7}$$

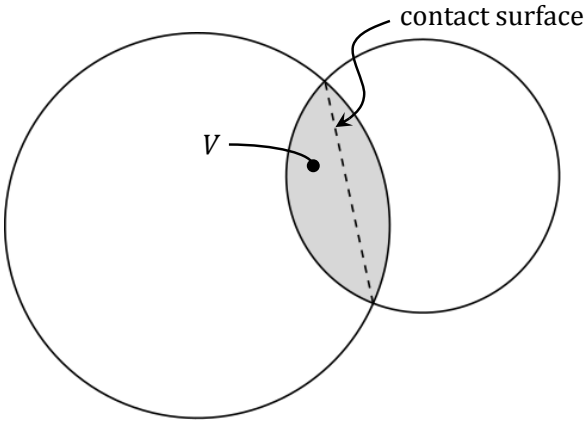

Figure 3.6: 2D representation of sphere-sphere intersection.

where a is the hysteretic damping parameter and v_n is the relative normal velocity between the colliding bodies. The damping parameter is chosen such that $(1 + av_n) > 1$ during compression and $(1+av_n) < 1$ during restitution [97], generating the signature asymmetric normal force histories observed during golf ball impacts [48, 50, 63]. The normal force is applied to the clubhead and ball at the center of an imaginary contact surface created by the intersection of the spherical surfaces. The intersection volume V and the contact surface are illustrated two-dimensionally in Fig. 3.6. The normal direction is simply defined by the relative position vector between the two sphere centers. In general, the clubhead CG does not coincide with the normal axis and thus the normal force will cause moments about the clubhead CG.

3.3.2 Friction Force and Tangential Compliance

Brown and McPhee's continuous velocity-based friction model [75] is used for the tangential force. The model was designed with a minimum number of parameters, all with physical meaning, facilitating the parameter identification process. Although the complete model of Brown and McPhee contains static, dynamic and viscous friction coefficients in order to capture stiction and the Stribeck effect, only the dynamic friction term, corresponding to Coulomb friction, is used in this impact model. Simple Coulomb friction was also used in the FE simulations of Tanaka et al. [63], where a coefficient of 0.3 was cited from experimental measurements [98]. Furthermore, Cross [99] observed that the more normal the impact, the more quickly an elastic ball will transition from slipping to sticking. Given the low loft of the driver, the transition likely occurs in the early stages of contact and

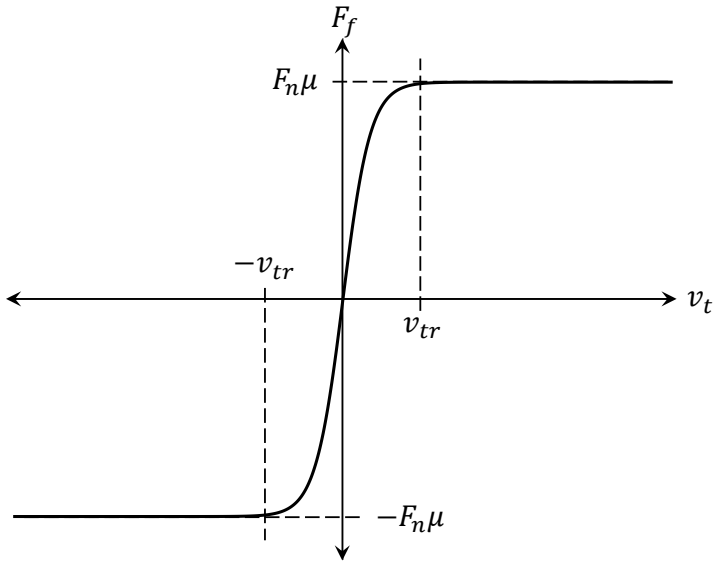

Figure 3.7: Continuous velocity-based Coulomb friction generated with Eq. 3.8 [75].

thus differentiating between dynamic and static friction will not affect spin generation significantly. The continuous, velocity-dependent Coulomb friction of Brown and McPhee is given by

$$F_f = F_n\mu \tanh\left(4\frac{v_t}{v_{tr}}\right) \tag{3.8}$$

where μ is the coefficient of friction, v_t is the relative tangential velocity between the colliding bodies at the impact point, and v_{tr} is the transition velocity. Fig. 3.7 shows the relationship between F_f and v_t for a constant normal force. F_f quickly approaches $F_n\mu$ as v_t increases from zero and settles to within 0.1% of its final value by v_{tr}. Before v_{tr}, the contact surface is said to be sticking. Beyond v_{tr}, the contact surface is said to be slipping. F_f is applied to the clubhead and ball in the direction of the relative tangential velocity vector at the center of the contact surface.

As a C^1 continuous function, Eq. 3.8 avoids any discontinuities in force at the onset of impact and transition from slipping to sticking. The slip-stick transition plays an important role in the tangential compliance recognized in the oblique impact of elastic spheres [99–103]. Cross [99] found through experimental measurements of the friction force and ball spin that in general, elastic balls do not roll when they bounce. Instead, the deformation of the contact region allows the ball to grip the surface when the bottom of the ball comes to rest. As a result, the ball vibrates in the tangential direction causing the friction force to

reverse during contact. These findings align with the analytical contact models presented by Maw et al. [100,101], Axe [102], and Stronge et al. [103]. Axe was specifically interested in this behavior as it applied to clubhead-ball impacts and found that, in qualitative agreement with his measurements, the friction force between a lofted clubface and ball initially acts to increase spin rate, but reverses in the late stage of impact. The USGA realized the same result while studying the effects of different groove geometries and surface textures on spin generation [104]. Naturally, the friction force reversal must also increase the launch angle of the golf ball. Since less spin and higher launch angle lead to greater distance [65], the friction force reversal has compelling implications regarding golf ball and clubhead design, most notably driver clubhead design, where distance is the primary performance indicator.

To capture the friction force reversal in the volumetric impact model, a two-layer golf ball model is proposed. The layers can rotate in 3D relative to each other, and are connected by a 3D rotational spring and damper with stiffness k_b and damping constant c_b. The outer layer has a relatively small thickness t_c, such that it quickly sticks to the clubface during a slip-stick transition while the inner layer continues to rotate. The inner layer eventually springs back and causes a friction force reversal. The layers in this model do not relate to the layers of a real two-piece golf ball in terms of geometry or physical properties. They are simply used to predict spin generation more accurately than a rigid ball model.

3.4 Ball Flight Model

Shortly after impact, the initial launch conditions of the golf ball are recorded. The launch conditions are the ball's initial velocity and angular velocity. These values initialize a ball flight model that simulates the trajectory of the shot. If the ball flight model is to be used in an optimization routine, it must be robust and computationally efficient. The model proposed by Quintavalla [39] is unsurpassed in terms of robustness and efficiency, and its aerodynamic coefficients were empirically determined.

In total, there are four loads acting on the golf ball: gravity, aerodynamic lift, aerodynamic drag, and aerodynamic spin-decay. The lift force $\boldsymbol{L}$ acts perpendicular to both the angular velocity $\boldsymbol{\omega_b}$ and velocity $\boldsymbol{v_b}$ of the ball in the direction $\hat{\boldsymbol{\omega}}_{\boldsymbol{b}} \times \hat{\boldsymbol{v}}_{\boldsymbol{b}}$, where $\hat{\boldsymbol{\omega}}_{\boldsymbol{b}}$ and $\hat{\boldsymbol{v}}_{\boldsymbol{b}}$ are unit vectors. It is given by

$$\boldsymbol{L} = \frac{1}{2}\rho A_b |\boldsymbol{v_b}|^2 C_L (\hat{\boldsymbol{\omega}}_{\boldsymbol{b}} \times \hat{\boldsymbol{v}}_{\boldsymbol{b}}) \tag{3.9}$$

where ρ is the air density, A_b is the projected area of the ball, and C_L is the lift coefficient.

The drag force $\boldsymbol{D}$ acts in the $-\hat{\boldsymbol{v}}_{\boldsymbol{b}}$ direction and is given by

$$\boldsymbol{D} = \frac{1}{2}\rho A_b |\boldsymbol{v_b}|^2 C_D(-\hat{\boldsymbol{v}}_{\boldsymbol{b}}) \tag{3.10}$$

where C_D is the drag coefficient. The spin-decay moment acts in the $-\hat{\boldsymbol{\omega}}_{\boldsymbol{b}}$ direction and is given by

$$\boldsymbol{\Gamma} = \frac{1}{2}\rho A_b |\boldsymbol{v_b}|^2 C_\Gamma D_b(-\hat{\boldsymbol{\omega}}_{\boldsymbol{b}}) \tag{3.11}$$

where C_Γ is the spin-decay coefficient and D_b is the ball diameter. The aerodynamic coefficients C_L, C_D and C_Γ depend on the dimensionless spin ratio S_p

$$S_p = \frac{|\boldsymbol{\omega_b}| r_b}{|\boldsymbol{v_b}|} \tag{3.12}$$

where r_b is the ball radius. The coefficients were empirically determined by Quintavalla:

$$\begin{aligned} C_L &= 0.083 + 0.885 S_p \\ C_D &= 0.171 + 0.62 S_p \\ C_\Gamma &= 0.0125 S_p \end{aligned} \tag{3.13}$$

The equations of motion for the golf ball were formulated using Eqs. 3.9 through 3.13 and the ball flight is numerically integrated in MATLAB. Fig. 3.8 shows an example ball trajectory using $\boldsymbol{v_{b,i}} = [70, 15, 5]^T$ m/s and $\boldsymbol{\omega_{b,i}} = [0, 400, 2500]^T$ rpm. The $\times$ marks the landing position of the ball.

3.5 Optimal Control

The usefulness of the golfer model comes from its ability to adapt to different equipment or configurations and produce an optimal golf swing in every scenario. This is accomplished using optimal control. Advances in golf club performance are typically based on the notion that golfer biomechanics do not change significantly when modifications are made to the golf club. For example, increasing the vertical MOI of a clubhead improves forgiveness during off-center hits. However, it could also make it more difficult to square the clubface at impact. A golfer must make biomechanical adjustments to account for this. The biomechanical adjustments required for subtle equipment changes are often overlooked by club designers as they are not easily evaluated.

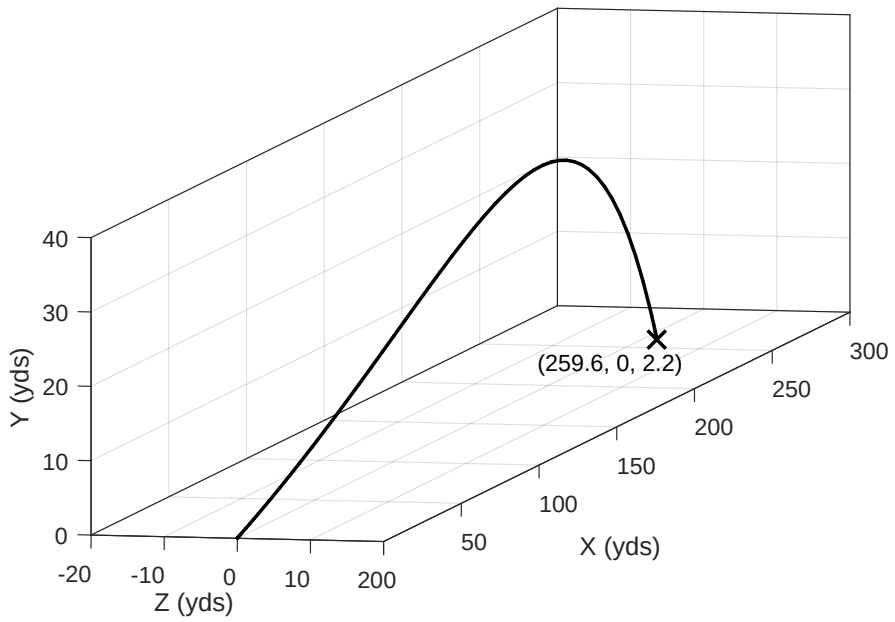

Figure 3.8: Example ball flight simulation.

A second example relates to the mass of the clubhead. If a golfer could swing the club the same way every time, a more massive clubhead would lead to greater momentum at impact and thus greater ball speed. But the mass of the clubhead significantly affects the golfer's ability to generate clubhead speed, which raises the question, what is the optimal clubhead mass? Clubhead designers obviously consider how clubhead mass affects biomechanics and performance, but the fact remains that the trade-off between clubhead mass and speed is not fully understood. In Section 5.3, the model is applied to investigate this trade-off and determine what the optimal clubhead mass should be for the model golfer.

3.5.1 Objective Function

The golf swing is controlled using the activation and deactivation times of each muscle torque generator and the shoulder torque ratio, r. A simple biomechanical optimization aims to find the optimal biomechanical timings and shoulder torque ratio by maximizing

carry distance, which is measured as the point to point distance the golf ball travels in the air. Shots that travel offline are not penalized because it is assumed that the golfer could adjust their alignment such that the same shot lands in the center of the fairway. This contrasts the objective function used by Balzerson et al. [37], who alternatively penalized shots landing offline using an exponential function. No offline penalization ensures the optimization finds the most efficient impact possible.

Rather than defining the initial ball position and forcing the model to make contact, the initial ball position is determined as follows: for each simulated swing, the impact and carry distance are calculated assuming a center-face (CF) impact at several points in the swing where the clubhead is within a height achievable using a maximum length tee of 101.6 mm (4"). If the model swings above the maximum achievable tee height or too close to the body, the swing is discarded. Moreover, if the clubhead touches the ground, or the clubface angle is such that the resulting impact would produce too much side spin, the swing is also discarded. The impact point in the swing resulting in the maximum carry distance determines the ball position for that particular swing.

3.5.2 Optimization Algorithm

The optimization problem is highly non-linear and may contain many local maxima. It is important that the global maximum is found in every optimization. This is not an easy task with numerous optimization variables. MathWorks' Global Optimization Toolbox carries a number of global algorithms that can be implemented in a parallel computing framework. The `patternsearch` algorithm employed by Balzerson et al. [37] is an efficient algorithm for a large number of variables, but depending on the initial guess and chosen settings, it is possible for it to converge on a local maximum. The genetic algorithm (`ga`) is an alternative algorithm that is stochastic and does not require an initial guess. The genetic algorithm is more reliable at finding the true global maximum; however, it is less efficient because it requires many more function evaluations. In this work, the genetic algorithm is used in a preliminary optimization to find the general location of the optimal solution, and then the `patternsearch` algorithm is used to refine the solution. More details on the optimization and the basic implementation of the golf drive model using default parameters is available in Section 4.4.

Chapter 4

Experimental Validation

A forward dynamic model can only provide meaningful insights if it has been validated against experiments. Through a research agreement with the University of Waterloo, PING Inc., a leading golf equipment manufacturer headquartered in Phoenix, Arizona, has shared data from a golf swing motion capture experiment involving high-caliber golfers. Furthermore, PING has shared the results of empirical tests performed on the shaft and clubhead used in the experiment. It should be noted that the author was employed by PING on a four-month internship and was involved in conducting said experiments. The physical properties of the golf club are confidential and therefore not disclosed in this work. However, the club properties are used extensively to support parameter identification and model validation. In this chapter, the results of the motion capture experiment are used to validate the flexible club, impact, and biomechanical models described in Chapter 3.

4.1 Golf Swing Motion Capture Experiment

4.1.1 Protocol

Ten elite male right-handed golfers (handicap ≤ 4.0) were recruited to participate in a golf swing motion capture experiment. An 8-camera passive optical system (Nexus, Vicon, Oxford, UK) was used, recording the motion of a driver fitted with reflective markers at 723 frames per second. Prior to the experiment, three important reference frames were calibrated: the inertial frame, the clubface frame, and the grip frame. The reference frames are illustrated in Fig. 4.1. The inertial frame's X axis points directly at the target and the

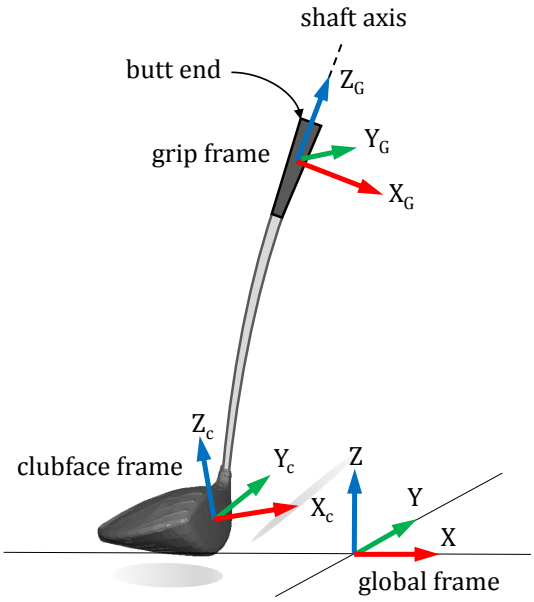

Figure 4.1: Motion capture calibrated reference frames

Z axis is perpendicular to the ground. It is important to note the distinction between the inertial frame in the experiment and the inertial frame in the golfer model, shown in Fig. 3.1. The clubface frame is positioned at CF with the X_C axis normal to the clubface and Y_C axis parallel with the grooves, directed towards the golfer. The grip frame is positioned on the shaft axis and is offset from the butt end of the club to coincide with the position of the golfer's hands. The Z_G axis is coincident with the shaft axis and points toward the butt end, while X_G lies in the $X_C Z_C$ plane (during static calibration).

Two additional video cameras were used to locate the golf ball. Using the golf ball's 3D coordinates, the motion capture software applies smoothing algorithms to the downswing and extrapolates the club kinematics to the precise moment of impact, also calculating the golf ball's impact location on the clubface. The players were requested to hit 10 drives with the main criterion that they were satisfied with the quality of their shot, so as to provide consistency among their 10 swings. The launch conditions for each drive were recorded using a launch monitor (GC2, Foresight Sports, San Diego, CA, USA) that measured ball speed, launch angle, azimuth, back spin and side spin. The driver used in the experiment had a nominal loft of 9.0 degrees and a 'stiff' rated shaft.

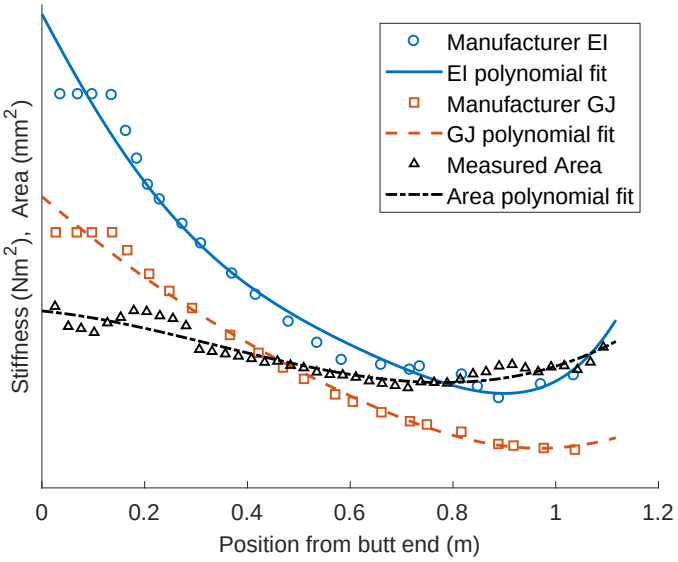

Figure 4.2: Third-order polynomial fits of the shaft's material properties

4.1.2 Golf Club Properties

The shaft's bending and torsional stiffness profiles were provided by the manufacturer. The profiles were generated from numerical models based on the construction of the golf shaft, where the stiffness was estimated from the number of layers of material in a particular region of the shaft. The outer diameter of the shaft was measured using an optical micrometer (LS-7030, Keyence, Osaka, Japan) and the wall thickness was measured using a magnetic thickness gauge (Magna-Mike 8500, Olympus, Tokyo, Japan). The cross-sectional area was calculated using the inner and outer radii and third-order polynomials were fit to the material properties to provide continuous functions of the shaft's length from the butt end. The polynomial fits for the bending stiffness (EI), torsional stiffness (GJ) and cross-sectional area are shown in Fig. 4.2 with their magnitudes hidden. The shaft length and mass were measured to be 1.12 m (44 in) and 63.4 g, resulting in a mean volumetric mass density of 1480 kg/m^3.

The clubhead mass, CG location, and MOI about the vertical (crown-sole) and horizontal (heel-toe) axes were empirically determined. Clubhead mass and CG measurements were obtained using a digital balance (EJ-1500, A&D Weighting, San Jose, CA, USA) and bespoke CG fixture, while clubhead MOI measurements were obtained using the USGA standard method and equipment [66]. The remainder of the inertia matrix was populated

using the clubhead solid model. All empirical measurements included the shaft sleeve, fastener, and motion capture markers.

4.1.3 Results

There are countless results from the motion capture experiment that are of interest. Select results are available in various sections of this work and include the following:

- the mean clubhead deliveries (i.e., the clubhead kinematics at the moment of impact) for each golfer (Table A.1),
- the mean launch conditions for each golfer (Table A.2),
- the mean shaft deflections and twist for each golfer (Figs. 4.5 and B.1),
- the mean grip kinematics of all the golf swings (Fig. 4.12), and
- the mean grip forces for each golfer, obtained through inverse dynamics (Fig. C.1).

4.2 Flexible Club Validation

The flexing of the golf shaft is a crucial component of the golf swing. In a typical driver swing, the shaft is dynamically loaded during the downswing and *kicks* forward just before impact, boosting clubhead speed and causing the shaft to bend forward. Not only does the golfer benefit from the kick velocity, but the *lead* deflection (forward bend) of the golf club increases dynamic loft[1]. Dynamic loft increases the launch angle of the golf ball and generally leads to greater carry distance. Looking at Tables A.1 and A.2, there is a clear correlation between dynamic loft and launch angle. Because the clubhead CG does not lie on the shaft axis, the inertia of the clubhead and its weight under gravity cause the shaft to *droop* (bend downward) near the bottom of the golf swing [105]. Droop, sometimes referred to as toe-down deflection, affects the dynamic lie[2]. However, the performance benefits of dynamic lie are less compelling than those of dynamic loft.

The flexible club model must be able to recreate the observed shaft deflections and clubhead delivery, given a grip motion as input. In this Section, the experimental grip

[1]Dynamic loft is the absolute clubface loft at the moment of impact.

[2]Dynamic lie is the absolute lie angle of the clubhead at impact. The static lie angle of a club is measured from the horizontal plane to the shaft, and is usually around 60° for the driver.

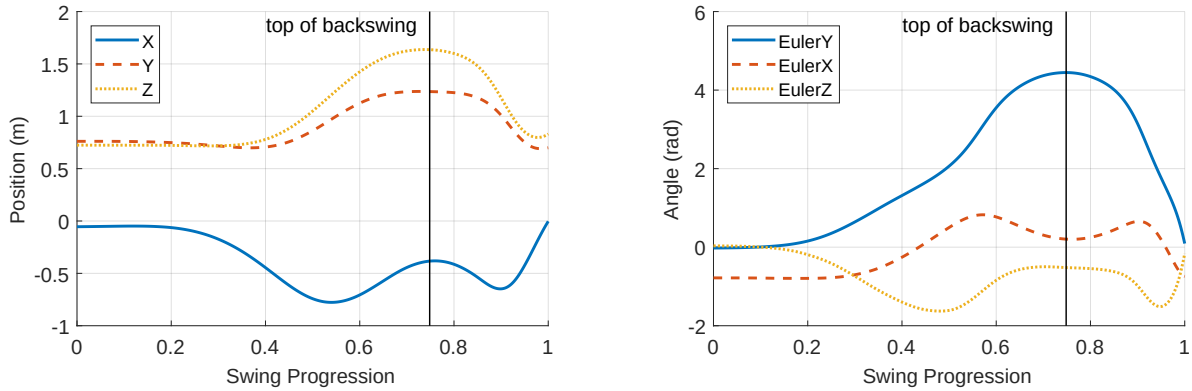

(a) Position

(b) Orientation (Y-X-Z Euler)

Figure 4.3: 6-DOF grip motion for a representative golf swing.

kinematics are used to drive the flexible club model in full swing simulations, and the simulated shaft deflections and clubhead deliveries are compared to those observed in the experiment. A convergence study was performed to determine a suitable number of elastic coordinates (see Section 3.2) for the shaft. It was found that one elastic coordinate for the transverse and torsional directions (i.e., $u0111$) provided good results and computational efficiency. Axial deformation was assumed to be negligible.

The 6-DOF grip position data consists of three translational (X, Y, Z) and rotational components (Y-X-Z Euler angles). The grip motion of a representative golf swing is plotted against the normalized progression of the swing in Fig. 4.3, where the swing begins at the address position and finishes at impact. The vertical line indicates the top of the backswing. To ensure continuous accelerations at the grip, cubic spline interpolation was applied between the position data points.

The mean simulated lead deflection, droop deflection and shaft twist for the 10 swings of one golfer are compared to the observed measurements in Fig. 4.4. The shaded bands represent one standard deviation. The lead and droop deflections were measured as the relative displacement of the hosel in the X_G and Y_G directions, respectively. The shaft twist angle is positive about Z_G, and was measured by calculating the relative Euler angles between the grip and an intermediate frame at the hosel, where the final Euler rotation represented the twist of the shaft. The simulation results indicate that the model flexes more than the actual club, but is able to reproduce the unique bending profiles of the golfer and the subtle patterns within them. The experimental shaft twist is noticeably noisier than the deflections, yet the simulated twist appears to follow the general trend of

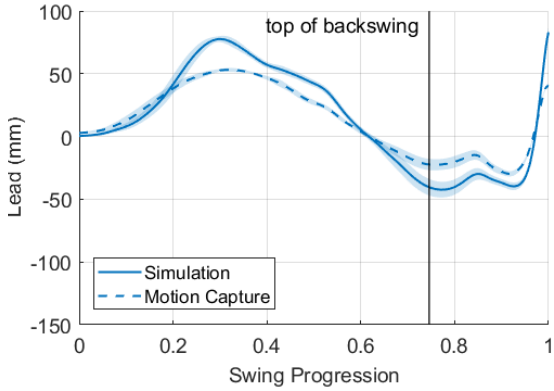

(a) Golfer 10 Lead

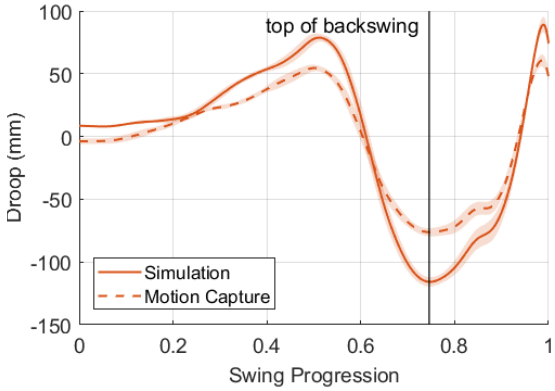

(b) Golfer 10 Droop

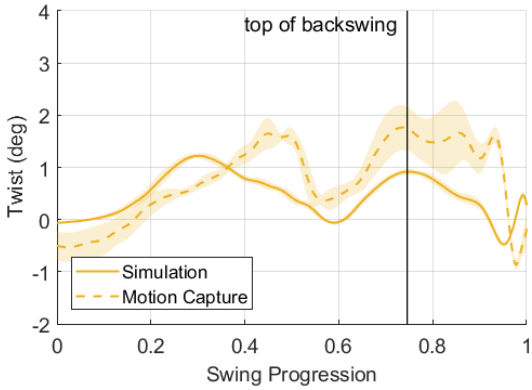

(c) Golfer 10 Twist

Figure 4.4: Simulated vs. experimental shaft deflections and twist (Golfer 10).

experimental twist, albeit with less accuracy. It should be noted that in the simulations, the grip position was held still for one second, allowing the shaft to reach static equilibrium through internal damping before the swing commences. Otherwise, the sudden effects of gravity would cause spurious oscillations at the beginning of the swing. The initial simulated droop resulting from static equilibrium under gravity is not observed in the experimental results as golfers typically rest the clubhead on the ground, so the different initial conditions may have affected the subsequent results in time.

It is possible that the numerically-generated stiffness profiles provided by the manufacturer do not provide good estimates for the shaft's actual stiffness, causing the errors observed in Fig. 4.4. It was found through optimization that the deflection errors could

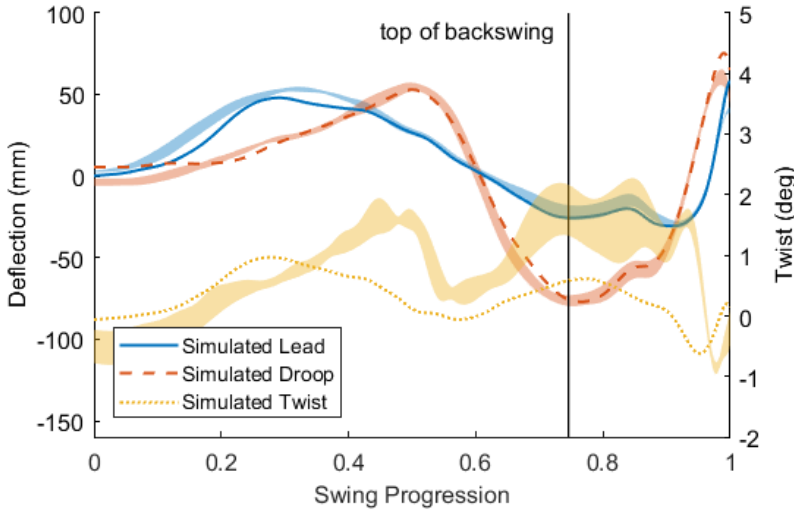

Figure 4.5: Simulated vs. experimental shaft deflections and twist using scaled bending stiffness (Golfer 10).

be minimized by scaling the bending stiffness (EI) by a factor of 1.5. However, scaling the torsional stiffness (GJ) did not prove to be effective. Furthermore, the shaft's damping parameters were determined in the same minimization routine and were found to be 0.006 s^{-1} for both bending and torsion. In Fig. 4.5, the mean simulated deflections and twist using the scaled bending stiffness and tuned damping parameters are plotted against the experimental data for the same golfer as in Fig. 4.4. The lead and droop deflection errors were effectively minimized, and the twist error did not change significantly. The scaled bending stiffness is used in the remaining work as it replicates the actual club behaviour with greater accuracy. Similar plots to those in Fig. 4.5 are available in Appendix B for the remaining nine golfers. For some golfers, the view of the markers on the clubhead was obstructed by the player and caused some noise in the experimental data.

The remaining errors, however small, ultimately affect the presentation of the clubhead at impact. The mean clubhead delivery errors (*simulated – experimental*) for each golfer are provided in Table 4.1. The flexible club model consistently overpredicts angle of attack and under predicts clubhead path, albeit by a small amount – roughly 1.5°. Nonetheless, the overall behaviour of the model and its capability to recreate the unique bending profiles and clubhead deliveries for each golfer, as demonstrated by Figs. 4.5 and B.1, and Table 4.1, provides confidence when using the flexible club model in conjunction with the biomechanical and impact models.

Table 4.1: Mean simulated clubhead delivery errors for each golfer (*simulated – experimental*)

Golfer	Clubhead Speed (km/h)	Angle of Attack (deg)	Clubhead Path (deg)	Face Angle (deg)	Dynamic Loft (deg)	Dynamic Lie (deg)	Closure Rate (rpm)	Loft Rate (rpm)	Lie Rate (rpm)
1*	-0.279 ± 0.43	1.6 ± 0.789	-1.6 ± 0.562	-0.647 ± 0.133	-1.1 ± 0.291	-2.96 ± 0.104	-13.8 ± 4	9.65 ± 5.13	0.192 ± 5.22
2	0.272 ± 0.519	1.63 ± 0.707	-1.32 ± 0.496	-1.43 ± 0.291	0.0371 ± 0.156	-2.64 ± 0.171	-7.63 ± 3.98	14.5 ± 6.98	-26.7 ± 5.05
3	-1.92 ± 0.241	1.1 ± 0.546	-1.49 ± 0.294	0.428 ± 0.166	-0.386 ± 0.157	-2.41 ± 0.0802	-15.7 ± 2.55	3.93 ± 3.17	3.55 ± 3.81
4	0.0551 ± 0.886	1.65 ± 0.659	-1.47 ± 0.299	-1.53 ± 0.181	0.0989 ± 0.22	-2.95 ± 0.187	-17.6 ± 5.32	11.3 ± 7.41	-31.3 ± 8.27
5	-1.98 ± 1.09	0.651 ± 0.583	-0.729 ± 0.381	0.796 ± 0.262	0.0733 ± 0.565	-1.8 ± 0.328	-56.3 ± 5.4	25.9 ± 15.2	-11.5 ± 9.61
6	-2.1 ± 0.61	0.736 ± 0.604	-0.891 ± 0.544	0.79 ± 0.313	-2.53 ± 0.2	-2.95 ± 0.145	-13.2 ± 3.4	-7.48 ± 3.77	-4.03 ± 5.98
7	0.0676 ± 0.544	1.51 ± 0.597	-1.8 ± 0.448	-0.797 ± 0.224	-0.592 ± 0.204	-2.5 ± 0.2	3.68 ± 4.23	-2.5 ± 6.82	-15.3 ± 2.33
8	-0.94 ± 0.349	1.2 ± 0.66	-1.44 ± 0.456	-0.107 ± 0.316	-1.05 ± 0.214	-2.07 ± 0.125	0.651 ± 4.3	-13 ± 3.16	14.4 ± 7.41
9	0.809 ± 1.45	2.07 ± 0.758	-2.28 ± 0.389	-1.69 ± 0.192	1.57 ± 0.284	-2.54 ± 0.33	-9.54 ± 7	8.45 ± 12.4	-19.7 ± 14.1
10	-0.318 ± 0.288	1.17 ± 0.682	-1.62 ± 0.461	-0.88 ± 0.168	-0.359 ± 0.322	-2.19 ± 0.156	-8.23 ± 6.16	4.72 ± 8.67	-2.54 ± 6.77

Clubhead speed and direction measured at CG. Angle of attack positive about -Y, beginning at X. Club path and face angle positive about -Z, beginning at X. Dynamic loft measured as the angle between X_C and the XY plane, positive about -Y. Dynamic lie measured by projecting the Y_C onto the YZ plane and adding the static lie angle. Closure rate, loft rate and lie rate positive about Z, Y, and X, respectively. Refer to Fig. 4.1 for different frames of reference.

*only 7 swings were recorded for Golfer 1.

4.3 Impact Model Validation

In this Section, the parameters of the volumetric impact model are identified using the data from the motion capture experiment. There are seven parameters in total, including the normal force parameters k_v and a, the friction parameters μ and v_{tr}, and the tangential compliance parameters k_b, c_b and t_c. The parameters are identified by minimizing the difference between the simulated and experimental launch conditions in full-club impact simulations. Inverse dynamics was performed to determine the simulated grip forces, which were used to drive the club during the 0.5 ms of impact. The experimental data was divided into training and test datasets in order to validate the model.

4.3.1 Full-club Impact Simulation

The simulated clubhead deliveries from the full swing simulations are very good but not perfect, as shown by Table 4.1. Therefore, tuning the impact model using the measured launch conditions in conjunction with full swing simulations is not logical (e.g., 1° of face angle error could generate a large amount of side spin). To correct for this, the flexible club model was initialized at the moment of impact using the experimental data.

Initializing the flexible club is accomplished by setting the initial conditions at the clubhead and grip and fitting the shaft between these two positions. However, defining all four sets of initial conditions (i.e., translational and rotational at the clubhead and grip) over-constrains the flexible club model. One set of initial conditions must be relaxed in order for the flexible club to initialize properly. The clubhead initial conditions are crucial to the outcome of the impact, so they cannot be relaxed. Since the grip orientation relative to the clubhead constrains the deformation of the shaft, it was chosen to enforce the rotational and relax the translational initial conditions at the grip. The translational initial conditions are then computed using algebraic constraints. It was found that the errors associated with relaxing the grip's initial position and velocity were acceptable. On average, the position of the grip relative to CF differed from the experiment by 1.9 mm (0.2%), and the grip speed differed from the experiment by 2.4 m/s (15%). For the same reason that the club cannot be initialized using all six degrees of freedom at the grip, it also cannot be driven kinematically using six degrees of freedom at the grip. Alternatively, the club may be driven dynamically using six-DOF grip *forces*.

Cochran and Stobbs [9] hypothesized that the golfer nor the shaft can affect the dynamics of the impact. It may be true that the forces applied at the grip do not affect the impact in a meaningful way, but it stands to reason that these forces are not zero, and

should be included in the full-club impact simulations. To get an estimate of the grip forces at impact, inverse dynamics was performed using the full-swing simulations described in Section 4.2. The mean simulated grip forces for Golfer 10 are given in the motion capture inertial and grip frames in Figs. 4.6 and 4.7, respectively. The shaded bands represent the standard deviation of the ten swings. Appendix C contains the simulated grip forces in the grip frame for golfers 1 through 9.

The simulated grip forces provide some interesting insights. Firstly, the application of force by each golfer is remarkably consistent. Secondly, the translational forces in the grip frame indicate that nearly all the grip force at impact is acting along the shaft axis Z_G. In other words, the force is nearly completely centripetal. In a way, this result concurs with the idea of "free-wheeling" through impact, as the golfer does not apply significant forces in any direction but the one required to keep the club moving in an arc. Lastly, there is minimal torque applied about the shaft axis throughout the whole swing. This is surprising because it is natural to think that the act of closing the clubface originates from a torque applied about the shaft axis. Evidently, this is not the case.

To drive the flexible club in the impact simulations, the grip forces were extrapolated for the 0.5 ms of impact. The golf ball was positioned such that it contacted the clubface at the measured impact location.

4.3.2 Parameter Identification

Approximately 100 shots with impact locations spanning the entire clubface are available for the parameter identification. However, the normal force model can only account for a single COR value [97]. The relationship between COR and impact location for the experimental clubhead is unknown, so a subset of 60 impacts within a 12 mm radius of CF were chosen for the parameter identification with the assumption that impacts within the *sweet-spot* of the clubface share a similar COR. The 60 impacts were divided into training and test datasets by randomly selecting 40 impacts for the training dataset.

A sensitivity analysis demonstrated that v_{tr} did not affect spin generation as long as it was relatively small. However, increasing v_{tr} reduced the stiffness of the system equations and improved simulation time. Therefore, to reduce the number of optimization parameters and improve computational efficiency, v_{tr} was set to a value of 1 m/s. Moreover, friction and tangential compliance interact to generate spin, and different combinations of these parameters can generate the same spin. To facilitate the tuning process, the coefficient of friction was set to 0.3, a value used in the FE simulations of Tanaka et al. [63, 70] and Tamaogi et al. [48]. The five remaining parameters were found by minimizing the following

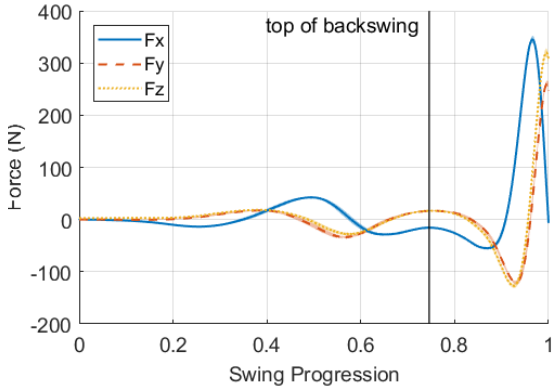

(a) Golfer 10 Force

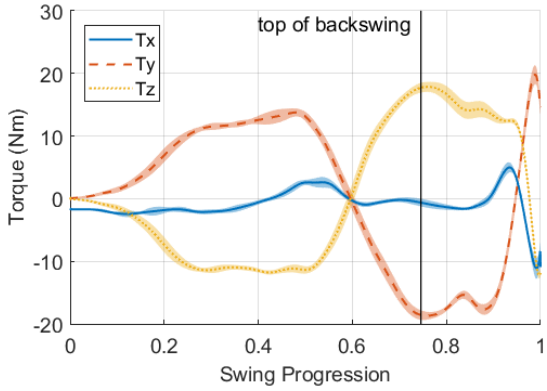

(b) Golfer 10 Torque

Figure 4.6: Simulated grip forces in motion capture inertial frame (Golfer 10)

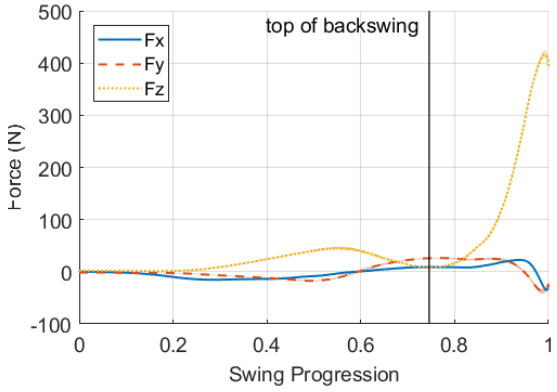

(a) Golfer 10 Force

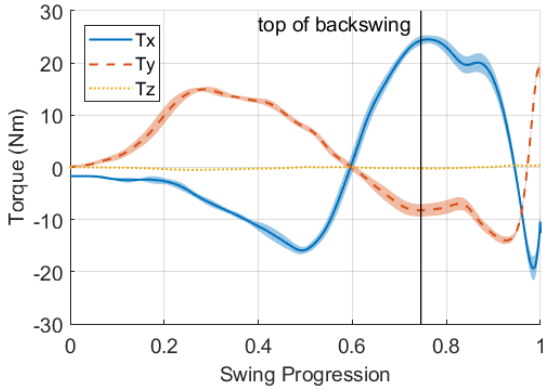

(b) Golfer 10 Torque

Figure 4.7: Simulated grip forces in grip frame (Golfer 10)

Table 4.2: Mean simulated launch condition errors (*simulated – experimental*) for training (n = 40) and test (n = 20) datasets

Dataset	Ball Speed (km/h)	Launch Angle (deg)	Azimuth (deg)	Back Spin (rpm)	Side Spin (rpm)
Training	-0.242 ± 1.6	0.996 ± 0.326	0.164 ± 0.691	-59.4 ± 334	184 ± 286
Test	0.169 ± 1.96	0.934 ± 0.389	-0.147 ± 0.54	-150 ± 287	239 ± 269

Positive launch angle is measured about the -Y axis, and positive azimuth and side spin about the -Z axis. Refer to Fig. 4.1 for motion capture inertial frame.
Volumetric impact model parameters: k_v = 5.234e+09 N/m^3, a = −7.315e−03 (m/s)$^{-1}$, μ = 0.3, v_{tr} = 1 m/s, k_b = 17.96 Nm/rad, c_b = 2.030e−03 Nm/rad· s^{-1}, t_c = 2.016 mm.

objective function using MATLAB's genetic algorithm

$$J = \sum_{i=1}^{40} \left| \frac{V_{s,i} - V_{e,i}}{V_{e,i}} \right| + \left| \frac{\Omega_{s,i} - \Omega_{e,i}}{\Omega_{e,i}} \right| \tag{4.1}$$

where $V_{s,i}$, $\Omega_{s,i}$ and $V_{e,i}$, $\Omega_{e,i}$ are the simulated and experimental ball speed and spin rate, respectively, after an impact i. The mean simulated launch condition errors (*simulated – experimental*) for the training and test datasets are shown in Table 4.2, and the identified parameters are provided in the table footer.

The volumetric impact model shows good agreement for ball speed and azimuth, and reasonable agreement for launch angle and back spin. Relatively large errors are reported for side spin, which may have been caused by imprecise calibration of the motion capture system and manually positioned launch monitor. A misalignment of just 2 degrees between the vertical axes of the inertial frame and the launch monitor could create 100 rpm of side-spin error. Furthermore, an elite golfer can typically sense the direction of side spin of the resulting shot based on the feel of the impact, and one golfer in the experiment claimed the launch monitor was returning substantial draw spin (i.e., negative side spin) for shots he felt were straight, or perhaps even fades[3]. Supporting his claim is the overwhelming amount of draw spin in Table A.2.

Simulated normal force (F_n) histories are compared to the experimental results of Tamaogi et al. [48] for two impacts with similar incident velocities in Fig. 4.8a. The model's peak normal force is greater than in the experiment and the contact time is noticeably shorter, but overall the model shows reasonable agreement with the experimental

[3]For a right-handed golfer, a *fade* is a shot with positive side spin, and a *draw* is a shot with negative side spin.

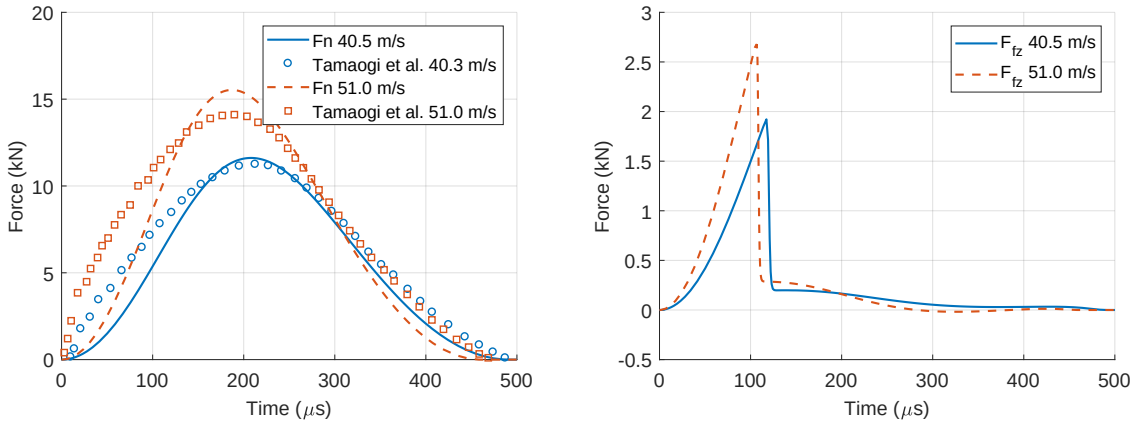

(a) Normal Force

(b) Vertical Friction Force

Figure 4.8: Normal force history comparison with Tamaogi et al. [48], and corresponding vertical friction force histories.

normal force histories. It should be noted that the experiments of Tamaogi et al. involved shooting a golf ball into a solid cylindrical Ti-alloy bar, and it is possible that the dynamics of clubhead-ball impacts are different. Roberts et al. [106] developed a technique to measure the duration of contact between a clubhead and ball by creating an electric circuit in which the ball and clubface formed a switch, completing the circuit while contact was maintained. They demonstrated that the contact time between the clubhead and ball varied greatly depending on the construction of the ball, its compression, the type of clubhead used, and the clubhead speed. The experimental contact times observed by Roberts et al. ranged from less than 430 μs to greater than 530 μs. The contact times of the simulated 40 m/s and 51 m/s impacts were 491 μs and 460 μs, respectively. The mean contact time of all 60 impacts was 466 μs.

The vertical friction force (F_{fz}) histories corresponding to the simulated impacts in Fig. 4.8a are shown in Fig. 4.8b. The spikes at the beginning of contact (around 100 μs) represent a brief period of slip between the golf ball cover and the clubface. The friction force drops sharply when the relative tangential velocity v_t between the cover of the ball and the clubface approaches zero. A small friction force reversal is observed for the 51.0 m/s impact.

To show that the impact model adequately predicts ball speed and spin rate for a variety of impact conditions, the simulated ball speeds and spin rates for the 60 impacts are plotted against their corresponding experimental values in Fig. 4.9. The overall performance of

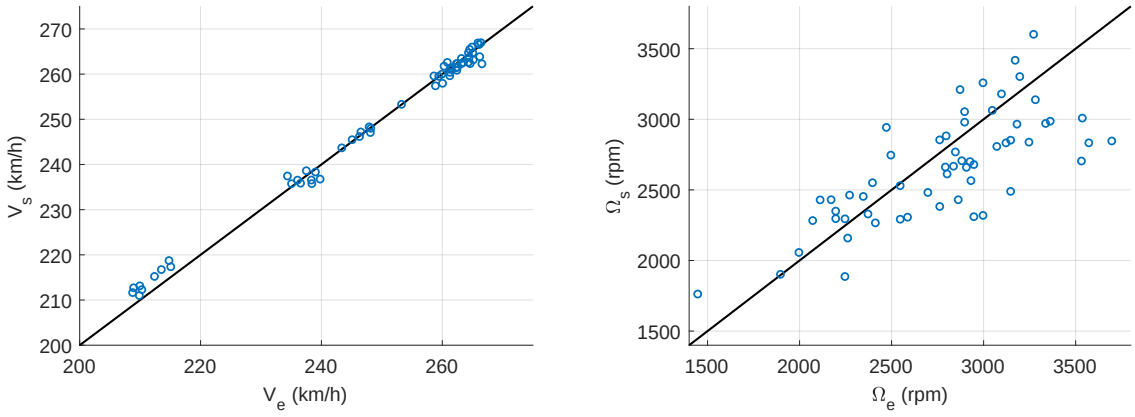

(a) Ball Speed

(b) Spin Rate

Figure 4.9: Simulated vs. experimental ball speeds and spin rates

the volumetric impact model is acceptable. However, more experimental data should be collected with a means for calibrating the launch monitor with the motion capture system to further investigate the accuracy of the model.

4.4 Biomechanical Validation

To validate the biomechanical model, the full golfer model is optimized by maximizing carry distance. The resulting simulated grip kinematics are compared to those of the elite golfers in the motion capture experiment.

4.4.1 Golfer Model Configuration

The address position (position and orientation of a golfer's joints before the swing commences) was predetermined. The pelvis and torso angles were taken from mean values in literature [41], and the remaining joint angles were determined by matching the golfer model's grip position and orientation to the mean grip position and orientation from the motion capture experiment.

Where applicable, the muscle torque generators were given the same parameters as used by MacKenzie and Sprigings [30]. The newly added pelvis is more proximal than

Table 4.3: Muscle torque generator parameters

Generator	T_m (Nm)	τ_{act} (ms)	τ_{deact} (ms)	ω_{max} (rad/s)	n	Γ	S	T_r
Pelvis	250	20	40	30	3.0	3.0	2.0	1.5
Torso	200	20	40	30	3.0	3.0	2.0	1.5
Shoulder	160	20	40	60	3.0	3.0	2.0	1.5
Arm	60	20	40	60	3.0	3.0	2.0	1.5
Wrist	90	20	40	60	3.0	3.0	2.0	1.5

the torso, so it was given a maximum isometric torque of 250 Nm, 25% greater than the torso, and a maximum angular velocity of 30 rad/s, equal to that of the torso. The default muscle torque generator parameters are summarized in Table 4.3. The maximum isometric shoulder torque is decomposed into horizontal and vertical components as described in Section 3.1.2. For this optimization, the maximum angular velocities for the backswing were scaled by a factor of 0.07 and the maximum isometric torques were scaled by a factor of 0.65 to create a realistic 3:1 tempo[4] and swing duration of approximately one second (i.e., from address to impact).

4.4.2 Golf Swing Optimization

The optimization variables are the activation and deactivation times of the muscle torque generators, the shoulder torque ratio r, and the height of the pelvis h_p, which was allowed to vary slightly to represent a small variance in knee flexion. To decrease the size of the solution space, some assumptions were made about the sequence of the swing:

1. the torso and the shoulder activate and deactivate simultaneously,
2. the pelvis, torso, shoulder and arm all activate at $t = 0$ to initiate the backswing, and
3. at the transition from backswing to downswing, the pelvis, torso and shoulder activate at a time τ_{deact} after their respective backswing deactivation times.

The optimization variables were given sufficient boundaries to permit the generation of diverse golf swings. An optimal swing was found after following the procedure outlined in

[4]Golf swing tempo is measured as the ratio of the duration of the backswing to the duration of downswing.

Table 4.4: Optimal biomechanical timings for the default model

Variable	Lower Bound	Upper Bound	Solution	Variable	Lower Bound	Upper Bound	Solution
r	0.3	1.2	0.856	$P_{off,down}$	0.8	1.0	1.000
h_p*	0.45	0.55	0.496	$TS_{off,down}$	0.8	1.0	1.000
$P_{off,back}$	0.5	0.8	0.688	$A_{on,down}$	0.7	1.0	0.888
$TS_{off,back}$	0.5	0.8	0.619	$A_{off,down}$	0.8	1.0	0.987
$A_{off,back}$	0.0	0.6	0.103	$W_{on,down}$	0.7	1.0	0.899
$W_{on,back}$	0.0	0.6	0.252	$W_{off,down}$	0.8	1.0	1.000
$W_{off,back}$	0.4	0.8	0.771				

*h_p is the ratio of model pelvis height to the overall height of the golfer standing upright. Besides r and h_p, which are unitless, all the values are given in seconds.

Section 3.5. The chosen boundaries and solution to the optimization problem are provided in Table 4.4, where P, TS, A, and W denote the pelvis, torso/shoulder, arm and wrist, respectively. Some timings were omitted from Table 4.4 as they can be inferred from the foregoing assumptions.

4.4.3 Results and Discussion

The optimized biomechanical timings in Table 4.4 indicate that the torso activates before the pelvis to commence the downswing. This result is inconsistent with real golf swings, where the rotation of the pelvis typically initiates the downswing [107]. The model is not exploiting the extra power that could be generated by creating separation between torso and pelvis, also known as the X-factor. It is possible that the biomechanical constraints render the model's X-factor ineffective at generating extra clubhead speed with a favorable clubhead delivery; one of the major limitations of the biomechanical model is the rigid body representation of the torso. In a real golf swing, the spine bends and contorts, causing a noticeable displacement of the thorax during the downswing [108]. The flexibility of the spine could be what permits the sequential driving of the pelvis followed by the torso during the downswing.

Other than the torso activating before the pelvis, the optimized timings seem reasonable. The late deactivation of the wrist during the backswing suggests the optimizer discovered the benefits of a large wrist cock and corresponding delayed wrist release, also known as *lag*. Furthermore, power was maximized during the downswing by deactivating

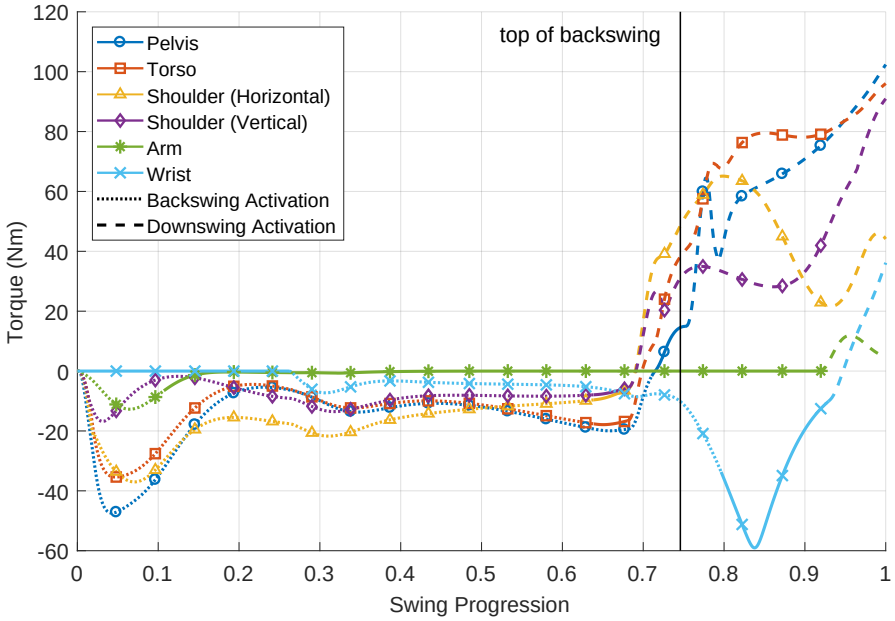

Figure 4.10: Golfer model active torques for optimized swing.

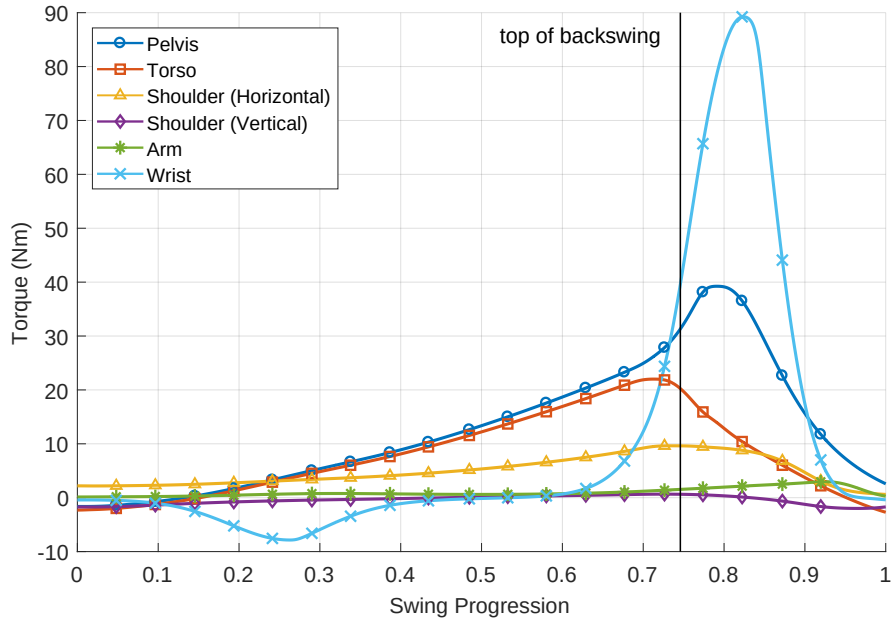

Figure 4.11: Golfer model passive torques for optimized swing.

the active muscle torques of the torso/shoulder, arm and wrist after impact, which occurred at $t = 0.968$ seconds. Figs. 4.10 and 4.11 show the active and passive torques (excluding joint damping) for the optimized golf swing, respectively, for each DOF. Fig. 4.11 exhibits a build up of passive torques at the top of the backswing that aids the generation of clubhead speed during the downswing. A large passive torque was created by the wrist lag during the downswing, as required to keep the wrist joint within its anatomical joint limits. The large passive torque is likely double what would be required by each wrist if both hands were used to drive the club.

The golf ball was teed far forward in the stance and as high as possible to allow for an ideal clubhead delivery with a large angle of attack (11.9°) and dynamic loft (21.9°), thus minimizing spin rate (1620 rpm) and maximizing launch angle (20.5°). The clubhead and ball speed were 164 km/h and 241 km/h, respectively. The *smash factor* is a golf statistic used as a measure of impact efficiency and is equal to the ratio of ball speed to clubhead speed. The simulated impact yielded a smash factor of 1.47. The average smash factor from the motion capture experiment was 1.42, and the average smash factor on the PGA Tour in 2017 was 1.48 [109]. The golf ball carried 257 yds.

To validate the optimized swing kinematics, the golfer model's grip kinematics were compared to those of the elite golfers from the motion capture experiment in Fig. 4.12. The shaded regions represent the standard deviation of the experimental measurements, which were shifted to align with the inertial reference frame of the golfer model (see Fig. 3.1). The grip orientation is represented using Y-X-Z Euler rotations. At some points in the swing, the simulated swing kinematics fall outside the standard deviation of the experimental measurements. The discrepancies in the final quarter of the swing arise from the forward ball position that was required for the ideal clubhead delivery. It is atypical for a golfer to place the ball so far forward in the stance, but based on the results of this optimization it may be advisable to do so in order to create a large angle of attack and increase dynamic loft. As a result of the forward ball position, the downswing of the golfer model is effectively longer than that of a real golfer, which explains the offsets in the kinematics for the downswing portion of the swing. Despite these discrepancies, the model is effectively recreating the motion of an elite golf swing with no prior knowledge of what such a swing should look like. The authenticity of the simulated golf swing lends credibility to the results of simulation experiments involving the use of the golfer model.

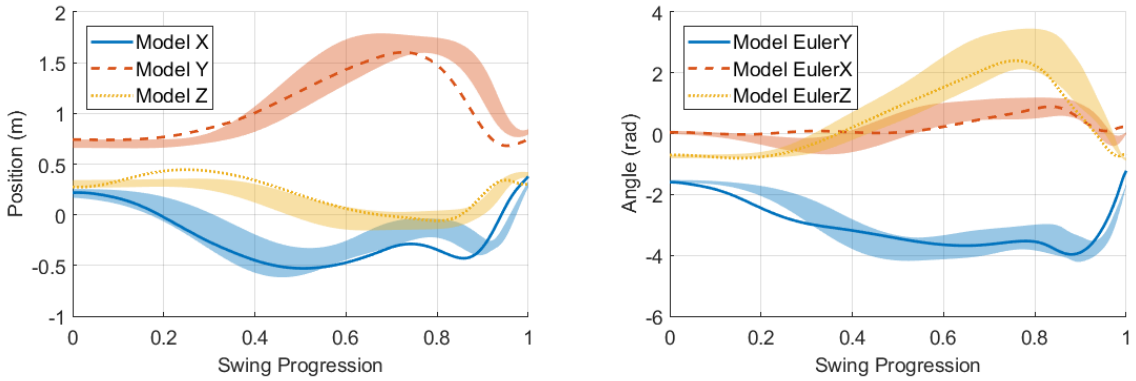

(a) Position

(b) Orientation (Y-X-Z Euler)

Figure 4.12: Optimized golfer model grip kinematics compared to elite golfers. The shaded regions represent the standard deviation of the experimental measurements for the ten elite golfers.

Chapter 5

Simulation Experiments

In this chapter, the validated models are used to run four simulation experiments. The first two simulation experiments focus solely on impact dynamics and therefore do not require the golf swing model to simulate the biomechanical interaction with the golf club. In the final two simulation experiments, the golf club is modified in such a way that would affect the swing mechanics. In these simulation experiments, the golf swing is optimized in tandem with golf club properties to account for biomechanical adjustments that should be made to provide an optimal golf swing with the modified golf club.

5.1 The Influence of the Shaft and Golfer on Impact Dynamics

A long-standing assumption in golf science is that neither the shaft nor golfer can influence clubhead-ball impact dynamics. As a result, free-body collisions between the clubhead and ball have been assumed to be an accurate representation of the driver impact. Many studies have exploited the free-body assumption to provide insights on optimal clubhead design, using both FE and analytical models. In industry, free-body FE simulations are used extensively by golf equipment manufacturers to assess the performance and structural integrity of prototype clubhead designs. Consequently, the free-body assumption plays a pivotal role in golf research and development, but there is limited evidence supporting it.

The free-body assumption dates back to the hinged driver experiment of Cochran and Stobbs [9], published in 1968 (details in Section 2.2.1). In 2008, Tanaka et al. [70] used FE models to investigate shaft effects and the claims of Cochran and Stobbs. However,

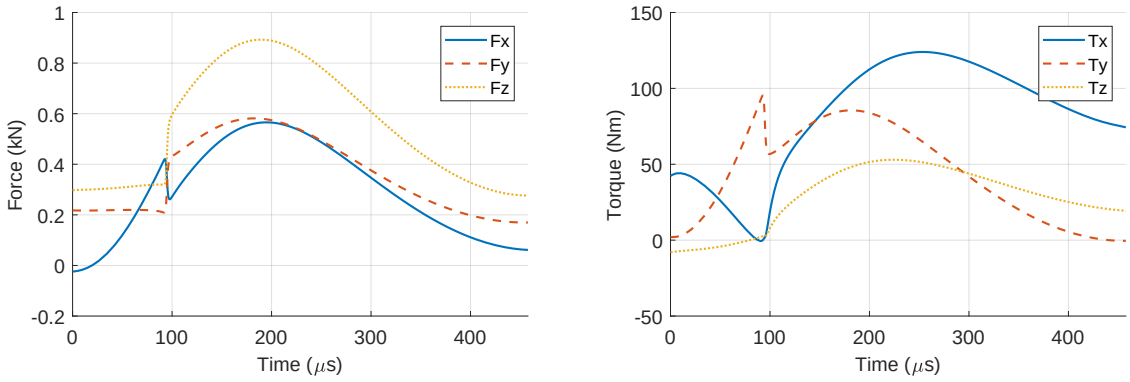

(a) Force

(b) Torque

Figure 5.1: Shaft reaction forces and torques at the hosel for a representative impact

the club used by Tanaka et al. was highly unrealistic (see description of simplified club in 2.2.4) and the experiment did not consider the dynamic loading of the shaft at impact. The work in this section extends the simple cylinder-pendulum club of Tanaka et al. to real golf clubs, leveraging the computational efficiency of the symbolic flexible club and impact models to investigate the influence of the shaft and golfer on impact dynamics.

Hosel Reaction Forces

Any differences between full-club and free-body impacts are fundamentally the result of the reaction forces that develop at the hosel during contact. The free-body assumption implies that these forces are negligible in comparison to the contact forces between the clubhead and ball. The multibody dynamics framework facilitates the observance of reaction forces during simulations, and so the shaft reaction forces for a representative full-club impact chosen from the 60 used in Section 4.3.2 are shown in Fig. 5.1, given in the global frame. The magnitude of the reaction force peaked at roughly 1.2 kN, or 7.7% of the peak normal force for this particular impact. Furthermore, the reaction torque was substantial, peaking at a magnitude of 150 Nm. The irregularities observed in the first 100 μs are the result of the large friction force created while the golf ball is slipping at the beginning of contact (see Fig. 4.8b). The golf ball transitions from slipping to sticking near t = 100 μs.

Table 5.1: Mean launch condition differences between full-club and free-body impact simulations (*full-club – free-body*) for 60 impacts from motion capture study within 12 mm of CF.

Ball Speed (km/h)	Launch Angle (deg)	Azimuth (deg)	Back Spin (rpm)	Side Spin (rpm)
4.24 ± 1.59	-0.305 ± 0.198	0.26 ± 0.148	194 ± 160	-134 ± 106

Full-club vs. Free-Body Launch Conditions

Although the reaction forces at the hosel do not seem negligible, it is difficult to say whether or not they are large enough to affect the launch conditions of the golf ball. To gauge the effects of the reaction forces on launch conditions, the 60 full-club impact simulations described in Section 4.3.1 are compared to corresponding free-body impact simulations by removing the shaft from the simulation and allowing the clubhead to behave as a free-body. Table 5.1 shows the mean differences (*full-club – free-body*) in launch conditions for the 60 impacts. Of the differences, ball speed is the most significant, with the full-club producing an extra 4.2 km/h on average. The differences in launch angle, azimuth, and spin are less remarkable, but can still be explained by the reaction at the hosel.

The hosel reaction forces stabilize the clubhead through impact and resist clubhead rotation. As a result, the hosel reaction forces are associated with a suppression of the gear-effect, which is the spin generated due to the ball engaging with the clubface without slip, similar to meshed gears [67, 71]. Essentially, the gear-effect creates a correlation between the final spin of the clubhead (i.e., at the end of contact) and the spin imparted to the golf ball. Considering a hypothetical CF impact, the normal force acts on a line that passes above the clubhead CG and creates a moment that rotates the clubface upward. This rotation increases launch angle and reduces back spin as a result of the gear-effect. The hosel reaction torque T_y effectively resists this rotation, as demonstrated by the decrease in launch angle and increase in back spin in Table 5.1.

A similar mechanism occurs in the horizontal plane and affects azimuth and side spin. In general, a heel[1] impact causes the clubhead to rotate positively about the Z axis, decreasing azimuth and increasing fade spin as a result of the gear-effect. Conversely, a toe impact causes the clubhead to rotate negatively about the Z axis, increasing azimuth and draw spin as a result of the gear-effect. The hosel reaction forces resist these respective rotations and suppress the associated gear-effects. However, an equal suppression of the gear-effect for heel and toe impacts does not explain the differences in azimuth and side-

[1]Relative to CF, the *heel* is located towards the hosel, and the *toe* is located away from the hosel

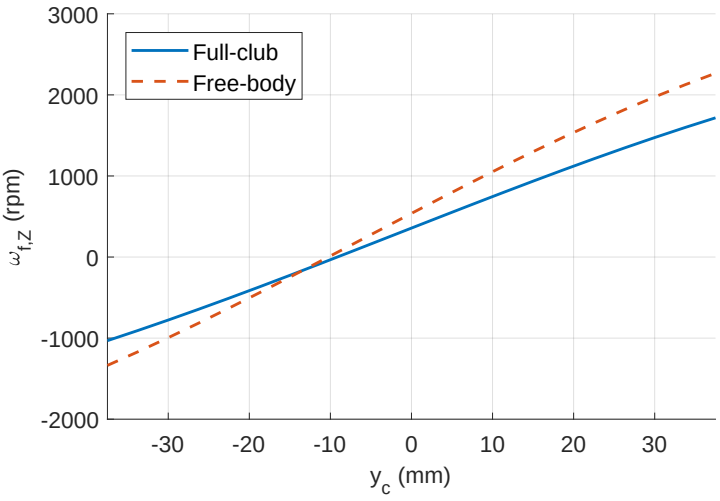

Figure 5.2: Final clubhead spin about the Z axis vs. horizontal impact location. A representative clubhead delivery was used.

spin observed in Table 5.1. Interestingly, it was found that the mean final spin (i.e., at the end of contact) of the clubhead about the Z axis for the 60 full-club impact simulations was 205 rpm; at CF, some of the clubhead's initial closure-rate is maintained through impact. Therefore, for CF impacts, the gear-effect acts to increase fade spin by default. Relative to the free-body impact simulations, this default gear-effect was suppressed, which increased azimuth and decreased fade spin, as shown in Table 5.1. To better understand the full-club's resistance to twisting about the vertical axis, Fig. 5.2 compares the final spin of the clubhead about the Z axis ($\omega_{f,Z}$) for full-club and free-body impacts using a representative clubhead delivery. The curves were generated by varying the impact location across the clubface from $y_c = -37.5$ mm (toe) to $y_c = 37.5$ mm (heel). For this particular clubhead delivery, $\omega_{f,Z}$ at CF was 315 rpm. Relative to $\omega_{f,Z} = 0$, the resistance to clubhead rotation (i.e., the suppression of the gear-effect) appears to increase equally in both directions.

To observe changes in ball speed with respect to impact location, the impact location was varied to cover a 75 x 37.5 mm area on the clubface using the representative clubhead delivery. Figs. 5.3a and 5.3b show contour plots of the simulated ball speed for full-club and free-body impacts, respectively. The dashed circle represents the area for which the impact model was tuned. Results outside this area should only be interpreted qualitatively. The full-club ball speeds are greater across the clubface, and the free-body ball speeds appear

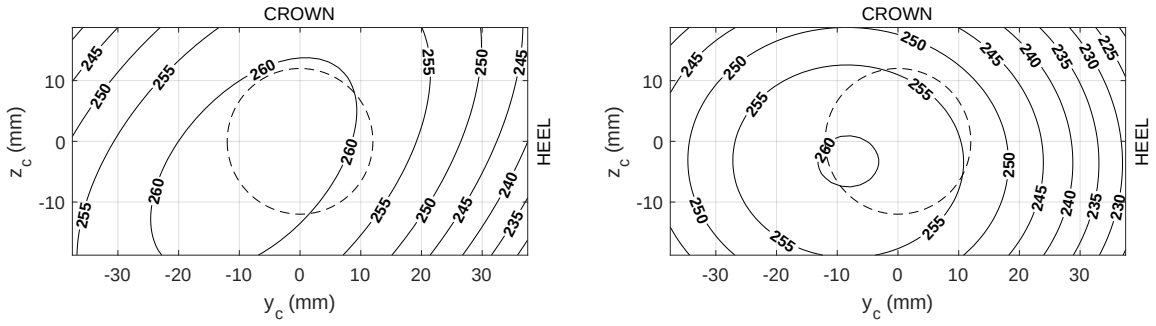

(a) Full-club ball speed (km/h)

(b) Free-body ball speed (km/h)

Figure 5.3: Contour plots of ball speed for full-club and free-body impacts. Impact location varied across the clubface using a representative clubhead delivery.

to drop off more drastically near the high heel area of the clubface, or in close proximity to the hosel. Note that the areas of maximum ball speed roughly correspond to the points where $\omega_{f,Z} = 0$ in Fig. 5.2. In these areas, less energy is lost to the final rotational kinetic energy of the clubhead, and thus energy is transferred to the ball with greater efficiency. Higher ball speeds on the toe have historically been thought to be caused by closure rate – the toe of the clubhead is traveling faster than the heel so it has a higher *effective* clubhead speed. An alternative explanation, elucidated by these results, is that this particular area on the toe produces greater ball speed because is it the area for which the final rotational kinetic energy of the clubhead is lowest.

Fig. 5.4 displays contours of the differences (*full-club – free-body*) in ball speed, launch angle, azimuth, side spin and back spin using the representative clubhead delivery. For this particular clubhead delivery, ball speed is the only launch condition that displays a significant difference at CF, with the full-club generating approximately 4 km/h more. The launch condition differences become more apparent for mishits outside the dashed circle, especially in the direction towards the hosel. Fig. 5.4a shows a remarkable increase in ball speed in the high heel area of the clubface. However, it is likely that a real clubhead suffers from a loss of COR in this area, whereas the model does not. Conversely, the difference in ball speed is much less toward the high toe area, where the full-club is most susceptible to clubhead rotation.

Another interesting observation is the large variance in back spin observed along the horizontal axis of Fig. 5.4d. There is a collective understanding among golfers that heel impacts generate more back spin than toe impacts. It was thought that this occurs because mishits are frequently distributed high on the toe and low on the heel and as a result,

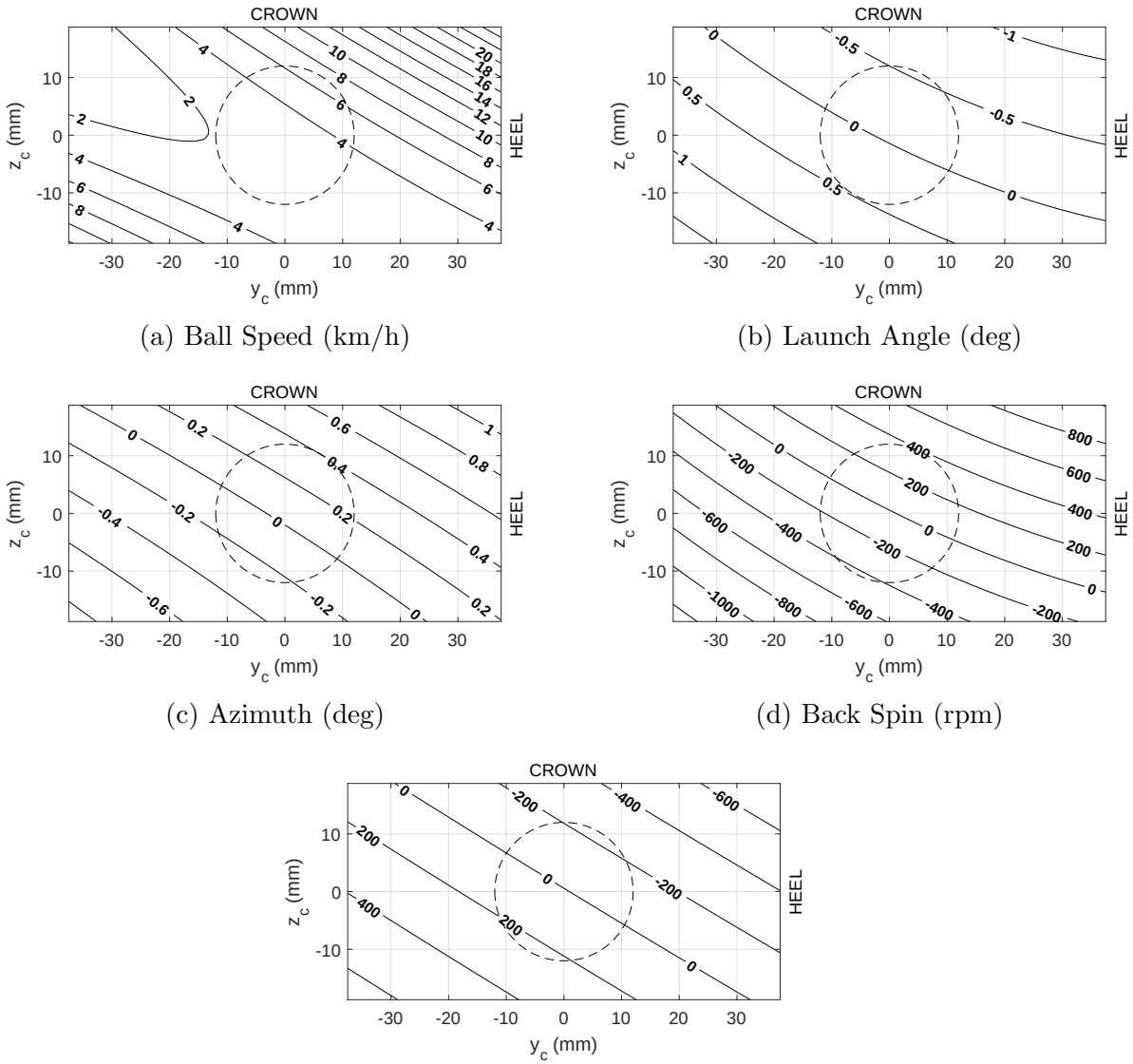

(a) Ball Speed (km/h)

(b) Launch Angle (deg)

(c) Azimuth (deg)

(d) Back Spin (rpm)

(e) Side Spin (rpm)

Figure 5.4: Differences in launch conditions across the clubface (*full-club – free-body*). Impact location varied across the clubface using a representative clubhead delivery.

Table 5.2: Mean differences in launch conditions between the driven club and free club (*driven club – free club*) for 60 impacts from motion capture study (within 12 mm of CF).

Ball Speed (km/h)	Launch Angle (deg)	Azimuth (deg)	Back Spin (rpm)	Side Spin (rpm)
0.397 ± 0.0524	0.0996 ± 0.0130	-0.0759 ± 0.0100	-92.7 ± 10.1	73.9 ± 10.4

vertical gearing reduces back spin for toe impacts and increases back spin for heel impacts. Knowing that for a free-body impact horizontally aligned shots should generate similar back spin, Fig. 5.4d demonstrates that heel impacts are naturally high-spinning, and toe impacts are naturally low-spinning, regardless of vertical impact location. The hosel reaction forces stiffen the clubhead for heel impacts, suppressing the vertical gear-effect relative to toe impacts.

In summary, Fig. 5.4 shows that the differences in launch conditions between full-club and free-body impacts are less compelling at CF, with ball speed being the only significant difference. The differences become more apparent moving away from CF, especially towards the hosel, where the reaction forces resist the rotation of the clubhead, leading to a suppression of the gear-effect relative to free-body impacts.

The Influence of the Golfer

To examine the influence of the golfer on impact dynamics, the grip forces used to drive the flexible club were removed from the full-club impact simulations. Table 5.2 shows the mean differences in launch conditions between the driven club and free club (*driven club – free club*) for the 60 impacts within 12 mm of CF. Although the differences are small, they should not be considered negligible from a modelling standpoint. The differences in spin are on the order of 3% and suggest that the boundary conditions at the grip play an relevant role with regards to spin generation. For example, if the grip were to be kinematically driven through impact instead of dynamically driven, the resulting spin may be considerably different. From the golfer's perspective, the results are much less meaningful. Knowing that a diverse set of golf swings lead to the generation of Table 5.2, the small standard deviations suggest that there is not much variance in grip force effects from golfer to golfer. Therefore, actively trying to influence the outcome of the impact by attempting to alter grip forces would not be effective.

5.2 Optimal Clubhead Loft

The loft of a driver is one of its most important characteristics. Depending on a golfer's skill level and swing mechanics, the loft best suited for a golfer can vary substantially. Consequently, golf equipment manufacturers typically offer multiple nominal loft angles for their drivers, ranging from 8.5° to 12°. Furthermore, most drivers now feature an adjustable hosel that accommodates fine-tuning of the loft angle for individual preferences. For example, PING's flagship driver in 2017, the G400, is available in nominal lofts of 9° and 10.5°. Their adjustable hosel technology allows further adjustment to within ±1°. Generally, higher lofted drivers are better suited for golfers with slower swings speeds to help launch the ball higher and carry further. However, unique swing mechanics can create an exception to this rule. Because golf swings are diverse, even among highly skilled golfers, selecting the nominal loft offerings as a manufacturer is not a straight-forward decision. In this section, the loft angle is varied in full-club impact simulations to determine if the nominal loft angle of the driver used is suitable for the elite golfer demographic.

The clubface is arguably the only physical clubhead characteristic that may be modified without affecting a golfer's swing. For that reason, the 60 full-club impact simulations described in Section 4.3.2 were leveraged to determine optimal clubhead loft for the experimental clubhead deliveries of elite golfers. Using the full-club impact simulations, the loft angle was varied from 4° to 14° in 0.5° increments. For each loft angle, the average carry distance was computed. Fig. 5.5 shows the change in average carry distance with respect to loft angle. A loft angle of 8.5° performed the best for this particular subset of clubhead deliveries, indicating that the 9° driver used in the experiment is more or less suitable for the elite golfer.

5.3 Optimal Clubhead Mass

Optimal driver clubhead mass has long been a matter of debate in the golf research community. There exists an obscure trade-off between clubhead mass, the golfer's ability to generate clubhead speed, and impact efficiency. Cochran and Stobbs [9] investigated this trade-off using a practical experiment. They asked several golfers to swing clubs whose head weights varied from 3.5 ounces to 12.3 ounces (100 – 350 g) and measured the clubhead speeds with each. From this, they estimated how far each shot would carry using simplified analytical models. Their estimates found that the optimal clubhead mass was around 7 ounces (200 g), but any clubhead between 5 and 10 ounces (140 – 280 g) made little practical difference to how far the ball carried. As a result, it was suggested that

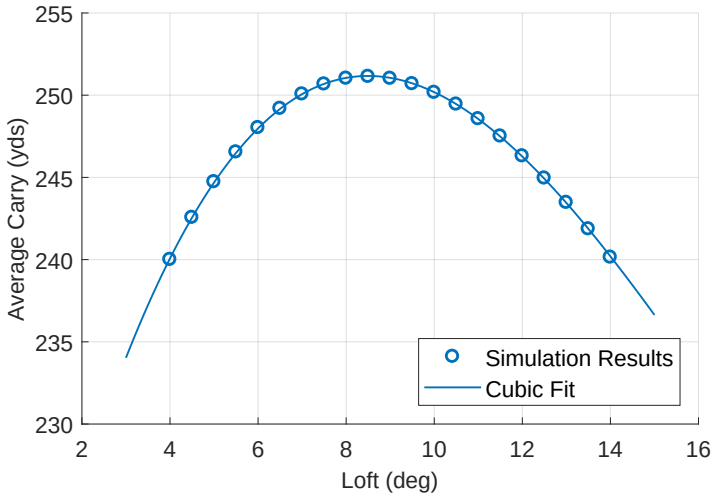

Figure 5.5: Simulated average carry distance vs. loft angle for elite goflers

clubhead mass should be chosen in order to promote consistent rhythm and timing. It should be noted that driver shafts were much heavier in these days. The standard driver shaft was quoted by Cochran and Stobbs to weigh 4.5 ounces (130 g), whereas the shaft used in the motion capture study in Section 4.1 weighed 63.4 g.

Typical modern driver clubheads have a mass of 200 g, a weight that has been backed by more recent simulation experiments involving golf swing models, including the double-pendulum model of White [110], and the three-dimensional forward dynamic model of Balzerson [111]. The golfer model presented in Chapter 3 features many advancements to the state-of-the-art and for that reason the optimal clubhead mass debate should be revisited using the latest model.

Modifications to clubhead mass should not be made without considering corresponding changes to the clubhead MOI. In the aforementioned studies, it was not disclosed how the clubhead MOI was modified in relation to clubhead mass. By definition, an object's MOI is proportional to its material density. Scaling the mass of a clubhead without modifying its shape or volume is equivalent to scaling the density of the material and leads to a corresponding linear scaling of the MOI (assuming the clubhead is made of a single material with a uniform density). For this simulation experiment, the clubhead mass was varied from 100 to 280 g in 10 g increments and the clubhead inertia matrix was linearly

scaled accordingly. Beginning with 190 and 210 g, the golfer model was optimized using `patternsearch`, where the results from Section 4.4 (i.e., using a 200 g clubhead) were used for the initial guesses. The same boundaries were used. The results from these first two optimizations were fed into subsequent optimizations using lighter and heavier masses until the range of clubhead masses were tested.

Fig. 5.6 displays the relationship between clubhead mass, clubhead speed, and carry distance. Some variance was observed in the optimization results so quadratic functions were fit to the data and plotted as solid lines. The dashed line represents the mass-speed curve of a professional golfer, as estimated by Cochran and Stobbs [9]. Cochran and Stobbs admitted that their mass-speeds curves were highly theoretical, and should only be considered for golfers of average strength. Interestingly, the model from Chapter 3 was able to hit the ball further using a lighter clubhead, and carry distance peaked using a 150 g clubhead. The natural inclination is to consider that lighter materials of similar strength (i.e., having a higher strength-to-weight ratio, or specific strength), so as to maintain the structural integrity of the clubhead, may provide performance benefits for a golfer, under the assumption that the clubface behaves similarly to current driver clubfaces. This assumption is not unrealistic, as driver clubfaces are often made of different materials than the body, so changing the body material without changing the behaviour of the clubface is plausible. Still, the golfer model is a very complex system, and it is possible that the mass-carry curve in Fig. 5.6 was not caused by clubhead mass explicitly, but some secondary effects. Other causes should be investigated before concluding that a lighter clubhead may be beneficial.

The clubhead mass affected the optimal swing mechanics significantly, and it was speculated that the different golf swings may have led to variations in the quality of the clubhead delivery and thus carry distance. Fig 5.7 shows traces of the clubhead path in the ZY_M plane using various clubhead masses. Because the biomechanical model lacks the support of the trailing arm, increasing clubhead mass weighed down the leading arm at the top of the swing and created flatter downswings. Nonetheless, all the swings converged near impact, indicating that the clubhead deliveries for each clubhead mass are very similar, and perhaps equally optimal.

Other measures may be used to assess the quality of a clubhead delivery. The smash factor is commonly used to gauge the quality of a clubhead delivery and impact efficiency. Yet, it is shown in Fig. 5.8 that using the smash factor to compare impacts resulting from golf swings with different clubhead masses is not helpful, as the smash factor increases with clubhead mass and does not correlate with carry distance. Equally perplexing is the trend of the clubhead's linear momentum at impact. It also does not correlate with carry distance. Based on these results, it was concluded that optimal clubhead mass does not

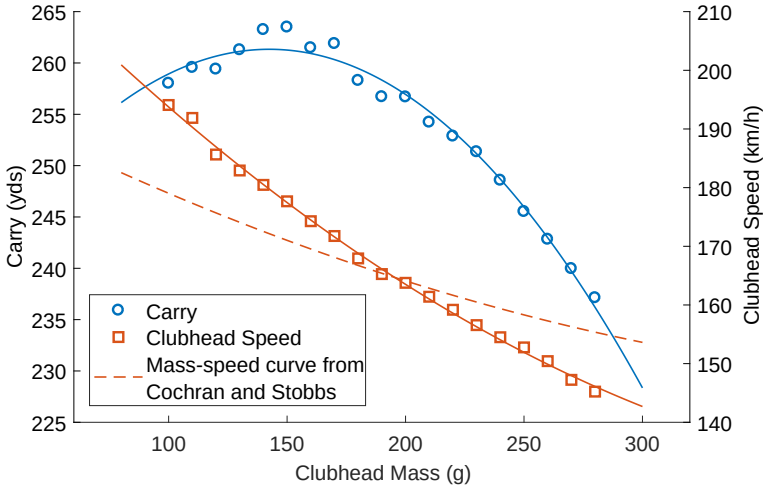

Figure 5.6: Relationship between clubhead mass, clubhead speed generation, and carry distance.

coincide with maximum clubhead momentum at impact. Finally, it was suspected that side spin played a role in the optimization, as minimal side spin leads to maximum carry distance. Nevertheless, the shots resulting from clubhead masses of 160 to 280 g all had less side spin than those 150 g and below.

Ball speed is the primary contributor to carry distance, and was the single impact characteristic that appeared to be linked to the mass-carry curve in Fig. 5.6. Therefore, there must be some interaction between the normal impulse and clubhead speed *generation* that is optimal using a 150 g clubhead. To finally rule out clubhead delivery as the cause, a series of idealized 1D free-body impact simulations were run, varying the clubhead mass and using the same normal force parameters k_v and a. The clubhead speed was determined using the mass-speed curves from Fig. 5.6 and the normal impulse was recorded for each ideal 1D impact. Fig. 5.9 plots the normal impulse versus clubhead mass for both mass-speed curves. As expected, the maximum normal impulse using the golf drive model mass-speed curve was located at 150 g. Using the mass-speed curve estimated by Cochran and Stobbs, the normal impulse was relatively unchanged for clubhead masses 200 g and above.

Fig. 5.9 demonstrates that optimal clubhead mass heavily depends on the golfer's ability to generate clubhead speed using different clubhead masses. If the biomechanical model accurately reflects a real golfer's ability to generate clubhead speed with different clubhead

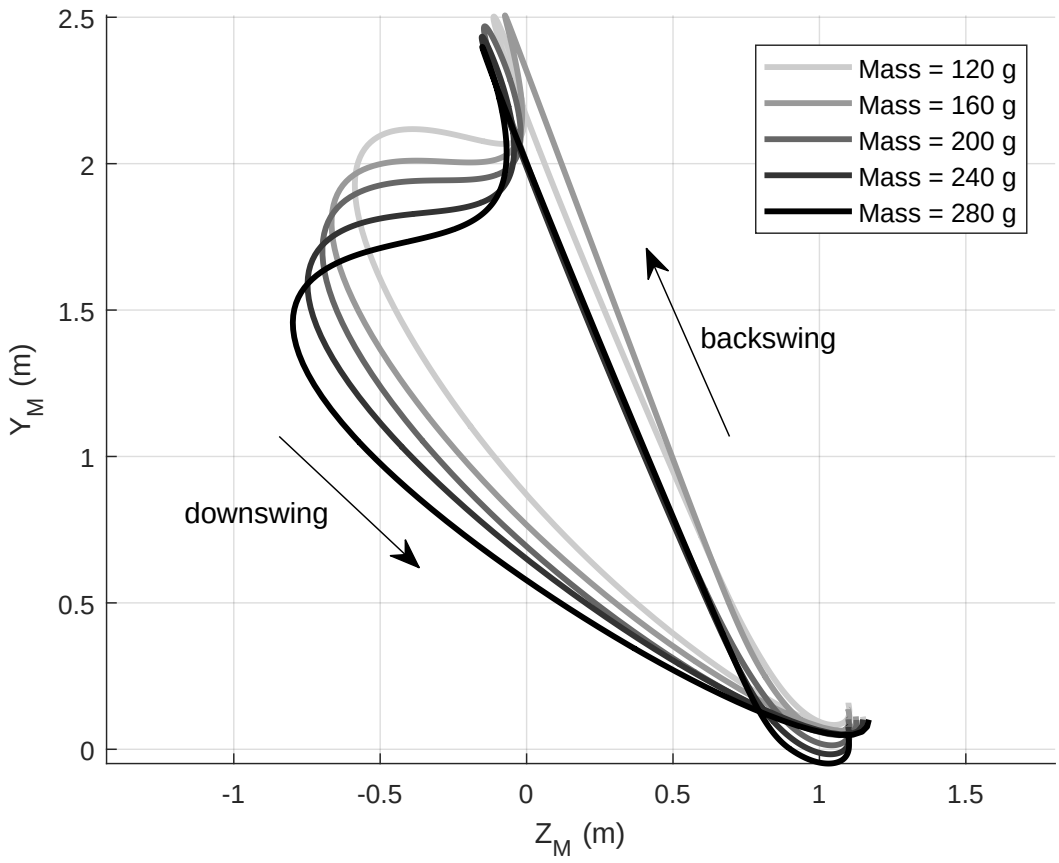

Figure 5.7: The effect of clubhead mass on optimal clubhead path.

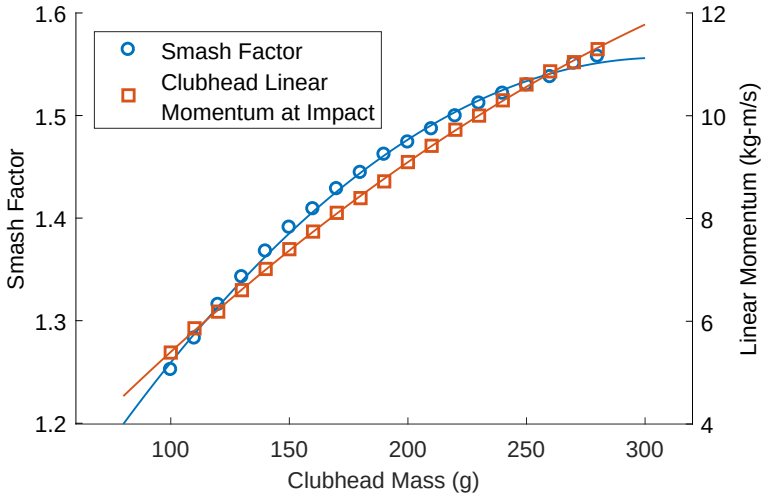

Figure 5.8: The effect of clubhead mass on smash factor and clubhead linear momentum at impact.

masses, then a clubhead of the same shape and 75% lighter material will in fact increase ball speed. However, it is presumed that mass-speed curves vary from golfer to golfer depending on their strength and swing mechanics. Therefore, mass-speed curves should be empirically tested in order to estimate subject-specific optimal clubhead masses.

5.4 Shaft Bending Stiffness Profile Optimization

A shaft's bending stiffness can alter a golf shot by affecting the clubhead delivery. In general, less stiff shafts flex more and are recommended for slower swing speeds to provide more dynamic loft at impact in order to launch the ball higher and carry further. Furthermore, shafts of the same nominal stiffness can vary based on their "kick point", also known as the flex point or bending point. The kick point is where the shaft bends the most and is measured as the point on the shaft with the smallest radius of curvature under a static load [112]. The kick point is classified as high, medium or low based on its position relative to the tip end of the club. Similar to shaft stiffness, a low kick point causes more flexing at the tip and promotes higher dynamic loft. Joyce et al. [113] investigated the effects of kick point on clubhead delivery and launch conditions using two stiff shafts with low and high

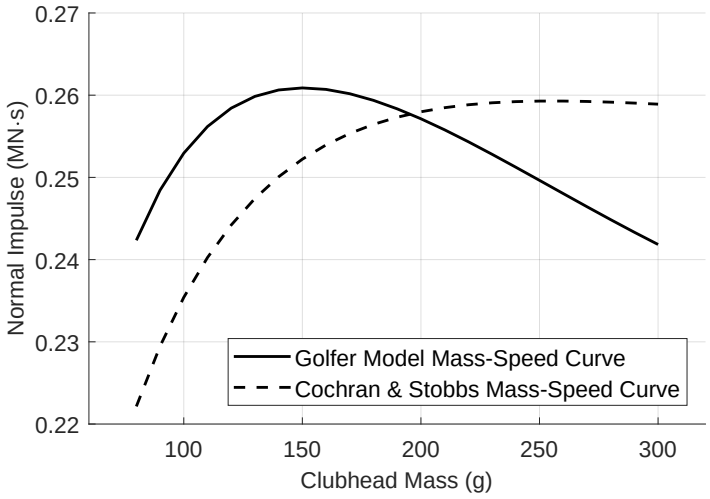

Figure 5.9: Simulated normal impulses for varying clubhead mass where clubhead speed was determined by mass-speed curves.

kick points. Twelve elite golfers were recruited for the experiment and it was found that the driver fitted with the higher kick point shaft displayed a more negative angle of attack corresponding to lower dynamic loft, lower launch angle and increased spin rate. There is limited information regarding how the kick point location is associated with the bending stiffness profile; however the bending stiffness profiles measured by Joyce et al. indicated that higher kick point shafts possess a higher bending stiffness at the tip.

A shaft's performance depends on the interaction with the golfer's swing mechanics and for this reason, shaft selection is typically performed on a case-by-case basis by a golf professional. The goal of the fitting process is to zero in on optimal launch conditions and involves testing shafts of various stiffnesses and kick points more or less through trial and error. In this section, an optimal golf shaft is fitted to the golfer model by modifying the shaft's bending stiffness profile in an optimization routine. The modification of the bending stiffness profile was accomplished by generating a "stiffness spline" that passed through five equally spaced points on the shaft (i.e., the butt, three points along the shaft, and the tip). The points on the spline were allowed to vary between 50% and 200% of the shaft's original bending stiffness at the respective positions of the spline points. The flexible club model requires the bending stiffness to be defined using a polynomial, so a polynomial was then fit to the spline to comply with the model. The density, cross-sectional area, and GJ

curves remained unchanged.

The golfer model was optimized in tandem with the bending stiffness profile to find the best combination of biomechanics and bending stiffness. The `patternsearch` algorithm was used for the golf swing, where the results from Section 4.4 were used as the initial guess and the same boundaries were used. For each swing in the top-level golf swing optimization, the bending stiffness profile was optimized by maximizing the carry distance, also using the `patternsearch` algorithm with an initial guess corresponding to the original bending stiffness. The result of the overall optimization is therefore a combination of optimal biomechanics and bending stiffness profile that provide the maximum carry distance.

A gain of only 1.2 yds was observed, so the optimization did not prove to be very effective. The optimized stiffness profile is shown in Fig. 5.10, where the dashed line represents the original stiffness and the shaded area represents the bounds of the spline points. The circles represent the points used to generate the stiffness spline, for which the optimal stiffness polynomial was fit. The fact that the optimization did not yield impressive gains is not surprising. The primary role of shaft stiffness is to alter the clubhead delivery in such way to improve the result of the shot. The golfer model likely found an optimal clubhead delivery with the original shaft, so it would be difficult to create an *improved* clubhead delivery with any modified shaft. Nonetheless, Tables 5.3 and 5.4 show that the optimized shaft enabled the golfer model to generate slightly more clubhead speed, angle of attack and dynamic loft, leading to a small increase in launch angle and reduction in back spin.

Because the optimized bending stiffness profile is so irregular, it is difficult to say whether the the kick point is higher or lower than the original shaft. Based on the measurements of Joyce et al. the higher tip stiffness is indicative of a higher kick point, yet the simulated clubhead delivery suggests a lower kick point. Furthermore, the biomechanics changed slightly so they could be partially responsible for the differences. In the end, the optimization was ineffective because the golfer model efficiently adapts to different equipment and can likely produce an optimal clubhead delivery with any equipment it is given. A real golfer would lack proficiency in altering their swing mechanics, so fitting a shaft to a real golfer's swing is more practical.

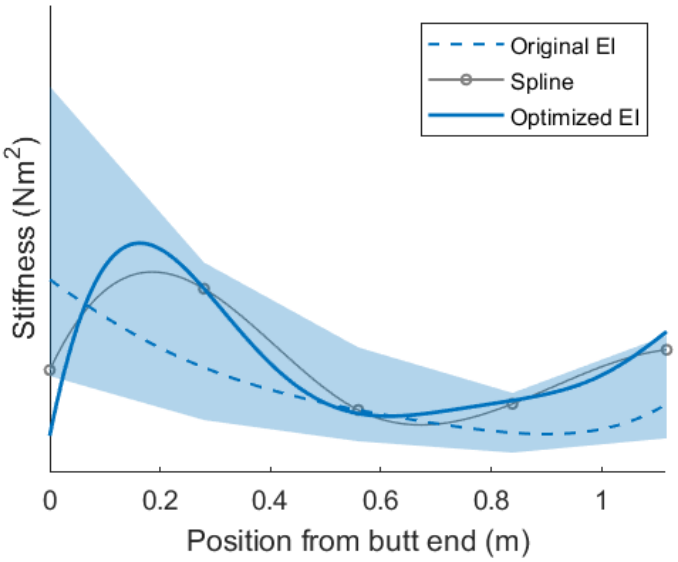

Figure 5.10: Optimized bending stiffness profile.

Table 5.3: Clubhead delivery differences for default and optimized shaft (*optimized – default*).

Clubhead Speed (km/h)	Angle of Attack (deg)	Clubhead Path (deg)	Face Angle (deg)	Dynamic Loft (deg)	Dynamic Lie (deg)	Closure Rate (rpm)	Loft Rate (rpm)	Lie Rate (rpm)
0.484	0.271	-0.057	0.000	0.179	-0.342	2.27	-3.91	1.93

Table 5.4: Launch conditions differences for default and optimized shaft (*optimized – default*).

Ball Speed (km/h)	Launch Angle (deg)	Azimuth (deg)	Back Spin (rpm)	Side Spin (rpm)
0.778	0.207	-0.0108	-124	8.38

Chapter 6

Conclusions

In this chapter, the completed work is summarized and recommendations are made based on the results of the simulation experiments. The project concludes with suggestions for future research to help improve the models presented.

6.1 Project Summary

One of the goals of this work was to advance the existing golfer model of Balzerson et al. [37]. Following the literature review in Chapter 2, many areas for improvement were identified. The improvements included modelling the backswing to eliminate shaft initialization issues, the inclusion of the pelvis to model the X-factor, the addition of another DOF in the shoulder joint enabling a dynamic arm plane, the incorporation of an internally damped shaft to mitigate unrealistic shaft deflections, and a new impact model that is compatible with the shaft and golfer in a multibody framework. After identifying these opportunities, the project progressed through the development of the golf drive, experimental validation, and finally application.

Golf Drive Model

Chapter 3 discussed all the improvements made to the golf drive model and its implementation using optimal control. With the modelling of the backswing, a new torque-velocity scaling function was required to avoid mathematical singularities during eccentric contraction. As a result, a continuous torque-velocity scaling function was formulated based on

the muscle lengthening experiments of Katz [81] using parameters from existing golf swing models. Furthermore, the active joint torque functions were modified slightly to reduce the stiffness of the system equations and reflect measured muscle force activations with greater accuracy. It was also shown in this chapter how the shoulder joint could be broken down into two degrees of freedom using the shoulder torque ratio r, which controls the plane of the golf swing.

Experimental Validation

Chapter 4 covered the experimental validation of the flexible club, impact, and biomechanical models. The use of the motion capture data provided by PING was crucial for these validations. The flexible club model was validated through comparison of the simulated and experimental shaft deflections and twist in the full-swings of elite golfers, where the simulations were driven by experimental grip kinematics. Very good agreement was observed for the shaft deflections after scaling the bending stiffness by a factor of 1.5. It was speculated that the numerically-generated stiffness profiles provided by the manufacturer underestimated the actual stiffness of the shaft.

The parameters of the impact model were identified by minimizing the difference between the simulated and experimental ball velocity and angular velocity using a training dataset. The impact model was then validated against a test dataset. Good agreement was reported for the simulated ball speed, launch angle, azimuth and backspin.

Finally, the biomechanical model was validated by comparing the simulated grip kinematics to the mean grip kinematics of the golfers in the motion capture experiment. Through optimization of carry distance, the biomechanical model reproduced the swing of an elite golfer.

Simulation Experiments

In Chapter 5, four simulation experiments were run using full-club impact simulations and the golf drive model. The first simulation experiment addressed a long-held assumption in golf engineering – that neither the shaft nor golfer can affect the impact dynamics between the clubhead and ball. By probing the reaction forces at the hosel in full-club impact simulations, it was shown that the shaft creates a stiffening effect that resists the twisting of the clubhead during contact, corresponding to a significant increase in ball speed and suppression of the gear-effect relative to free-body impacts. In the same simulation

experiment, it was shown that golfer grip forces affect the outcome of the impact in a meaningful way.

The second simulation experiment used full-club impacts to show that a nominal loft of around 8.5° is generally suitable for the elite golfer.

The third simulation experiment investigated the interaction between the golfer and clubhead mass (more specifically, clubhead material density). It was found that optimal clubhead mass greatly depends on a golfer's ability to generate clubhead speed using different masses. If the biomechanical model accurately reflects a golfer's ability to generate clubhead speed with different masses, then using a clubhead material with 75% of its original density may increase ball speed and carry distance.

A final simulation experiment investigated the possibility of optimizing a shaft's bending stiffness profile to maximize carry distance. Using the golf drive model, very little performance benefits were observed. For an actual golfer, the flexibility of the shaft can help promote a beneficial clubhead delivery. The biomechanical model adapts to different shaft flexes very effectively and thus is able to create an optimal clubhead delivery with any shaft it is given. As a result, a customized shaft stiffness profile does not benefit the biomechanical model, but may be practical for a real golfer who is less inclined to alter their biomechanics.

6.2 Recommendations

Based on the golf swing optimization performed in Section 4.4 and the results of the simulation experiments in Chapter 5, the following recommendations are made.

1. A golfer may benefit from teeing the ball far forward in the stance and as high as possible in order to maximize angle of attack and dynamic loft and increase carry distance.

2. Shaft reaction forces during impact alter the launch conditions of the golf ball significantly and should be taken into consideration when designing a driver clubhead.

3. Grip forces affect spin generation and should be included in full-club impact simulations.

4. A nominal loft angle of 8.5° is suitable for the elite golfer demographic.

5. Optimal clubhead mass largely depends on a golfer's ability to generate clubhead speed using different clubhead masses and should therefore be evaluated on a case-by-case basis.

6.3 Future Research

As is, the golf drive model could be used to run countless more simulation experiments. To name a few, the model could be used to:

- investigate the effect of vertical clubhead MOI on golfer biomechanics,
- investigate the effect of clubhead CG position on golfer biomechanics and impact efficiency,
- determine the optimal clubface curvature (bulge/roll radius),
- examine the role of shaft stiffness in generating clubhead speed, or
- assess the benefits of a longer/shorter backswing.

However, the core focus of future research should be concerned with improving the accuracy of the model. Improvements to the model would strengthen the significance of simulation experiment results. Outlined below are some recommended modelling improvements that could be pursued in future research.

Biomechanics

1. A biomechanical dynamometer (Biodex Medical Systems, Shirley, NY, USA) could be used to obtain subject-specific passive and active torque curves for some of the degrees of freedom in the biomechanical model. The passive and active torque function parameters may be identified using the collected data, or the experimental data may be used to drive the model directly.
2. Measurement of the passive resistance of the pelvis in rotation relative to the ground. A typical biomechanical dynamometer will not accommodate such a movement so a custom experiment would need to be designed. The results would help improve the pelvis behaviour in the model and enhance the significance of the model's X-factor.

3. There are many biomechanical degrees of freedom that could be added, at the expense of computational resources required for optimization. Options include the trailing arm, the lower limbs, and torso rotation in the sagittal plane (lean).

4. The joint torque framework could be replaced with a high-fidelity musculoskeletal model, including muscle kinematics and dynamics [114, 115]. Motion may be controlled using muscle synergies, as demonstrated by Razavian et al. [116]. If such a model were pursued, it is recommended that the model be applied to the shoulder complex. A musculoskeletal model could be used to determine which muscles contribute most to the golf swing, and which muscles may be at a higher risk for injury.

Flexible Club

1. More work should be completed to address the twist error of the flexible club model. Experiments utilizing a more accurate method for measuring torsional deformation, such as strain gauges, should be pursued and compared with simulations using the flexible club model. If the torsional deformation error persists, modifications to the analytical formulation of the flexible beam should be considered to improve its accuracy.

2. There is a need for a device that measures the bending (EI) and torsional (GJ) stiffness profiles of a golf shaft empirically. Some manufacturers use simple numerical models to estimate stiffness profiles, but these models may not be accurate, as demonstrated in this work. Using the empirically determined stiffness profiles, the static and dynamic behaviour of MapleSim's flexible beam component should then be verified using experiments.

Impact

1. Additional golf swing motion capture experiments should be conducted to provide a richer dataset for the impact model parameter identification. Using measured ball speeds and impact locations, the degradation of COR across the clubface should be accommodated so that the impact model can be validated for off-center impacts.

2. Alternative friction/tangential compliance models should be considered in attempt to reproduce experimental tangential force histories [99, 104]. The large spike in friction

created by the current model during slip (see Fig. 4.8b) is not observed in empirical tangential force histories.

Ball Flight

1. New golf ball aerodynamic coefficients should be obtained through experiments using modern golf balls. Golf ball aerodynamics have advanced considerably since the ball flight model of Quintavalla [39] was developed in 2002. Some high-end launch monitors such as the TrackMan 4 (TrackMan Golf, Copenhagen, Denmark) exploit radar technology to track the golf ball's entire flight. Aerodynamic coefficients could be determined through optimization, by minimizing the difference between simulated and measured ball flights.

2. Currently, the golf drive model does not consider the run of the golf ball (bounce and roll after initial contact with the ground). Penner [117] developed a model for the run of the golf ball, but did not provide experimental validation. Including the run of the golf ball may affect optimization results. For example, a shot with a higher trajectory may carry further than a shot with a lower trajectory, but the latter may roll-out further than the former, providing greater overall distance. Ground conditions on golf courses vary considerably so a run model should be developed and validated for a perfectly flat, archetypal fairway.

References

[1] HSBC, "Golf's 2020 vision: The HSBC report," 2012. Available at http://www.golf.org.au/site/_content/document/00017543-source.pdf.

[2] R&A, "Golf around the world 2017," 2017. Available at https://www.randa.org/~/media/Files/DownloadsAndPublications/Golf-around-the-world-2017.ashx.

[3] Statistics Canada, "Sport participation 2010," February 2014. Available at http://publications.gc.ca/collections/collection_2013/pc-ch/CH24-1-2012-eng.pdf.

[4] S. Stinson, "Golf industry scrambles to innovate in trying times," July 2017. Available at http://torontosun.com/2017/07/20/stinson-golf-industry-forced-to-innovate-in-period-of-decline/wcm/52dab002-c0ce-443e-95f0-f843920ad92b.

[5] R. Fuhrmann, "The future outlook of the golf industry," August 2015. Available at https://www.investopedia.com/articles/personal-finance/081815/future-outlook-golf-industry.asp.

[6] National Golf Foundation, "Golf participation in the U.S. 2017 edition," 2017. Available at http://www.mobilegolfevents.net/uploads/2/2/7/9/22799670/2017ngf_golferparticipation.pdf.

[7] E. Matuszewski, "Here's why we should be bullish about golf in 2017," January 2017. Available at https://www.forbes.com/sites/erikmatuszewski/2017/01/23/heres-why-we-should-be-bullish-about-golf-in-2017/.

[8] D. Dusek, "Average driving distance on PGA Tour hasn't changed much in more than a decade," December 2015. Available at http://golfweek.com/2015/12/22/average-driving-distance-pga-tour-hasnt-changed-much-decade/.

[9] A. J. Cochran and J. Stobbs, *The Search for the Perfect Swing: An account of the golf society of great Britain scientific study.* Heinemann, 1968.

[10] S. M. Nesbit, "A three dimensional kinematic and kinetic study of the golf swing," *Journal of Sports Science & Medicine*, vol. 4, no. 4, pp. 499–519, 2005.

[11] E. Otten, "Inverse and forward dynamics: models of multi–body systems," *Philosophical Transactions of the Royal Society of London B: Biological Sciences*, vol. 358, no. 1437, pp. 1493–1500, 2003.

[12] N. Betzler, S. Monk, E. Wallace, S. Otto, and G. Shan, "From the double pendulum model to full-body simulation: Evolution of golf swing modeling," *Sports Technology*, vol. 1, no. 4-5, pp. 175–188, 2008.

[13] S. M. Nesbit and M. Serrano, "Work and power analysis of the golf swing," *Journal of Sports Science & Medicine*, vol. 4, no. 4, pp. 520–533, 2005.

[14] D. E. Anderson, M. L. Madigan, and M. A. Nussbaum, "Maximum voluntary joint torque as a function of joint angle and angular velocity: model development and application to the lower limb," *Journal of Biomechanics*, vol. 40, no. 14, pp. 3105–3113, 2007.

[15] T. Jorgensen Jr, "On the dynamics of the swing of a golf club," *American Journal of Physics*, vol. 38, no. 5, pp. 644–651, 1970.

[16] M. Lampsa, "Maximizing distance of the golf drive: an optimal control study," *Journal of Dynamic Systems, Measurement, and Control, Transactions ASME*, vol. 97, no. Series G), Dec, pp. 362–367, 1975.

[17] W. Pickering and G. Vickers, "On the double pendulum model of the golf swing," *Sports Engineering*, vol. 2, no. 3, pp. 161–172, 1999.

[18] K. Miura, "Parametric acceleration–the effect of inward pull of the golf club at impact stage," *Sports Engineering*, vol. 4, no. 2, pp. 75–86, 2001.

[19] C. Chen, Y. Inoue, and K. Shibara, "Numerical study on the wrist action during the golf downswing," *Sports Engineering*, vol. 10, no. 1, pp. 23–31, 2007.

[20] R. D. Milne and J. P. Davis, "The role of the shaft in the golf swing," *Journal of Biomechanics*, vol. 25, no. 9, pp. 975–983, 1992.

[21] T. P. Jorgensen, *The physics of golf.* Springer Science & Business Media, 1999.

[22] E. J. Sprigings and S. Mackenzie, "Examining the delayed release in the golf swing using computer simulation," *Sports Engineering*, vol. 5, no. 1, pp. 23–32, 2002.

[23] E. J. Sprigings and R. J. Neal, "An insight into the importance of wrist torque in driving the golfball: a simulation study," *Journal of Applied Biomechanics*, vol. 16, no. 4, pp. 356–366, 2000.

[24] A. Hill, "The heat of shortening and the dynamic constants of muscle," *Proceedings of the Royal Society of London B: Biological Sciences*, vol. 126, no. 843, pp. 136–195, 1938.

[25] R. M. Alexander, "Optimum take-off techniques for high and long jumps," *Philosophical Transactions of the Royal Society of London B: Biological Sciences*, vol. 329, no. 1252, pp. 3–10, 1990.

[26] P. De Leva, "Adjustments to zatsiorsky-seluyanov's segment inertia parameters," *Journal of Biomechanics*, vol. 29, no. 9, pp. 1223–1230, 1996.

[27] E. J. Sprigings, "Simulation of the force enhancement phenomenon in muscle," *Computers in Biology and Medicine*, vol. 16, no. 6, pp. 423–430, 1986.

[28] R. Neal, D. Burko, E. Sprigings, and R. Landeo, "Segment interactions during the golf swing: 3 segments in 3d," in *International Society of Biomechanics XVIIth Congress*, pp. 690–690, University of Calgary, 1999.

[29] M. J. Powell, "An efficient method for finding the minimum of a function of several variables without calculating derivatives," *The Computer Journal*, vol. 7, no. 2, pp. 155–162, 1964.

[30] S. J. MacKenzie and E. J. Sprigings, "A three-dimensional forward dynamics model of the golf swing," *Sports Engineering*, vol. 11, no. 4, pp. 165–175, 2009.

[31] C. Vaughan, "A three-dimensional analysis of the forces and torques applied by a golfer during the downswing," *Biomechanics VII-B*, pp. 325–331, 1981.

[32] R. J. Neal and B. D. Wilson, "3d kinematics and kinetics of the golf swing," *International journal of sport biomechanics*, vol. 1, no. 3, pp. 221–232, 1985.

[33] F. Tinmark, J. Hellström, K. Halvorsen, and A. Thorstensson, "Elite golfers' kinematic sequence in full-swing and partial-swing shots," *Sports Biomechanics*, vol. 9, no. 4, pp. 236–244, 2010.

[34] S. MacKenzie, *Understanding the role of shaft stiffness in the golf swing.* PhD thesis, University of Saskatchewan, 2005.

[35] S. J. MacKenzie and E. J. Sprigings, "Understanding the role of shaft stiffness in the golf swing," *Sports engineering*, vol. 12, no. 1, pp. 13–19, 2009.

[36] S. J. MacKenzie and D. E. Boucher, "The influence of golf shaft stiffness on grip and clubhead kinematics," *Journal of sports sciences*, vol. 35, no. 2, pp. 105–111, 2017.

[37] D. Balzerson, J. Banerjee, and J. McPhee, "A three-dimensional forward dynamic model of the golf swing optimized for ball carry distance," *Sports Engineering*, vol. 19, no. 4, pp. 237–250, 2016.

[38] W. Petersen and J. McPhee, "Comparison of impulse-momentum and finite element models for impact between golf ball and clubhead," in *Science and Golf V: proceedings of the World Scientific Congress of Golf, Phoenix*, 2008.

[39] S. Quintavalla, "A generally applicable model for the aerodynamic behavior of golf balls," *Science and Golf IV, Routledge*, 2002.

[40] J. Myers, S. Lephart, Y.-s. Tsai, T. Sell, J. Smoliga, and J. Jolly, "The role of upper torso and pelvis rotation in driving performance during the golf swing," *Journal of sports sciences*, vol. 26, no. 2, pp. 181–188, 2008.

[41] A. M. Burden, P. N. Grimshaw, and E. S. Wallace, "Hip and shoulder rotations during the golf swing of sub-10 handicap players," *Journal of sports sciences*, vol. 16, no. 2, pp. 165–176, 1998.

[42] P. Cheetham, P. Martin, R. Mottram, and B. St Laurent, "The importance of stretching the x factor in the golf downswing," in *International Congress on Sport Science, Sports Medicine and Physical Education., Brisbane, QLD*, pp. 7–12, 2000.

[43] S. M. Lephart, J. M. Smoliga, J. B. Myers, T. C. Sell, and T. Yung-Shen, "An eight-week golf-specific exercise program improves physical characteristics, swing mechanics, and golf performance in recreational golfers," *Journal of Strength and conditioning Research*, vol. 21, no. 3, p. 860, 2007.

[44] Y. Chu, T. C. Sell, and S. M. Lephart, "The relationship between biomechanical variables and driving performance during the golf swing," *Journal of sports sciences*, vol. 28, no. 11, pp. 1251–1259, 2010.

[45] J. An, G. Wulf, and S. Kim, "Increased carry distance and x-factor stretch in golf through an external focus of attention," *Journal of Motor Learning and Development*, vol. 1, no. 1, pp. 2–11, 2013.

[46] G. S. Gluck, J. A. Bendo, and J. M. Spivak, "The lumbar spine and low back pain in golf: a literature review of swing biomechanics and injury prevention," *The Spine Journal*, vol. 8, no. 5, pp. 778–788, 2008.

[47] K. Arakawa, T. Mada, H. Komatsu, T. Shimizu, M. Satou, K. Takehara, and G. Etoh, "Dynamic deformation behavior of a golf ball during normal impact," *Experimental mechanics*, vol. 49, no. 4, pp. 471–477, 2009.

[48] T. Tamaogi, Y. Sogabe, Z. Wu, and T. Yokoyama, "Identification of mechanical models for golf ball materials using a viscoelastic split hopkinson pressure bar," *Journal of Dynamic Behavior of Materials*, pp. 1–14, 2017.

[49] B. Lieberman and S. Johnson, "An analytical model for ball-barrier impart, part 1 and part 2," in *Proceedings of the 1994 World Scientific Congress of Golf, St. Andrews, Scotland*, pp. 309–319, 1994.

[50] A. J. Cochran, "Development and use of one-dimensional models of a golf ball," *Journal of sports sciences*, vol. 20, no. 8, pp. 635–641, 2002.

[51] T. Yamaguchi and T. Iwatsubo, "Optimum design of golf club considering the mechanical impedance matching," in *Science and golf III: proceeding of the World Scientific Congress of Golf, St Andrews*, 1998.

[52] P. Chou, D. Liang, J. Yang, and W. Gobush, "Contact forces, coefficient of restitution, and spin rate of golf ball impact," *Science and Golf II, E & FN Spon*, 1994.

[53] S. Ujihashi, Y. Hirahara, T. Adachi, and H. Matsumoto, "Measurement and evaluation of restitution characteristic of golf balls," *Trans Jpn Soc Mech Eng C*, vol. 60, no. 577, pp. 3150–3156, 1994.

[54] USGA and R&A, "Initial velocity test procedure," February 2011. Available at https://www.usga.org/content/dam/usga/pdf/Equipment/TPX3007-initial-velocity-test-procedure.pdf.

[55] USGA and R&A, "Procedure for measuring the flexibility of a golf clubhead," May 2008. Available at https://www.usga.org/content/dam/usga/pdf/Equipment/TPX3004-procedure-for-measuring-the-flexibility-of-a-golf-clubhead.pdf.

[56] D. Winfield and T. E. Tan, "Optimization of clubhead loft and swing elevation angles for maximum distance of a golf drive," *Computers & structures*, vol. 53, no. 1, pp. 19–25, 1994.

[57] D. Winfield and T. E. Tan, "Optimization of the clubface shape of a golf driver to minimize dispersion of off-center shots," *Computers & structures*, vol. 58, no. 6, pp. 1217–1224, 1996.

[58] A. R. Penner, "The physics of golf: The optimum loft of a driver," *American journal of physics*, vol. 69, no. 5, pp. 563–568, 2001.

[59] A. R. Penner, "The physics of golf: The convex face of a driver," *American Journal of Physics*, vol. 69, no. 10, pp. 1073–1081, 2001.

[60] W. Petersen, "Dynamics of impact between golf clubhead and ball," *Diplomathesis, Institute for Mechanics and Ocean Engineering, Hamburg University of Technology*, 2007.

[61] D. Roylance, "Engineering viscoelasticity," *Department of Materials Science and Engineering–Massachusetts Institute of Technology, Cambridge MA*, vol. 2139, pp. 1–37, 2001.

[62] C. Van Sligtenhorst, D. S. Cronin, and G. W. Brodland, "High strain rate compressive properties of bovine muscle tissue determined using a split hopkinson bar apparatus," *Journal of biomechanics*, vol. 39, no. 10, pp. 1852–1858, 2006.

[63] K. Tanaka, F. Sato, H. Oodaira, Y. Teranishi, F. Sato, and S. Ujihashi, "Construction of the finite-element models of golf balls and simulations of their collisions," *Proceedings of the Institution of Mechanical Engineers, Part L: Journal of Materials: Design and Applications*, vol. 220, no. 1, pp. 13–22, 2006.

[64] T. Iwatsubo, S. Kawamura, K. Miyamoto, and T. Yamaguchi, "Numerical analysis of golf club head and ball at various impact points," *Sports Engineering*, vol. 3, no. 4, pp. 195–204, 2000.

[65] M. Kai, "Science and engineering technology behind bridgestone tour golf balls," *Sports Technology*, vol. 1, no. 1, pp. 57–64, 2008.

[66] USGA, "Procedure for measuring the moment of inertia of golf clubheads," 2006. Available at https://www.usga.org/content/dam/usga/pdf/Equipment/TPX3005-procedure-for-measuring-the-moment-of-inertia_of_golf_clubheads.pdf.

[67] W. McNally, D. Balzerson, D. Wilson, and J. McPhee, "Effect of clubhead inertial properties and driver face geometry on golf ball trajectories," *Procedia Engineering*, vol. 147, pp. 407–412, 2016.

[68] A. Hocknell, S. R. Mitchell, R. Jones, and S. Rothberg, "Hollow golf club head modal characteristics: determination and impact applications," *Experimental mechanics*, vol. 38, no. 2, pp. 140–146, 1998.

[69] W. Petersen and J. McPhee, "Shape optimization of golf clubface using finite element impact models," *Sports Engineering*, vol. 12, no. 2, pp. 77–85, 2009.

[70] K. Tanaka, H. Oodaira, Y. Teranishi, F. Sato, and S. Ujihashi, "Finite-element analysis of the collision and bounce between a golf ball and simplified clubs (p271)," *The Engineering of Sport 7*, pp. 653–662, 2008.

[71] R. Cross and A. M. Nathan, "Experimental study of the gear effect in ball collisions," *American Journal of Physics*, vol. 75, no. 7, pp. 658–664, 2007.

[72] Y. Gonthier, J. McPhee, C. Lange, and J.-C. Piedbœuf, "A contact modeling method based on volumetric properties," in *Proceedings of the ASME 5th International Conference on Multibody Systems, Nonlinear Dynamics, and Control*, vol. 5, pp. 477–486, 2005.

[73] M. Boos and J. McPhee, "Volumetric modeling and experimental validation of normal contact dynamic forces," *Journal of Computational and Nonlinear Dynamics*, vol. 8, no. 2, p. 021006, 2013.

[74] P. Brown, "Contact modelling for forward dynamics of human motion," Master's thesis, University of Waterloo, 2017.

[75] P. Brown and J. McPhee, "A continuous velocity-based friction model for dynamics and control with physically meaningful parameters," *Journal of Computational and Nonlinear Dynamics*, vol. 11, no. 5, p. 054502, 2016.

[76] A. C. Smith, J. R. Roberts, E. S. Wallace, P. Kong, and S. E. Forrester, "Comparison of two-and three-dimensional methods for analysis of trunk kinematic variables in the golf swing," *Journal of applied biomechanics*, vol. 32, no. 1, pp. 23–31, 2016.

[77] F. S. Grassia, "Practical parameterization of rotations using the exponential map," *Journal of graphics tools*, vol. 3, no. 3, pp. 29–48, 1998.

[78] V. Zatsiorsky, V. Seluyanov, and L. Chugunova, "Methods of determining mass-inertial characteristics of human body segments," *Contemporary problems of biomechanics*, vol. 272, p. 291, 1990.

[79] C. Moler, "Stiff differential equations." Available at https://www.mathworks.com/company/newsletters/articles/stiff-differential-equations.html.

[80] I. E. Brown and G. E. Loeb, "Measured and modeled properties of mammalian skeletal muscle: Iv. dynamics of activation and deactivation," *Journal of muscle research and cell motility*, vol. 21, no. 1, pp. 33–47, 2000.

[81] B. Katz, "The relation between force and speed in muscular contraction," *The Journal of Physiology*, vol. 96, no. 1, pp. 45–64, 1939.

[82] A. J. van Soest and M. F. Bobbert, "The contribution of muscle properties in the control of explosive movements," *Biological cybernetics*, vol. 69, no. 3, pp. 195–204, 1993.

[83] Y. Yoon and J. Mansour, "The passive elastic moment at the hip," *Journal of biomechanics*, vol. 15, no. 12, pp. 905–910, 1982.

[84] P. Hoang, R. Gorman, G. Todd, S. Gandevia, and R. Herbert, "A new method for measuring passive length–tension properties of human gastrocnemius muscle in vivo," *Journal of biomechanics*, vol. 38, no. 6, pp. 1333–1341, 2005.

[85] G. T. Yamaguchi, *Dynamic modeling of musculoskeletal motion: a vectorized approach for biomechanical analysis in three dimensions*. Springer Science & Business Media, 2005.

[86] S. McGill, J. Seguin, and G. Bennett, "Passive stiffness of the lumber torso in flexion, extension, lateral bending, and axial roatation: Effect of belt wearing and breath holding.," *Spine*, vol. 19, no. 6, pp. 696–704, 1994.

[87] A. Engin and S.-M. Chen, "Statistical data base for the biomechanical properties of the human shoulder complex—i: Kinematics of the shoulder complex," *Journal of biomechanical engineering*, vol. 108, no. 3, pp. 215–221, 1986.

[88] A. Engin and S.-M. Chen, "Statistical data base for the biomechanical properties of the human shoulder complex—ii: passive resistive properties beyond the shoulder complex sinus," *Journal of biomechanical engineering*, vol. 108, no. 3, pp. 222–227, 1986.

[89] A. E. Engin, "Passive resistive torques about long bone axes of major human joints.," *Aviation, space, and environmental medicine*, vol. 50, no. 10, pp. 1052–1057, 1979.

[90] D. Formica, S. K. Charles, L. Zollo, E. Guglielmelli, N. Hogan, and H. I. Krebs, "The passive stiffness of the wrist and forearm," *Journal of neurophysiology*, vol. 108, no. 4, pp. 1158–1166, 2012.

[91] P. Shi, J. McPhee, and G. Heppler, "A deformation field for euler–bernoulli beams with applications to flexible multibody dynamics," *Multibody System Dynamics*, vol. 5, no. 1, pp. 79–104, 2001.

[92] C. Schmitke and J. McPhee, "Using linear graph theory and the principle of orthogonality to model multibody, multi-domain systems," *Advanced Engineering Informatics*, vol. 22, no. 2, pp. 147–160, 2008.

[93] P. Shi, J. McPhee, and G. Heppler, "Polynomial shape functions and numerical methods for flexible multibody dynamics," 2001.

[94] S. Sandhu, M. Millard, J. McPhee, and D. Brekke, "3d dynamic modelling and simulation of a golf drive," *Procedia Engineering*, vol. 2, no. 2, pp. 3243–3248, 2010.

[95] M. Strangwood, A. Johnson, and S. Otto, "Energy losses in viscoelastic golf balls," *Proceedings of the Institution of Mechanical Engineers, Part L: Journal of Materials: Design and Applications*, vol. 220, no. 1, pp. 23–30, 2006.

[96] R. Cross, "The bounce of a ball," *American Journal of Physics*, vol. 67, no. 3, pp. 222–227, 1999.

[97] Y. Gonthier, J. McPhee, C. Lange, and J.-C. Piedboeuf, "A regularized contact model with asymmetric damping and dwell-time dependent friction," *Multibody System Dynamics*, vol. 11, no. 3, pp. 209–233, 2004.

[98] M. Nakasuga and R. Hashimoto, "Measurement of tangential force of golf ball impact," *Proceedings of the Japan Society of Mechanical Engineers*, pp. 97–10, 1997.

[99] R. Cross, "Grip-slip behavior of a bouncing ball," *American Journal of Physics*, vol. 70, no. 11, pp. 1093–1102, 2002.

[100] N. Maw, J. Barber, and J. Fawcett, "The oblique impact of elastic spheres," *Wear*, vol. 38, no. 1, pp. 101–114, 1976.

[101] N. Maw, J. Barber, and J. Fawcett, "The role of elastic tangential compliance in oblique impact," *Journal of Lubrication Technology*, vol. 103, no. 1, pp. 74–80, 1981.

[102] J. Axe, "Spin dynamics," in *Proceedings of the 1994 World Scientific Congress of Golf, St. Andrews, Scotland*, 1994.

[103] W. Stronge, R. James, and B. Ravani, "Oblique impact with friction and tangential compliance," *Philosophical Transactions of the Royal Society of London A: Mathematical, Physical and Engineering Sciences*, vol. 359, no. 1789, pp. 2447–2465, 2001.

[104] USGA and R&A, "Second report on the study of spin generation," 2011.

[105] S. J. MacKenzie and E. J. Sprigings, "Understanding the mechanisms of shaft deflection in the golf swing," *Sports Engineering*, vol. 12, no. 2, pp. 69–75, 2009.

[106] J. R. Roberts, R. Jones, and S. Rothberg, "Measurement of contact time in short duration sports ball impacts: an experimental method and correlation with the perceptions of elite golfers," *Sports Engineering*, vol. 4, no. 4, pp. 191–203, 2001.

[107] D. W. Meister, A. L. Ladd, E. E. Butler, B. Zhao, A. P. Rogers, C. J. Ray, and J. Rose, "Rotational biomechanics of the elite golf swing: benchmarks for amateurs," *Journal of Applied Biomechanics*, vol. 27, no. 3, pp. 242–251, 2011.

[108] S. A. Horan, K. Evans, N. R. Morris, and J. J. Kavanagh, "Thorax and pelvis kinematics during the downswing of male and female skilled golfers," *Journal of biomechanics*, vol. 43, no. 8, pp. 1456–1462, 2010.

[109] PGA Tour, "Smash factor statistics, 2017." Available at https://www.pgatour.com/stats/stat.02403.2017.html.

[110] R. White, "On the efficiency of the golf swing," *American Journal of Physics*, vol. 74, no. 12, pp. 1088–1094, 2006.

[111] D. Johnson, "A three-dimensional forward dynamic model of the golf swing," Master's thesis, University of Waterloo, 2015. Available at https://uwspace.uwaterloo.ca/handle/10012/9158.

[112] D. Howell, "The design of filament wound graphite/epoxy golf shafts," *Materials Working for You in the 21 st Century*, pp. 1392–1405, 1992.

[113] C. Joyce, A. Burnett, A. Reyes, and S. Herbert, "A dynamic evaluation of how kick point location influences swing parameters and related launch conditions," *Proceedings of the Institution of Mechanical Engineers, Part P: Journal of Sports Engineering and Technology*, vol. 228, no. 2, pp. 111–119, 2014.

[114] N. Mehrabi, R. S. Razavian, and J. McPhee, "A physics-based musculoskeletal driver model to study steering tasks," *Journal of Computational and Nonlinear Dynamics*, vol. 10, no. 2, p. 021012, 2015.

[115] N. Mehrabi, R. Sharif Razavian, B. Ghannadi, and J. McPhee, "Predictive simulation of reaching moving targets using nonlinear model predictive control," *Frontiers in Computational Neuroscience*, vol. 10, p. 143, 2017.

[116] R. S. Razavian, N. Mehrabi, and J. McPhee, "A model-based approach to predict muscle synergies using optimization: application to feedback control," *Frontiers in computational neuroscience*, vol. 9, 2015.

[117] A. R. Penner, "The run of a golf ball," *Canadian Journal of Physics*, vol. 80, no. 8, pp. 931–940, 2002.

APPENDICES

Appendix A

Mean Clubhead Deliveries and Launch Conditions from Motion Capture Experiment

Table A.1: Mean clubhead deliveries from motion capture experiment

Golfer	Clubhead Speed (km/h)	Angle of Attack (deg)	Clubhead Path (deg)	Face Angle (deg)	Dynamic Loft (deg)	Dynamic Lie (deg)	Closure Rate (rpm)	Loft Rate (rpm)	Lie Rate (rpm)
1*	185 ± 0.438	-3.65 ± 0.565	2.2 ± 1.69	1.08 ± 1.47	12.2 ± 0.37	58.2 ± 0.256	400 ± 12.5	193 ± 13.4	7.95 ± 8.34
2	173 ± 1.26	0.616 ± 1.22	4.32 ± 0.894	2.58 ± 1.27	17.4 ± 1.5	55.4 ± 0.515	442 ± 13.5	107 ± 13	-2.77 ± 7.23
3	183 ± 0.829	2.31 ± 0.525	6.3 ± 0.723	4.62 ± 0.935	12.7 ± 0.653	57.5 ± 0.44	389 ± 10.4	204 ± 8.81	-33.8 ± 5.23
4	184 ± 1.18	2.32 ± 0.773	4.48 ± 1.52	2.74 ± 2.43	17.7 ± 1.53	58.1 ± 0.75	517 ± 16.6	104 ± 19.2	-25.5 ± 9.66
5	148 ± 1.42	3.76 ± 1.06	6.04 ± 0.462	2.34 ± 2.54	17.6 ± 1.88	58.5 ± 0.443	601 ± 24	-33 ± 16.6	-41.4 ± 11.9
6	169 ± 0.714	1.15 ± 1.23	4.94 ± 0.778	4.69 ± 1.76	13.4 ± 1.28	57.8 ± 0.474	381 ± 35.1	194 ± 33.2	1.25 ± 9.97
7	184 ± 1.9	-0.0664 ± 0.765	1.13 ± 1.17	0.569 ± 1.61	15.6 ± 1.19	52.9 ± 0.546	466 ± 8.47	138 ± 12	13.7 ± 6.81
8	182 ± 1.12	1.72 ± 0.754	6.12 ± 0.997	3.72 ± 1.42	14.8 ± 1.03	55.9 ± 0.694	372 ± 12.3	211 ± 10.5	-43 ± 6.21
9	193 ± 1.59	0.604 ± 0.921	4.78 ± 0.861	3.38 ± 1.07	15.3 ± 0.715	58.6 ± 0.563	503 ± 15.3	158 ± 14.6	-23.2 ± 13.8
10	181 ± 1.33	2.74 ± 0.95	4.25 ± 1.21	2.3 ± 1.12	15.7 ± 0.762	56.9 ± 0.78	461 ± 15.2	121 ± 10.9	-32.6 ± 7.59

Clubhead speed and direction measured at CG. Angle of attack positive about -Y, beginning at X. Club path and face angle positive about -Z, beginning at X. Dynamic loft measured as the angle between X_C and the XY plane, positive about -Y. Dynamic lie measured by projecting the Y_C onto the YZ plane and adding the static lie angle. Closure rate, loft rate and lie rate positive about Z, Y, and X, respectively. Refer to Fig. 4.1 for different frames of reference.

*only 7 swings were recorded for Golfer 1.

Table A.2: Mean launch conditions from motion capture experiment

Golfer	Ball Speed (km/h)	Launch Angle (deg)	Azimuth (deg)	Back Spin (rpm)	Side Spin (rpm)
1*	264 ± 2.39	10.1 ± 0.501	0.763 ± 1.64	3170 ± 234	-201 ± 302
2	242 ± 3.61	15.9 ± 1.54	0.422 ± 1.12	3020 ± 307	-455 ± 327
3	264 ± 1.74	12.1 ± 0.822	2.69 ± 0.741	1960 ± 239	-179 ± 281
4	258 ± 4.13	16.8 ± 1.18	3.13 ± 1.33	2630 ± 318	-778 ± 384
5	212 ± 2.62	15.4 ± 1.52	0.725 ± 2.27	2460 ± 374	-696 ± 366
6	243 ± 5.62	13.1 ± 1.53	2.39 ± 1.37	1990 ± 416	42.5 ± 368
7	258 ± 6.51	14.5 ± 1.15	-1.62 ± 2.06	2980 ± 352	119 ± 368
8	261 ± 2.38	13.1 ± 1.48	1.92 ± 1.82	2560 ± 326	-403 ± 213
9	267 ± 4.41	14.7 ± 0.975	0.61 ± 1.86	2710 ± 257	-216 ± 237
10	261 ± 1.88	13.7 ± 1.03	2.85 ± 1.47	2610 ± 364	-485 ± 257

Positive launch angle is measured about the -Y axis, and positive azimuth and side spin about the -Z axis. Refer to Fig. 4.1 for global reference frame.
*only 7 swings were recorded for Golfer 1.

Appendix B

Simulated versus Experimental Shaft Deflection (Golfers 1-9)

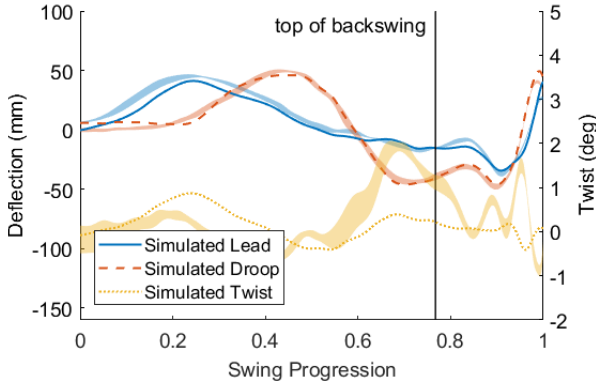

(a) Golfer 1

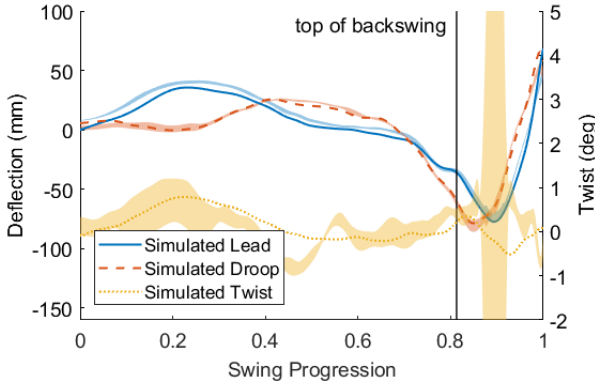

(b) Golfer 2

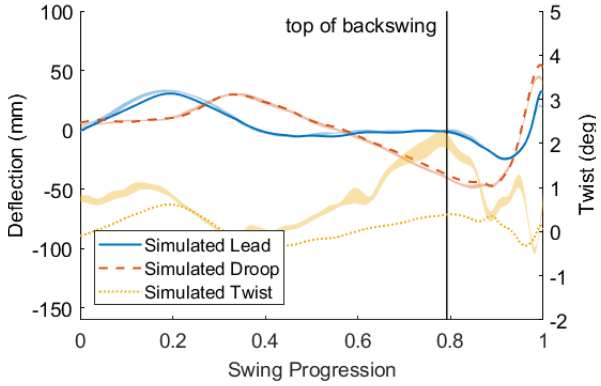

(c) Golfer 3

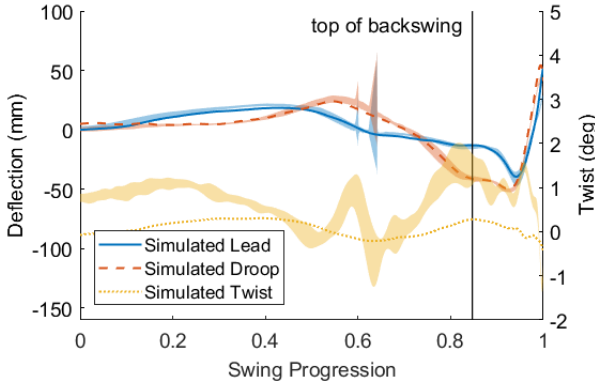

(d) Golfer 4

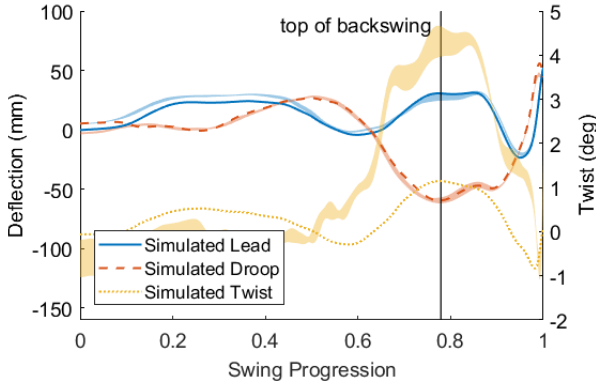

(e) Golfer 5

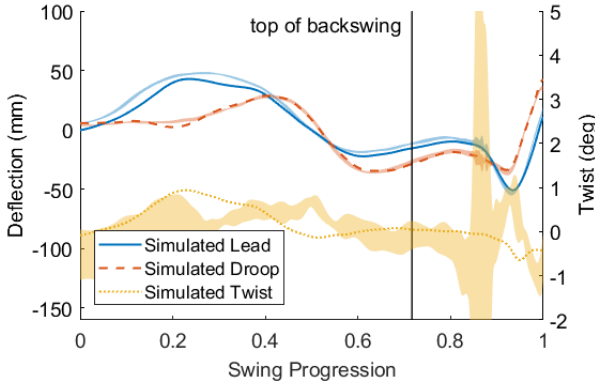

(f) Golfer 6

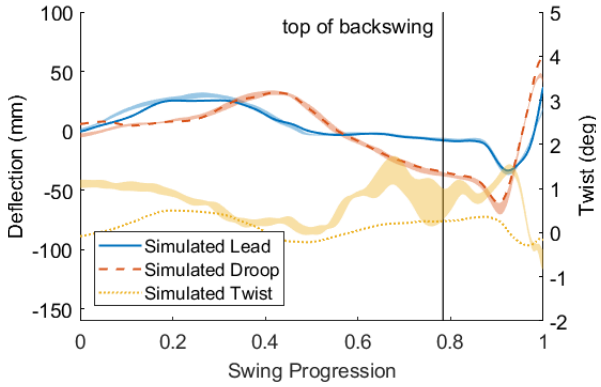

(g) Golfer 7

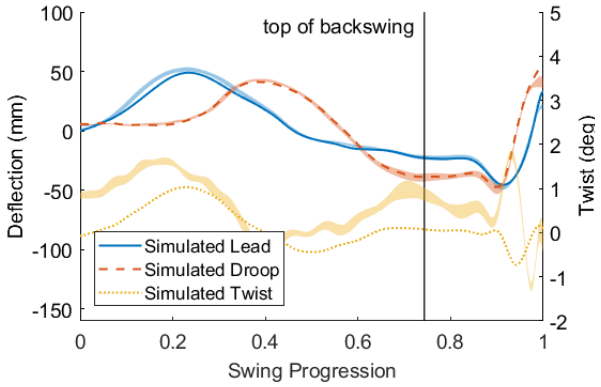

(h) Golfer 8

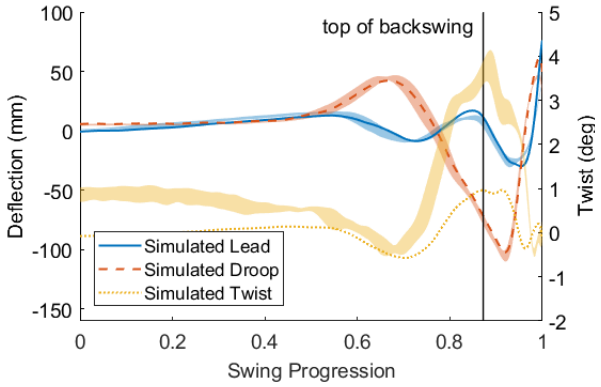

(i) Golfer 9

Figure B.1: Simulated vs. experimental shaft deflections and twist using scaled bending stiffness (Golfers 1 - 9)

Appendix C

Simulated Grip Forces (Golfers 1-9)

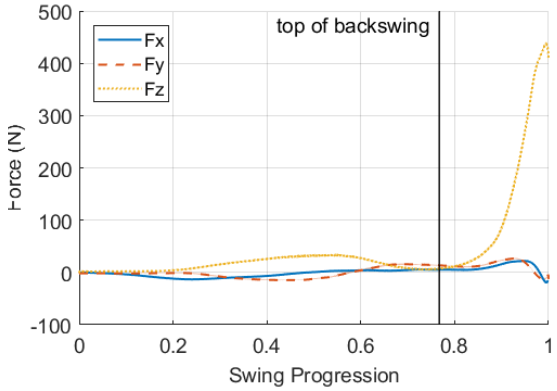

(a) Golfer 1 Force

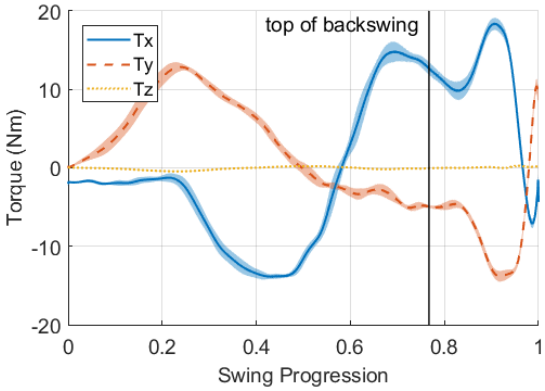

(b) Golfer 1 Torque

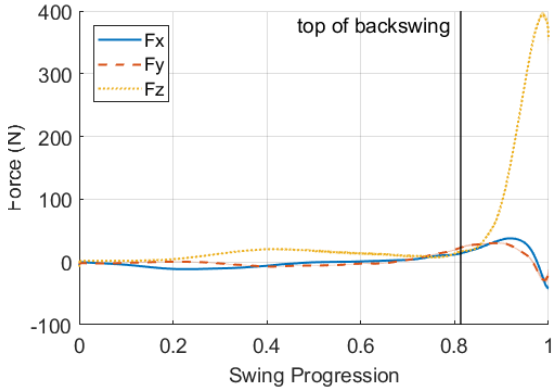

(c) Golfer 2 Force

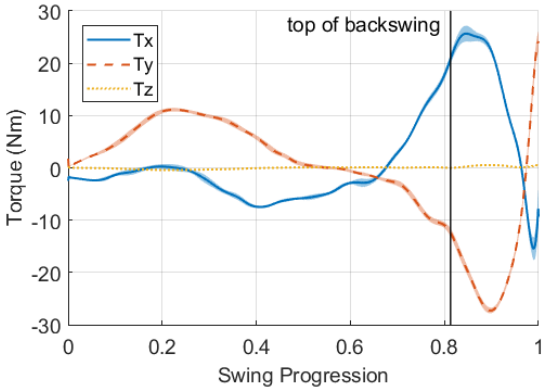

(d) Golfer 2 Torque

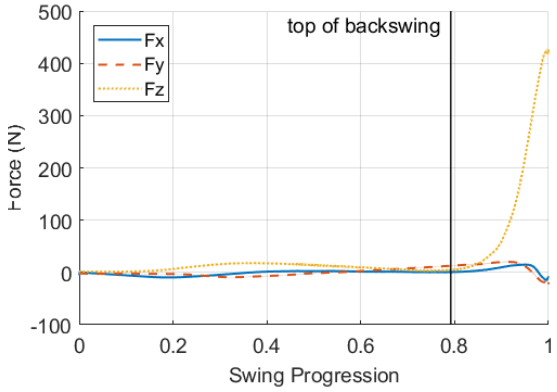

(e) Golfer 3 Force

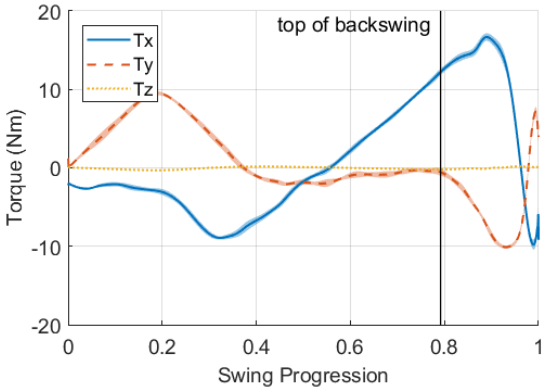

(f) Golfer 3 Torque

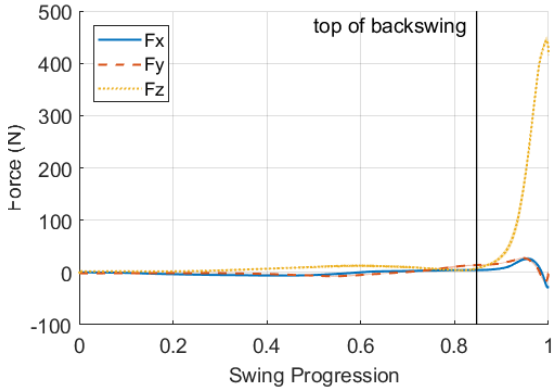

(g) Golfer 4 Force

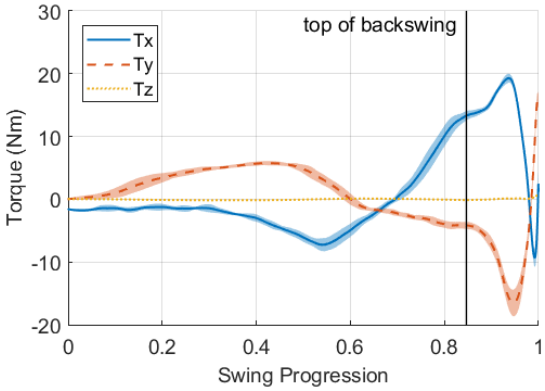

(h) Golfer 4 Torque

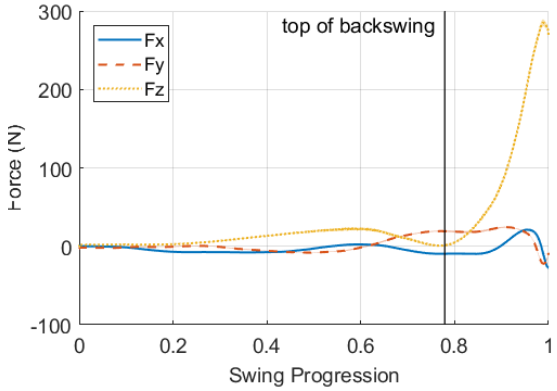

(i) Golfer 5 Force

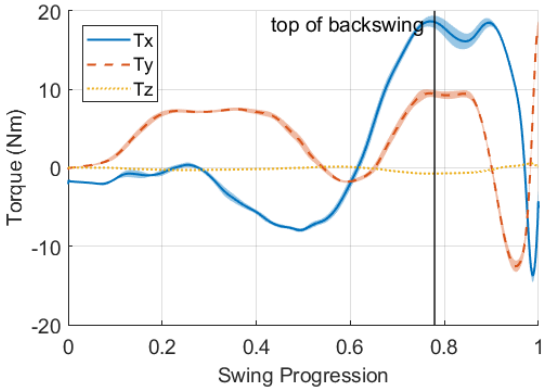

(j) Golfer 5 Torque

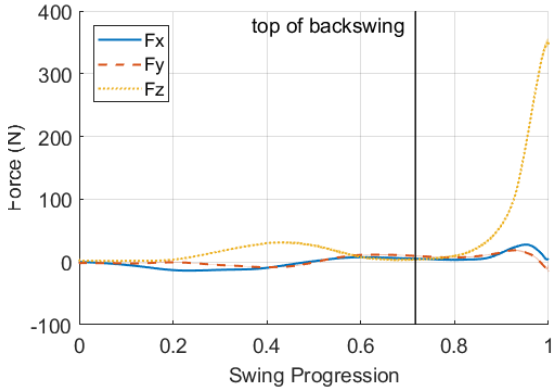

(k) Golfer 6 Force

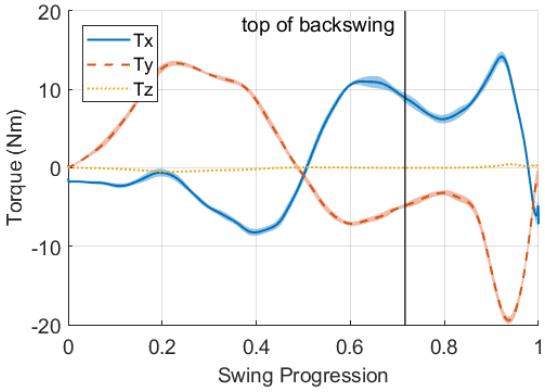

(l) Golfer 6 Torque

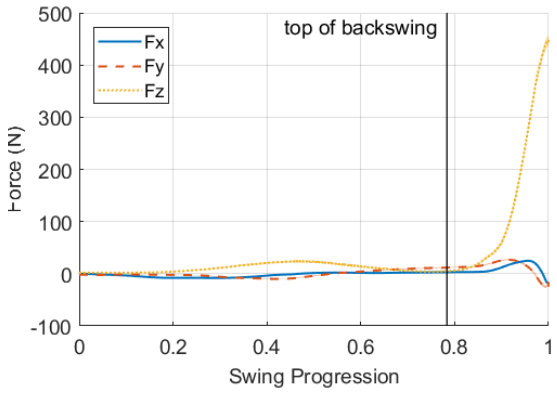

(m) Golfer 7 Force

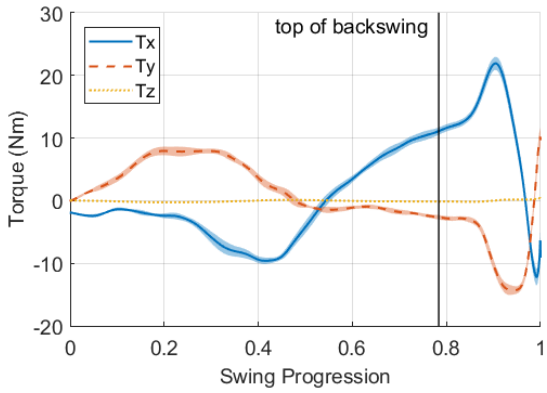

(n) Golfer 7 Torque

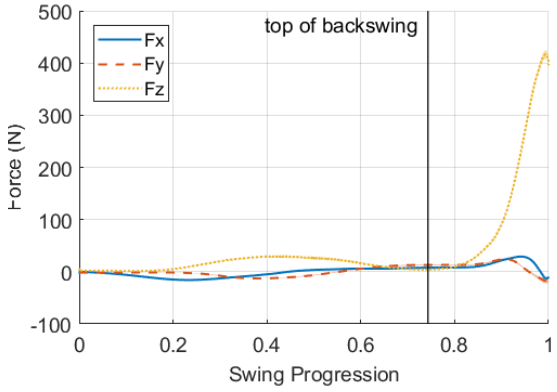

(o) Golfer 8 Force

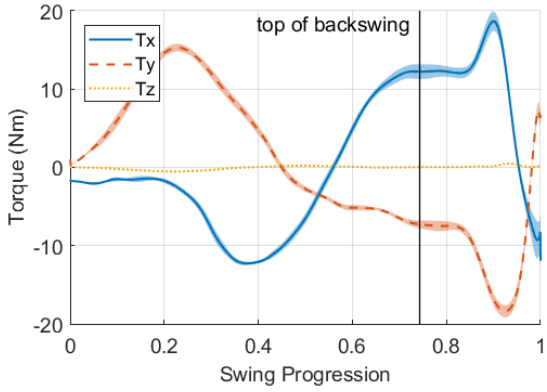

(p) Golfer 8 Torque

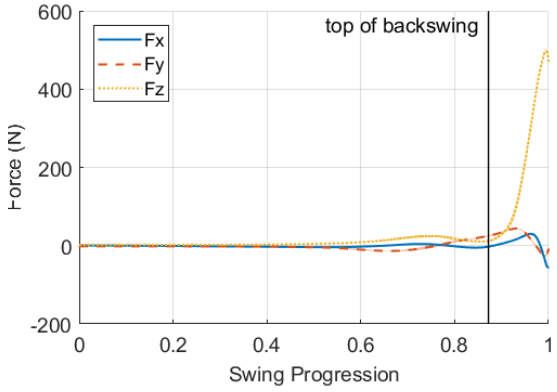

(q) Golfer 9 Force

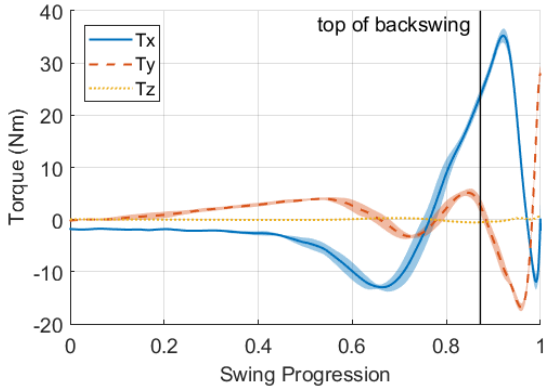

(r) Golfer 9 Torque

Figure C.1: Simulated grip forces in grip frame (Golfers 1-9)